The Hong Kong Polytechnic University
Department of Electrical Engineering

Optimisation Studies of a Wind Power Generation System

WONG, Ka Chung

A thesis submitted in partial fulfilment of the requirements for the Degree of Doctor of Philosophy

August 2008

CERTIFICATE OF ORIGINALITY

I herby declare that this thesis is my own work and that, to the best of my knowledge and belief, it reproduces no material previously published or written, nor material that has been accepted for the award of any other degree or diploma, except where due acknowledgement has been made in the text.

_____ (Signed)

WONG, Ka Chung (Name of Student)

Dedication

To my beloved parents, Siu Hing and Kwok Ming

Abstract

Studies on wind power generation systems are becoming a topical research area because of the increasingly scarcity of hydrocarbon fuels. The rise in petroleum price is also creating heavy demands on renewable energy sources such as wind, hydro, solar, bio-mass and so on. Hitherto, wind energy is most promising in terms of cost effectiveness. Among existing wind generation systems, variable speed wind turbines with doubly fed induction generators (DFIGs) are most common because of their high energy yields and ease of implementation that allows the users to control the reactive power of these wind generators with relatively simple and low power rating control gears. Only simple algorithms are needed for effective and robust control of wind power generation using DFIG.

In this research, direct control algorithms for normal operations of DFIGs, including synchronization and power generation, are developed. Mathematical models, computer simulation, and experimental results are included for the validation of various schemes being studied. The algorithms developed in the research are model-based designs with direct feedback of the control variables to minimize the number of parameters and to simplify numerical operations, with no compromise in performance. A direct voltage control scheme for the synchronization of DFIGs to grids is therefore presented. The beauty of the proposed methodology is that the scheme is a single loop design with no current control loops, and only those parameters which are required for tuning the voltage controller are needed. In comparison with conventional control schemes for DFIGs, the proposed controller

requires no mathematical coordinate transformation of currents and hence is simpler and faster.

Direct torque control of DFIGs with constant switching frequency is also developed in the research. The control scheme utilizes direct feedback of torque and reactive power to avoid the need to build current control loops. Hence, the scheme does not require alignment of currents to the synchronous frames, as torque and reactive power can be evaluated in any coordinate frames. The proposed scheme inherits the simplicity of classical direct torque control scheme, but not the disadvantages of classical schemes such as variable switching frequencies and relatively poor steady state accuracy. Overall, the power quality of power generation is improved in the proposed scheme.

Direct torque control of DFIGs in grids with large source impedances is proposed. The control method automatically adjusts the controller parameters in accordance to changes in grid voltage, in that the control performance and dynamics of the power generation systems are decoupled from fluctuations in the grid voltage, which is a common constraint in wind farms having weak connection to grids due to the presence of long transmission lines.

A control scheme for DFIGs to operate in grids with voltage unbalance is also developed. Variables of the DFIGs are separated into sequence components and are independently controlled. As the degree of freedom is increased by the separation of sequence components, coordination of the components can be performed in the scheme to achieve different objectives, to suit the needs of grids with different operating conditions.

Publications Arising from the Thesis

[1] Wong, K.C., Ho, S.L., and Cheng, K.W.E.: 'Direct voltage control for grid synchronization of doubly fed induction generators', *Electric Power Components and Systems*, 2008, **36**, (9), pp. 960–976

[2] Wong, K.C., Ho, S.L., and Cheng, K.W.E.: 'Direct control algorithm for doubly-fed induction generators in weak grids', *IET Electric Power Applications*, to be published

[3] Wong, K.C., Ho, S.L., and Cheng, K.W.E.: 'Direct torque control of a doubly-fed induction generator with space vector modulation', *Electric Power Components and Systems*, 2008, **36**, (12), pp. 1337–1350

[4] Wong, K.C., Ho, S.L., and Cheng, K.W.E.: 'Direct torque control of doubly fed induction generators connected to grids with unbalanced voltage', *Electric Power Components and Systems*, to be published

[5] Wong, K.C., Ho, S.L., and Cheng, K.W.E.: 'Minimization of current stress on the grid synchronization of doubly-fed induction generators for wind power generation', 3rd International Conference on Power Electronics Systems and Applications, 2009, to be published

Acknowledgements

I would like to express my pleasure and gratitude to Professor S.L. Ho, the Head of the Department of Electrical Engineering, The Hong Kong Polytechnic University. His supervision and guidance nourish me and help me overcome obstacles in the study. Without his knowledge and encouragement, the work would never be completed.

It is appreciated that the co-supervisors, Prof. K.W.E. Cheng and Dr. T.F. Chan, are also providing me with useful suggestions and advices on the research. Mr. C.K. Cheung of the Electrical Machines Laboratory is also acknowledged for his technical support.

The studentship support from the Department of Electrical Engineering is gratefully acknowledged.

Table of Contents

List of Figures

List of Tables

List of Symbols

i	Current in Ampere
n_{+-}	Negative sequence ratio
p	Number of pole pairs
s	Laplace variable
t	Time in second
v	Voltage in Volt
v_{dc}	DC link voltage in Volt
δ	Small change
θ_r	Rotor mechanical angle in radian per second
λ	Flux linkage in Weber-turn
τ	Torque in Newton-meter
ω_r	Rotor mechanical frequency in radian per second
ω_s	Electrical synchronous frequency in radian per second
$\boldsymbol{C}$	Controller model
$\boldsymbol{D}$	Diagonal component of the internal machine model
$\boldsymbol{G}$	Machine model
$\boldsymbol{I}$	Identity matrix
K_p	Proportional constant
$\boldsymbol{L}$	Transfer function of a low pass filter
L	Inductance (referred to the stator for machine quantities) in Henry
P	Real power in Watt
Q	Reactive power in Volt-ampere reactive
R	Resistance (referred to the stator for machine quantities) in Ohm

S Apparent power in Volt-ampere

T_{cl} Closed-loop time constant in second

T_i Integral time constant in second

$\boldsymbol{W}$ Off-diagonal component of the internal machine model

* Complex conjugate

^ Internal model

~ Disturbance

° Estimated value

‘ Mismatched parameter

$\angle\lambda_{s+-}$ Difference in argument between the negative and positive sequence components of the stator flux

Subscripts:

90 Variable delayed for one-fourth of the fundamental period

a Phase A variable

ab Difference between phase A and phase B variables

abc Three phase variables

b Phase B variable

bc Difference between phase B and phase C variables

c Phase C variable

d Real (direct) part of the variable in the stator flux reference frame

dq Variable in the stator flux reference frame

g Grid variable

m Magnetizing variable

q Imaginary (quadrature) part of the variable in the stator flux reference frame

r	Rotor variable
ref	Reference variable
ripple	Ripple term
s	Stator variable
x	Real (direct) part of the variable in the grid voltage reference frame
xy	Variable in the grid voltage reference frame
y	Imaginary (quadrature) part of the variable in the grid voltage reference frame
α	Real (direct) part of the variable in the stator reference frame
$\alpha\beta$	Variable in a stator reference frame
β	Imaginary (quadrature) part of the variable in the stator reference frame
σ	Leakage
A	Real (direct) part of the variable in the rotor reference frame
AB	Variable in the rotor reference frame
B	Imaginary (quadrature) part of the variable in the rotor reference frame
+	Positive sequence component
+-	Positive and negative sequence component
-	Negative sequence component

1 Introduction

1.1 Background

Because of increasing public awareness of global warming, fast depletion of existing non-renewable energy sources, and the introduction of Kyoto Protocol, researchers are seeking for new alternative energy sources that are sustainable and renewable. Among the possible energy sources, wind energy is one of the most promising and feasible sources in densely populated areas like Hong Kong [1]. Wind energy, as a renewable energy source, has the potential of being cost effective and has a high capacity factor. Currently, most commercially operating wind turbines have horizontal axis designs with variable speed electric power generation. Variable speed wind power generation is superior to fixed speed generation in that, when compared to the latter, it has a high energy yield [2], allows good and robust control of power generation, and has lower power and torque pulsations [3].

A typical configuration of a wind energy generation system is shown in Fig. 1.1. Naturally, the blades interact with wind and convert wind energy into mechanical energy at the shaft. The wind turbine, which includes couplings, dampers, and gear boxes, conveys the mechanical energy harvested at the blade shaft to the shaft of the generator system. The generator system, with its generator and power electronics, performs electro-mechanical energy conversion to generate electrical power to the power grid. Typical wind turbine characteristics are shown in Fig. 1.2 [4]. The turbine speed has to vary, according to the wind speed, to maximize the energy being harvested. If the wind speed is higher than the rated wind speed, the turbine speed has to be decreased to limit the power output to its rated value. As

controlling the blade pitch angle can only limit but not to maximize the power output, a good design to the control of the generator system becomes essential for variable speed systems so as to maximize as well as to limit the power generation [5].

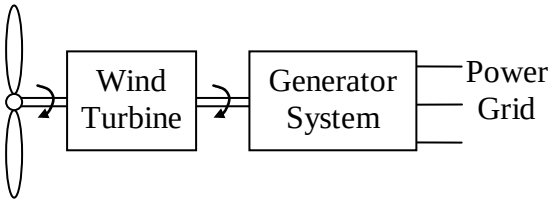

Fig. 1.1 Configuration of a wind energy generation system

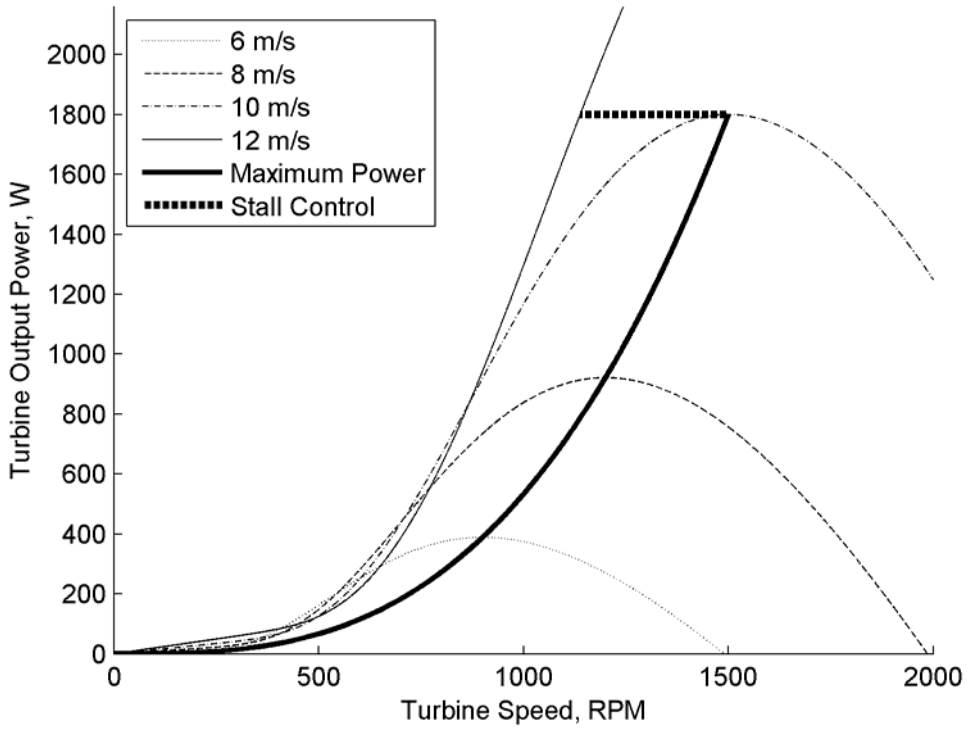

Fig. 1.2 Wind turbine characteristics

There are several types of generators for variable speed wind power generation, which are, namely, cage induction generators, synchronous generators, wound rotor induction generators with variable rotor resistances, doubly fed induction generators (DFIGs), brushless doubly fed induction generators, and switched reluctance

generators [6, 7]. Among them, cage induction generators, synchronous generators and switched reluctance generators require power electronic converters having the same ratings as that of generators, because all generated electric power has to be processed by the converters. The large ratings of these converters, apart from being very costly, will lead to large size and hence overall heavy generation units. In contrast, the ratings of the power electronic converters of DFIGs and brushless doubly fed induction generators are only fractions of the total generator output power, hence these controllers are cheaper, simpler and more reliable. For wound rotor induction generators with variable rotor resistances, slip rings are unnecessary, however, the feasible operating speed range is limited to 100% to 110% of the synchronous speed of the generators. They also suffer from having poor control of real and reactive power. The rotor power in wound rotor induction generators with variable rotor resistances is dissipated as heat, instead of being recovered as electrical energy in DFIGs [8]. In the wind power industry, brushless doubly fed induction generators are however not popular because they are conceptually new to the wind turbine manufacturers [9]. On the other hand, DFIGs have the largest market share and highest annual growth rate in the wind power industry [8, 10], because of their low converter power ratings, high energy output, good utilization of the generators [11] and features that allow independent control of real and reactive output power over a wide speed range.

1.2 Literature Review

1.2.1 General Characteristics of Doubly Fed Induction Generators

The static and dynamic operation of DFIGs has been well known for more than half a century [12]. At times before the wide applications of power electronics for

machine drives, DFIGs have been commonly used as series or shunt induction machines. They are also operated together with rotary frequency changers connected to the rotors for variable speed operation, because of the absence of power electronics for machine control at that time. Most reported researches on DFIGs are focused on their steady state characteristics [13] and operating limits [14]. The most important characteristic is that the rotor power of DFIGs is proportional to the product of the slip and stator power, by assuming the power losses are negligible. It implies that if DFIGs are operated with relatively low slips, the rotor power will only be fractions of the stator power. In other words, within speed ranges around the synchronous frequency, the rotor converters in DFIGs only need to process a portion of the total input mechanical power to the wind turbine.

1.2.2 Synchronization of Doubly Fed Induction Generators

In order to make the best use of generated power from the wind turbines, it is desirable to connect the power output from these turbines to a common grid. To connect the DFIGs to a common grid, these machines must have their stator voltages synchronized to the power grids [15]. The most basic form of synchronization is to employ field-oriented control (FOC) to regulate the rotor currents in order to adjust the stator voltage before synchronization [16]. For simple FOC method with no stator voltage feedback, there may be voltage differences between the stator and the grid voltage at the synchronization stage, thus there might be large current inrush at the instant at which the DFIGs are connected to the grids. In [17 –21], outer voltage control loops providing the reference rotor currents for the inner current control loops are proposed to regulate the stator voltage to track the grid voltage. Once the

discrepancy between output from the DFIG and the grid supply are minimized during the synchronization process, soft synchronization can be realized.

Direct torque control (DTC) of DFIG for synchronization is proposed in [22]. In the scheme, the inner current control loops in FOC are replaced by feedbacks of the rotor flux, together with the hysteresis controllers. Outer control loops are formed by regulating the frequency and magnitude of the stator voltage to the grid values. A further outer loop is formed with a phase controller, which compares the phase difference between the stator and the grid voltage, to provide the frequency reference of the outer loop. Although DTC has no current control loops, the complexity of the overall structure is comparable to the FOC approach because of the outer loops. DTC has an additional disadvantage in that a large amount of harmonic contents with variable frequencies are generated in the stator voltage due to the hysteresis control method, thereby degrading the power quality of the generation system [23].

1.2.3 Control of Doubly Fed Induction Generators in Balanced Grids

Before the advent of modern high speed electronic switches, power electronics control of DFIG was implemented using thyristors [24, 25]. Since the firing angles of the thyristors are the only control variables and thyristors are naturally commutated devices, only scalar control can be implemented.

As high frequency force commutated switching devices emerge, vector control of DFIG could be implemented. The most common vector control algorithm for DFIGs is FOC, which is realized by converting firstly all three-phase variables to two-phase orthogonal variables with Clark transformation. The two-phase rotor

current is then transformed to the air gap flux [26], stator flux [5, 16, 18–21, 27], or stator voltage [28] reference frames, using Park transformation. The direct and quadrature components of the transformed rotor current are compared with their respective reference values for the current controllers to compute the required orthogonal components of the rotor voltage. The rotor voltage is transformed from the reference frame to the rotor natural frame, and modulated using three-phase sinusoidal pulse width modulation (SPWM) [27] or space vector modulation (SVM) [18] for the rotor side converter to control the voltage being applied to the rotor winding of the DFIG. The DC link of the rotor side converter is connected to a grid side converter, which regulates the DC link voltage by controlling the power flow between the DC link and the grid. One of the rotor current references is provided by an outer loop controller, which computes the difference between the reference and feedback speeds [15, 16, 27, 29], torque [26, 30, 31], or stator real power [5, 18–20, 28, 32 –38]. The other current reference is given by another outer loop controller, which compares the reference and feedback reactive power.

As FOC requires inner loops for current regulation and outer loops for reactive power control and torque or stator real power control, the implementation of FOC requires a processor with high computational power, because of the large number of Park transformations and numerous controllers in FOC. Therefore, DTC is proposed in [39–41] to simplify the controller design and reduce the parameter dependence of the system. In DTC, the current control loops in FOC are replaced by a torque loop together with a flux loop and hysteresis controllers. Since both the torque and magnitude of the rotor flux can be estimated without the transformation of the currents to any synchronous frame, the number of Park transformation in DTC is less

than that in FOC. However, DTC inherits the disadvantages of hysteresis control, including the need to operate at variable switching frequencies, large current distortions, and the requirement of high sampling frequencies for digital implementation [23, 42]. Moreover, in DTC, the control of reactive power requires an additional outer loop controller, which compares the reference and the feedback reactive powers to provide the reference rotor flux for the hysteresis controller to regulate the rotor flux.

Similar to DTC, direct power control (DPC) is developed to eliminate the current control loop [43 –46], but DPC employs the feedback of real and reactive power instead of torque and rotor flux. As the computation of the instantaneous real and reactive power also requires no Park transformation of the currents to any synchronous frame, the computational burden is also reduced. However, as hysteresis control is used in DPC, the disadvantages of DTC also exist in DPC. DPC with constant switching frequency deadbeat controllers, instead of hysteresis controllers, is proposed in [47] to address those problems arising from variable frequency switching based on hysteresis control. It is well known that, in order to control the rotor speed accurately, the total output power of the DFIG must be evaluated. However, as the rotor power of the DFIG is not considered explicitly in DPC, the tuning of the speed controller in DPC is complicated because insufficient information is available to the speed controller. Under such circumstances, the controller parameters have to be adjusted adaptively as the turbine speed changes in order to optimize the performance of the system.

In prior arts on the control of DFIGs, voltage fluctuations and source impedances of the grids are not considered. Nonetheless, there are significant voltage

fluctuations in wind farms, especially in systems having weak links due to long transmission lines [48]. More specifically, weak connection is characterised by high source impedances and rapid and significant changes of grid voltage as the generated output power fluctuates. In order to address these issues arising from transmission over long lines, high voltage direct current (HVDC) is proposed in [49]. However, the majority of the offshore wind farms still employs AC transmission because it is less expensive [50, 51].

1.2.4 Control of Doubly Fed Induction Generators in Grids with Unbalanced Voltage

Most of the analyses on DFIG are based on the assumption that DFIGs are connected to girds with balanced voltages [13–22, 24–47]. However, field measurement on the power qualities of wind farms indicates that most grids have various degrees of voltage unbalance [52]. Induction generators operating in a grid with voltage unbalance would generate unbalanced currents, which increase the winding temperature, and introduce torque and power pulsations [53]. Even if the negative sequence voltage is within the limit of 3% of the positive sequence voltage as stipulated in the European standard [54], the negative sequence stator current of a DFIG may be as high as 18.3% of the positive sequence current [55].

In [56], the torque and reactive power ripples of the DFIG resulting from voltage unbalance are eliminated by the addition of auxiliary control loops to the current control loops of the FOC designed for balanced grid voltage operation. Each auxiliary control loop comprises a band-pass filter tuned to twice synchronous frequency, and a high gain controller, to take care of the additional rotor voltage. The

auxiliary control loops have high gains at twice synchronous frequency such that the torque and reactive power ripples at twice mains frequency are attenuated by the injection of the compensating rotor voltage at the same frequency. An alternative method, as proposed in [57], can be exploited to reduce the torque and reactive power ripples by incorporating compensating rotor currents into the reference currents. In such schemes, the compensating rotor currents are derived from the oscillating amplitudes of the magnetizing currents. Both methods, however, are limited to the reduction of torque and reactive power ripples only, and they are not capable of reducing stator real power ripples or maintaining balanced stator currents. Minimization of stator current ripples with fuzzy controller is proposed in [58]. However, the method has the limitation of being able to address one specific minimization objective only.

Independent control of the positive and negative sequence components of stator currents is proposed in [59, 60]. The sequence components of the stator current are extracted and transformed from the stator frame to their respective stator flux reference frames. The transformed current components are compared with their reference values to act on the appropriate controllers. The controllers compute the required rotor voltages, which are transformed to the rotor frame and then combined before controlling the voltage to be impressed on the rotor windings through the rotor converter.

Coordination of the negative sequence real and reactive power in accordance to the minimization objectives and the magnitude of the negative sequence voltage is proposed in [61]. The positive and negative sequence components of the stator current are regulated to their respective reference values, whereas the reference

currents are derived from the positive and negative power controllers. The power controllers compare the differences between the power and their reference values in the same manner as that of FOC for balanced grid voltages. The method is capable of minimizing the torque and reactive power ripples, stator real power ripples or restoring balanced stators current. It is also possible to reduce the torque and power ripples by coordinating the positive and negative sequence currents, instead of coordinating the real and reactive power [62]. In [63, 64], the negative sequence reference rotor currents are derived from the positive sequence rotor currents, according to the minimization objective.

1.3 Research Objectives and Scope

As the power ratings of newly built wind turbines increase [65] and wind farms, especially those operating offshore, are emerging, most of the wind turbines are now connected to power grids. Furthermore, since DFIGs have the largest market share, the research project shall focus on grid-connected control of DFIGs. Because of the complicated designs and sophisticated tuning of existing control methods for grid connected DFIGs, the objective of this research project is to investigate and develop direct control methods to realize simple and robust operation of DFIGs with different network conditions.

The existing synchronization methods for DFIGs either have no stator voltage feedback, which may introduce current inrushes upon connections of the DFIGs; or involve cascaded current and voltage control loops, which are computationally demanding and require complicated tuning of controller parameters. On the other hand, the use of DTC for synchronization generates harmful harmonics having a

wide range of frequencies, thereby degrading the power quality. A direct voltage control (DVC) scheme for DFIGs is developed in the research to synchronize a DFIG to the grid with voltage feedback. The scheme is a stator-voltage-orientated single-loop design, which can minimize the impact on the DFIG as well as on the power system upon connection. As the stator voltage is directly controlled, instead of passing through a chain of cascaded loops, the number of parameters and hence the demand on the computational power are significantly reduced.

As FOC for DFIGs has current loops, cascaded with a reactive power loop, and a stator real power or torque control loop, FOC requires the tuning of several parameters and a large number of coordinate transformation and controllers. Even DTC and DPC reduce the number of control loops, the hysteresis switching may degrade the quality of the generated currents. DPC with constant frequency also suffer from having the disadvantage of requiring the feedback of part of the power generated, and this limits its use in speed control of DFIG. A direct torque control with space vector modulation (DTC-SVM) scheme is proposed in the research to utilize direct feedback of torque and reactive power to simplify the controller design, and it also makes use of a constant switching frequency to avoid switching harmonics of variable frequencies and other problems arising from hysteresis switching.

As some of the DFIGs are weakly connected to existing grids with significant source impedance, the effects of the source impedance on the operations and control of DFIG are investigated. A direct control algorithm, which automatically adjusts the parameters of the controllers in accordance to the voltage level of the grid, is developed to ensure that the control targets of the DFIGs are met.

Voltage unbalance is not uncommon in wind farms. However, existing control methods are incapable of achieving objectives such as reducing stator real power ripples, or require complicated FOC that independently regulates the sequence components of currents, together with power regulating outer control loops. A direct control scheme, with torque and reactive power feedback for independent regulation of the positive and negative sequence components of the torque and reactive power, is developed in the research. Similar to the FOC, the scheme can achieve different ripple minimization objectives to suit the needs of different grids in various grid conditions. For the proposed direct control scheme, the computational demand is less, and tuning of the algorithm is simpler than that in FOC because of the direct feedback of the control variables.

1.4 Thesis Organization

The direct voltage control for the synchronization of DFIGs to the power grids is presented in Chapter 2. In Chapter 3, direct torque control of DFIG with space vector modulation in grids with balanced voltage is developed. An algorithm to alleviate the impact of source impedances on the operations of DFIGs with DTC is discussed in Chapter 4. An algorithm for direct torque control of DFIGs in grids with voltage unbalance is reported in Chapter 5. Conclusions on the research and possible further developments are given in Chapter 6.

2 Direct Voltage Control for Grid Synchronization

2.1 Introduction

A scheme for synchronization of DFIGs to grids is developed in this chapter. The proposed topology is a vector control scheme with direct feedback of the stator voltage for the minimization of the differences in voltage between the stator and the grid. Since no current feedback is required and the scheme is a single-loop design, the scheme is less demanding, when compared to existing methods, on the processing power of the controllers.

2.2 Topology

The topology of a DFIG during synchronization is shown in Fig. 2.1. The DFIG is mechanically coupled to a wind turbine. The rotor converter is a three-phase full-bridge inverter that controls the voltage applied to the rotor winding of the DFIG. The grid converter controls the power flow between the DC link and the grid to keep the DC link voltage constant. The controllers monitor i) the grid, stator and DC link voltages, ii) the rotor current, and iii) the rotor position. All these information are used intelligently to control the operations of the two converters.

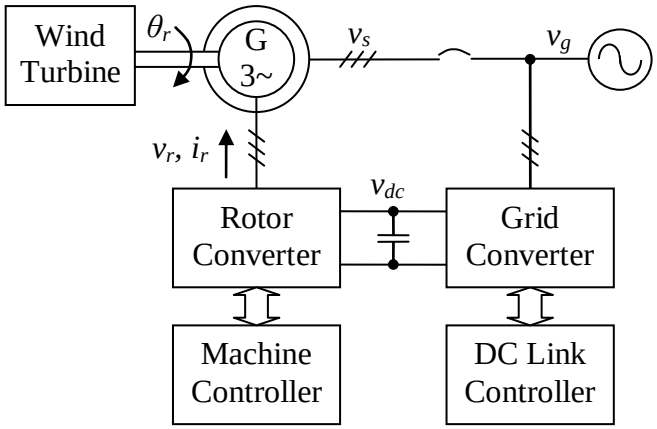

Fig. 2.1 Topology of a DFIG during synchronization to the grid

2.3 Mathematical Model

The three-phase rotor current in Fig. 2.1 is transformed into a complex value with Clark transformation:

$$i_{rA} = i_{ra}\sqrt{3/2} \tag{2.1}$$

$$i_{rB} = \left(i_{ra} + 2i_{rb}\right)/\sqrt{2} \tag{2.2}$$

$$\bar{i}_{rAB} = i_{rA} + ji_{rB} \tag{2.3}$$

Similarly, the stator voltage v_s and grid voltage v_g are transformed from line-to-line quantities to phasors with Clark transformation as given below:

$$v_\alpha = \left(v_{ab} + v_{bc}/2\right)\sqrt{2/3} \tag{2.4}$$

$$v_\beta = v_{bc}/\sqrt{2} \tag{2.5}$$

$$\bar{v}_{\alpha\beta} = v_\alpha + jv_\beta \tag{2.6}$$

As all voltage and current quantities of the DFIG are controllable with the rotor converter, the grid voltage is the only quantity not affected by the operation of the

DFIG before the machine is connected to the grid. Therefore, the grid voltage is taken as the reference value. Park transformation of the rotor current to the grid voltage reference frame yields

$$\bar{i}_{rxy} = \bar{i}_{rAB} \exp\left(- j\left(\arg\left(\bar{v}_{g\alpha\beta}\right) - p\theta_r\right)\right). \tag{2.7}$$

The stator voltage is transformed into the grid voltage reference frame with

$$\bar{v}_{sxy} = \bar{v}_{s\alpha\beta} \exp\left(- j \arg\left(\bar{v}_{g\alpha\beta}\right)\right). \tag{2.8}$$

The complex equations describing the operation of the DFIG in a synchronous reference frame aligned to the grid voltage are:

$$\bar{v}_{gxy} = \left|\bar{v}_{gxy}\right| = \left|\bar{v}_{g\alpha\beta}\right| \tag{2.9}$$

$$\bar{v}_{sxy} = \frac{d\bar{\lambda}_{sxy}}{dt} + j\omega_s \bar{\lambda}_{sxy} \tag{2.10}$$

$$\bar{v}_{rxy} = \bar{i}_{rxy} R_r + \frac{d\bar{\lambda}_{rxy}}{dt} + j\left(\omega_s - p\omega_r\right)\bar{\lambda}_{rxy} \tag{2.11}$$

$$\bar{\lambda}_{rxy} = \left(L_m + L_{r\sigma}\right)\bar{i}_{rxy} \tag{2.12}$$

$$\bar{\lambda}_{sxy} = L_m \bar{i}_{rxy} \tag{2.13}$$

$$\omega_r = \frac{d\theta_r}{dt} \tag{2.14}$$

The real parts of the complex variables are direct variables aligned to the grid voltage, and the imaginary parts of them are the quadrature variables orthogonal to the grid voltage.

The equivalent circuit of (2.9)–(2.14) is shown in Fig. 2.2. The stator leakage inductance $L_{s\sigma}$ is not included in the above equations because there is no stator current before the machine is connected to the grid.

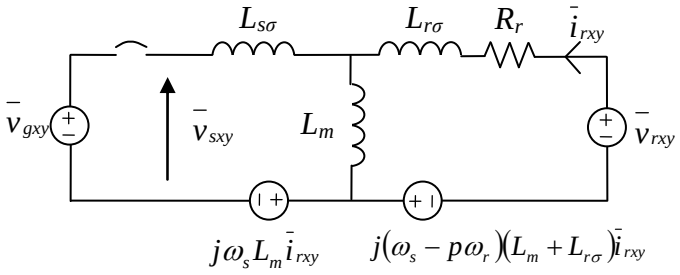

Fig. 2.2 Equivalent circuit of DFIG in the grid voltage reference frame

2.4 Control Strategy

The control objective is to control the stator voltage in a grid voltage reference frame, such that the stator voltage and the grid voltage will have equal magnitude, frequency, and zero phase difference. The controller has a general structure as shown in Fig. 2.3.

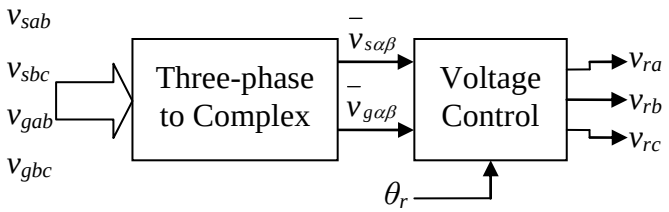

Fig. 2.3 Machine controller structure

The three-phase to complex operation transforms the stator and grid voltages using (2.4)–(2.6). The voltage controller computes the required rotor voltage and it will be described fully in section 2.4.1. The SVM operation in the voltage control

modulates the required rotor voltage into pulse-width patterns to control the switching state of the rotor converter.

2.4.1 Voltage Controller Design

To relate the stator voltages to the rotor voltages, (2.11) is firstly expressed as the following Laplace equations:

$$v_{rx}(s) = i_{rx}(s)R_r + s\lambda_{rx}(s) - (\omega_s - p\omega_r)\lambda_{ry}(s) \tag{2.15}$$

$$v_{ry}(s) = i_{ry}(s)R_r + s\lambda_{ry}(s) + (\omega_s - p\omega_r)\lambda_{rx}(s) \tag{2.16}$$

Substituting the Laplace form of (2.12) into (2.15) and (2.16) gives

$$v_{rx}(s) = i_{rx}(s)R_r + s(L_m + L_{r\sigma})i_{rx}(s) - (\omega_s - p\omega_r)(L_m + L_{r\sigma})i_{ry}(s) \tag{2.17}$$

$$v_{ry}(s) = i_{ry}(s)R_r + s(L_m + L_{r\sigma})i_{ry}(s) + (\omega_s - p\omega_r)(L_m + L_{r\sigma})i_{rx}(s). \tag{2.18}$$

The last terms in (2.17) and (2.18) can be compensated with feed-forward compensation. It can also be regarded as a disturbance, especially when the magnitude of the last term is much smaller than that of the second term in transient state. With

$$\bar{v}_{rxy}' = \bar{v}_{rxy} - j(\omega_s - p\omega_r)(L_m + L_{r\sigma})\bar{i}_{rxy}, \tag{2.19}$$

equation (2.17) and (2.18) become

$$v_{rx}'(s) = i_{rx}(s)(s(L_m + L_{r\sigma}) + R_r) \tag{2.20}$$

$$v_{ry}'(s) = i_{ry}(s)(s(L_m + L_{r\sigma}) + R_r). \tag{2.21}$$

Rearranging (2.20) and (2.21) yields

$$i_{rx}(s) = v_{rx}'(s)/(s(L_m + L_{r\sigma}) + R_r) \tag{2.22}$$

$$i_{ry}(s) = v_{ry}'(s)/(s(L_m + L_{r\sigma}) + R_r). \tag{2.23}$$

From (2.13), (2.22) and (2.23), the stator flux can be expressed as

$$\lambda_{sx}(s) = v_{rx}'(s)L_m/(s(L_m + L_{r\sigma}) + R_r) \tag{2.24}$$

$$\lambda_{sy}(s) = v_{ry}'(s)L_m/(s(L_m + L_{r\sigma}) + R_r). \tag{2.25}$$

As the stator voltage and flux have a multi-input multi-output relationship, appropriate pairs of the voltage and flux components have to be identified to close the control loop correctly. The degrees of relevance between the input and output variables can be calculated using the relative gain array (RGA) methodology [66]. RGA is an array with elements indicating the open-loop gain to closed-loop gain ratio between the corresponding input and output variables. The closer the open-loop gain and the closed-loop gain, the closer is the interaction between the corresponding variables. RGA is computed as an element-by-element product of the system transfer matrix and the inverse of its transposed matrix. An RGA element close to unity indicates that the input and output variables constitute a suitable pair to form a control loop, while a small positive RGA element implies low correlation between the input and output variables. As the row and column sums of the RGA elements must be unity, any element larger than one will result in negative values in other elements, which implies that the gain of the input-output pairs will be reversed upon closing the control loops. The RGA is usually evaluated at zero frequency to have valid control input and output pairs at steady state.

Separating (2.10) into real and imaginary parts, the following system of Laplace equations is formed:

$$\begin{pmatrix} v_{sx}(s) \\ v_{sy}(s) \end{pmatrix} = \begin{pmatrix} s & -\omega_s \\ \omega_s & s \end{pmatrix} \begin{pmatrix} \lambda_{sx}(s) \\ \lambda_{sy}(s) \end{pmatrix} \tag{2.26}$$

The RGA of the matrix is

$$\begin{pmatrix} s & -\omega_s \\ \omega_s & s \end{pmatrix} \times \left(\begin{pmatrix} s & -\omega_s \\ \omega_s & s \end{pmatrix}^T \right)^{-1} = \frac{1}{s^2 + \omega_s^2} \begin{pmatrix} s^2 & \omega_s^2 \\ \omega_s^2 & s^2 \end{pmatrix}, \tag{2.27}$$

where '×' is the element-by-element multiplication operator.

As the RGA becomes $\begin{pmatrix} 0 & 1 \\ 1 & 0 \end{pmatrix}$ when the Laplace variable approaches zero, the direct stator flux controls the quadrature voltage and the quadrature stator flux controls the direct voltage at steady state. The following matrix is obtained by decomposing (2.26):

$$\begin{pmatrix} v_{sx}(s) \\ v_{sy}(s) \end{pmatrix} = \left(\begin{pmatrix} 0 & -\omega_s \\ \omega_s & 0 \end{pmatrix} + \begin{pmatrix} s & 0 \\ 0 & s \end{pmatrix} \right) \begin{pmatrix} \lambda_{sx}(s) \\ \lambda_{sy}(s) \end{pmatrix} \tag{2.28}$$

The cross coupling term composing of *s* can be regarded as a disturbance again. Therefore, at steady state, (2.28) becomes

$$\begin{pmatrix} v_{sx}(s) \\ v_{sy}(s) \end{pmatrix} = \begin{pmatrix} 0 & -\omega_s \\ \omega_s & 0 \end{pmatrix} \begin{pmatrix} \lambda_{sx}(s) \\ \lambda_{sy}(s) \end{pmatrix}, \tag{2.29}$$

or, in complex notation:

$$\bar{v}_{sxy} = j\omega_s \bar{\lambda}_{sxy} \tag{2.30}$$

Substitutions of (2.24) and (2.25) into (2.29) yield

$$\begin{pmatrix} v_{sx}(s) \\ v_{sy}(s) \end{pmatrix} = \frac{L_m}{s(L_m + L_{r\sigma}) + R_r} \begin{pmatrix} 0 & -\omega_s \\ \omega_s & 0 \end{pmatrix} \begin{pmatrix} v'_{rx}(s) \\ v'_{ry}(s) \end{pmatrix}. \tag{2.31}$$

Since the transfer equation between the stator and rotor voltages is established in (2.31) and the appropriate control pairs are identified, the control system shown in Fig. 2.4 is designed, in which the $e^{-j\theta}$ and $e^{j\theta}$ blocks represent the Park and inverse Park transformations, respectively. The blocks denoted by PI are proportional-integral controllers.

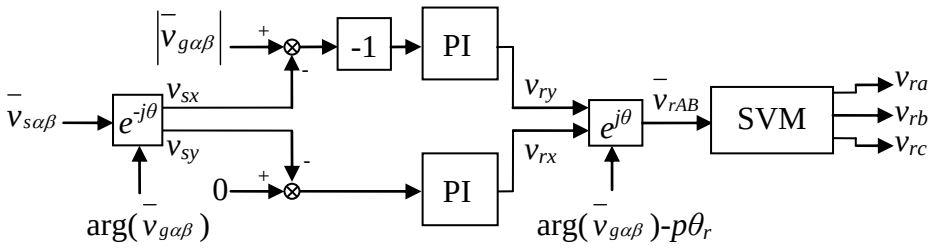

Fig. 2.4 Voltage control diagram of direct voltage control

As the variables are aligned to the grid voltage reference frame, the direct and quadrature controller reference voltages should correspond to the magnitude of the grid voltage and zero, respectively, before one can synchronize the stator voltage of the DFIG to the grid voltage. The proportional-integral controller for the direct stator voltage is implemented with the following equation:

$$v_{ry} = K_p \left(\left(v_{sx} - \left| \bar{v}_{gxy} \right| \right) + \int \frac{\left(v_{sx} - \left| \bar{v}_{gxy} \right| \right)}{T_i} dt \right) \tag{2.32}$$

To have a first order closed-loop step response to the reference input, pole placement is implemented with the proportional and integral time constants which are designed as:

$$K_p = \frac{L_m + L_{r\sigma}}{L_m \omega_s T_{cl}} \tag{2.33}$$

$$T_i = \frac{L_m + L_{r\sigma}}{R_r} \tag{2.34}$$

Similar implementation for the quadrature stator voltage is used with the same parameters, but with an opposite sign for the proportional gain, because of the similarity between the direct and quadrature stator voltages. The outputs of the proportional-integral controllers are transformed into the rotor coordinate with inverse Park transformation:

$$\bar{v}_{rAB} = \bar{v}_{rxy} \exp\left(j\left(\arg\left(\bar{v}_{g\alpha\beta}\right) - p\theta_r\right)\right) \tag{2.35}$$

The output rotor voltage is modulated with SVM to form a constant frequency pulse-width modulation pattern to control the switching operations of the rotor converter.

2.4.2 Comparison with Existing Methods

In comparison to the control diagram of cascaded synchronization scheme as shown in Fig. 2.5 [17, 18], the direct voltage control scheme has two voltage control loops only, whereas the cascaded voltage control scheme has two inner current control loops and two outer stator voltage control loops. If the feed-forward compensation is not implemented, the direct voltage control has a further advantage

as no Park transformation on the rotor currents is needed. Because the number of control loops is reduced by half, the proposed direct voltage control requires less tuning parameters and is less demanding on the computational power of the controller.

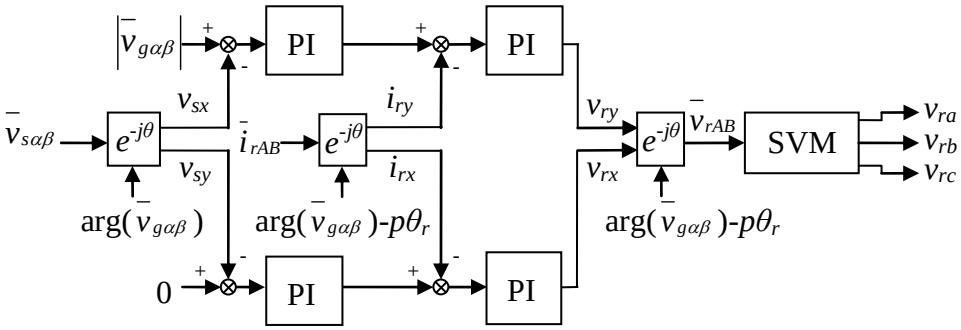

Fig. 2.5 Voltage control diagram of cascaded synchronization scheme

A direct torque control scheme is shown in Fig. 2.6 [22]. It is comprised of two cascaded loops with hysteresis controllers in the inner loops and a switching look-up table to synthesize the rotor voltage. Even it requires no Park transformation to align the variables to a common reference frame, the hysteresis switching look-up table based modulation has drawbacks as there are severe sub-harmonic components with variable frequencies in the output voltage. In comparison, the proposed direct voltage control is implemented with a constant switching frequency and has a relatively simple single loop design.

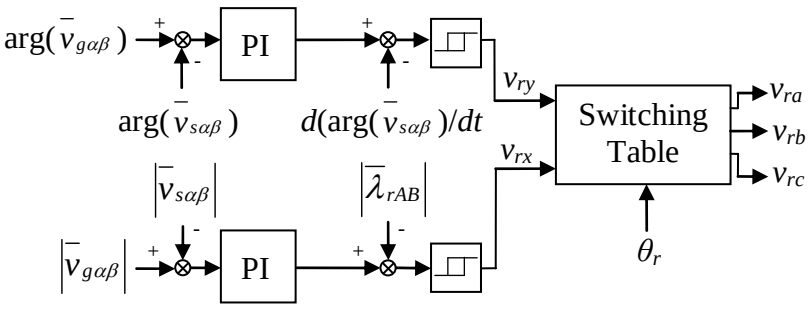

Fig. 2.6 Voltage control diagram of direct torque control

2.5 Conditions of Synchronization

The steady state equations of (2.17) and (2.18) become

$$v_{rx} = R_r i_{rx} - (\omega_s - p\omega_r)(L_m + L_{r\sigma}) i_{ry} \tag{2.36}$$

$$v_{ry} = R_r i_{ry} + (\omega_s - p\omega_r)(L_m + L_{r\sigma}) i_{rx}. \tag{2.37}$$

Rearranging (2.13) and substituting into (2.36) and (2.37) give

$$v_{rx} = \frac{R_r}{L_m}\lambda_{sx} - (\omega_s - p\omega_r)\frac{(L_m + L_{r\sigma})}{L_m}\lambda_{sy} \tag{2.38}$$

$$v_{ry} = \frac{R_r}{L_m}\lambda_{sy} + (\omega_s - p\omega_r)\frac{(L_m + L_{r\sigma})}{L_m}\lambda_{sx}. \tag{2.39}$$

Substituting the rearranged form of (2.30) into (2.38) and (2.39) gives

$$v_{rx} = \frac{R_r}{\omega_s L_m} v_{sy} + (\omega_s - p\omega_r)\frac{(L_m + L_{r\sigma})}{\omega_s L_m} v_{sx} \tag{2.40}$$

$$v_{ry} = -\frac{R_r}{\omega_s L_m} v_{sx} + (\omega_s - p\omega_r)\frac{(L_m + L_{r\sigma})}{\omega_s L_m} v_{sy}. \tag{2.41}$$

Since the direct and quadrature stator voltage is the same as the direct and quadrature grid voltages, respectively, at steady state, the direct stator voltage is the

same as the grid voltage, while the quadrature stator voltage is zero, because, as shown in (2.9), the direct component of the grid voltage is equal to the magnitude of the grid voltage. Furthermore, as the rotor resistance and the product of the synchronous frequency and the rotor leakage inductance are much smaller than the product of the synchronous frequency and the magnetizing inductance, (2.40) becomes

$$v_{rx} = \left|\bar{v}_{g\alpha\beta}\right|\left(1 - p\omega_r / \omega_s\right), \tag{2.42}$$

while the quadrature rotor voltage is zero at or after synchronization.

With SVM, the maximum line-to-line output voltage of the rotor converter is given by [23]:

$$\left|\bar{v}_{rxy}\right| = v_{dc} / \sqrt{2} \tag{2.43}$$

Substituting (2.42) into the (2.43), the minimum DC link voltage required is

$$v_{dc} = \sqrt{2}\left|\bar{v}_{g\alpha\beta}(1 - p\omega_r / \omega_s)\right|. \tag{2.44}$$

(2.44) shows that the rotor voltage required to bring the stator voltage to the grid voltage is dependent on the rotor speed. The required rotor voltage decreases as the rotor speed increases from zero to synchronous speed. On the other hand, the required rotor voltage will increase as the rotor speed increases beyond synchronous speed. As the rotor converter of DFIG is usually designed to handle a fraction of the gross power output [17], the DFIG would not generate adequate stator voltage if the rotor speed is outside its designed speed range.

In addition to the conditions stated above, the stator voltage and the grid voltage must have the following quantities equalized before synchronization in order to minimize the impact to the power system:

- voltage
- frequency
- phase

Since the proportional-integral controllers in Fig. 2.4 adjust the rotor voltage until the error between the stator voltage and grid voltage is zero, the direct stator voltage will be the same as the grid voltage and the quadrature stator voltage will be zero at steady state. Therefore, the voltages and the phases will be equal. As for the frequency, the stator voltage will have the same frequency as that of the gird voltage because the stator voltage rotates in a synchronous frame that is aligned to the grid voltage.

2.6 Simulation Results

The direct voltage control scheme is simulated with Matlab/Simulink. The machine parameters are given in the Appendices and the controllers are tuned to have a closed-loop time constant of 0.04 s. The rotor converter is modelled as a voltage source to simulate the state-averaged operation of the converter. The A-phase to B-phase grid and stator voltages of the DFIG are shown in Fig. 2.7 at a rotor speed of 1200 RPM, and the corresponding direct and quadrature voltages are shown in Fig. 2.8. The grid voltage is applied at time equals to 0.05 s. The stator voltage tracks the grid voltage rapidly and has its amplitude, frequency and phase equalized to those of the grid voltage at 0.33 s. Fig. 2.8 shows that the stator direct

voltage follows the grid voltage and shows a first order response, while the cross coupling between the stator direct and quadrature voltages are compensated at steady state as the quadrature voltage converges to zero. The simulation results are very similar for turbine speeds from 1200 RPM (20 % slip) to 1800 RPM (-20 % slip) as shown in Fig. 2.7 to Fig. 2.14, respectively. It verifies that the control scheme is capable of synchronizing the DFIG over a wide speed range.

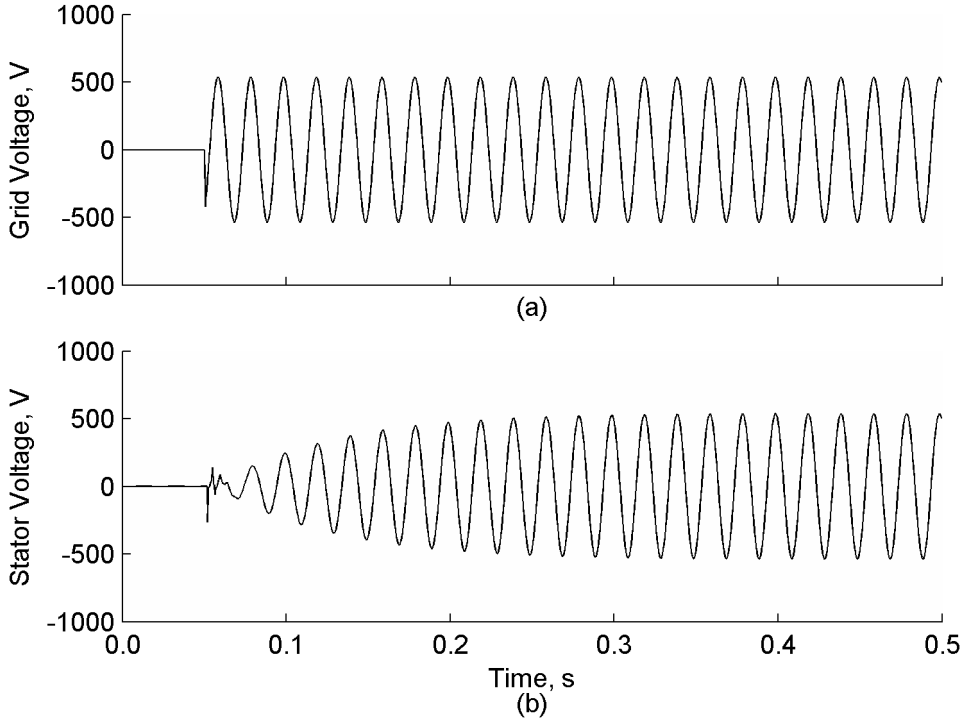

Fig. 2.7 Simulated line-to-line voltages during synchronization at 1200 RPM

(a) Grid, (b) Stator

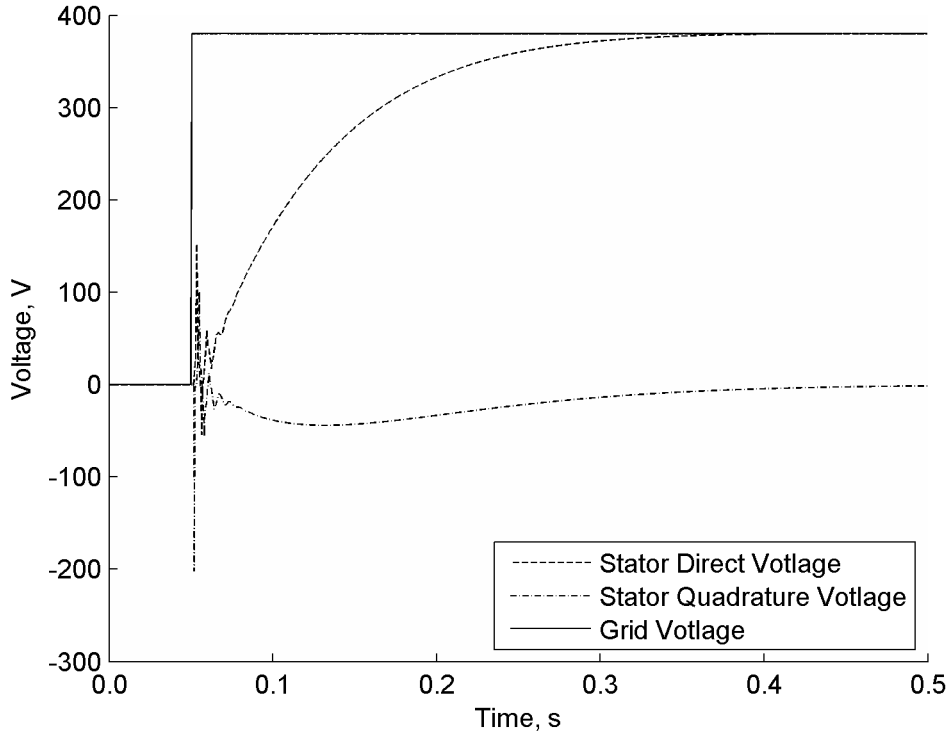

Fig. 2.8 Simulated grid, stator direct and quadrature voltages during synchronization at 1200 RPM

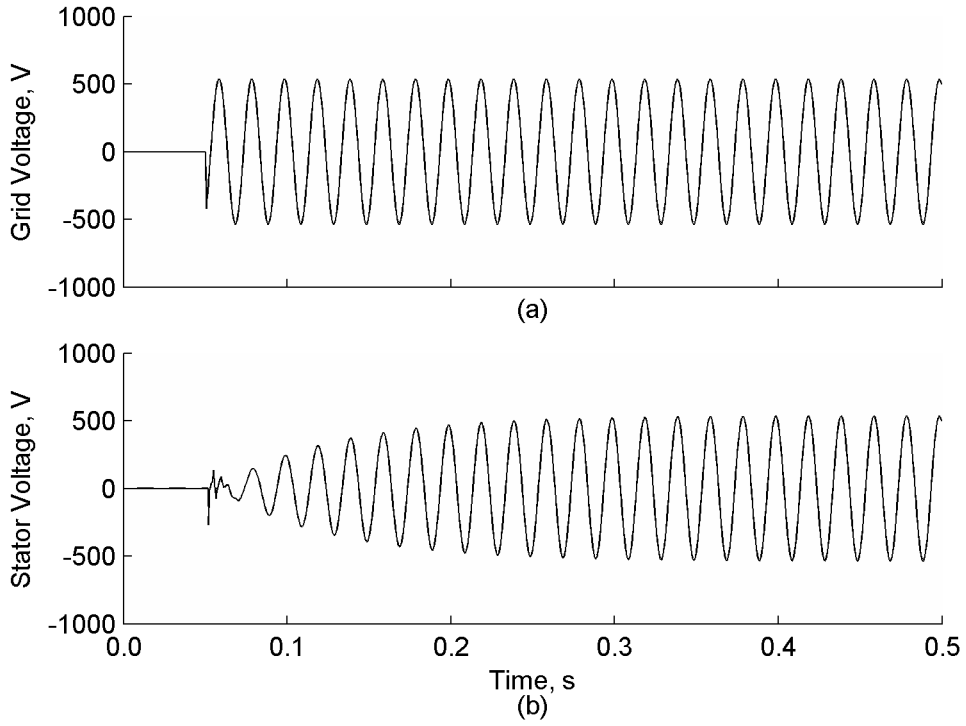

Fig. 2.9 Simulated line-to-line voltages during synchronization at 1325 RPM (a) Grid, (b) Stator

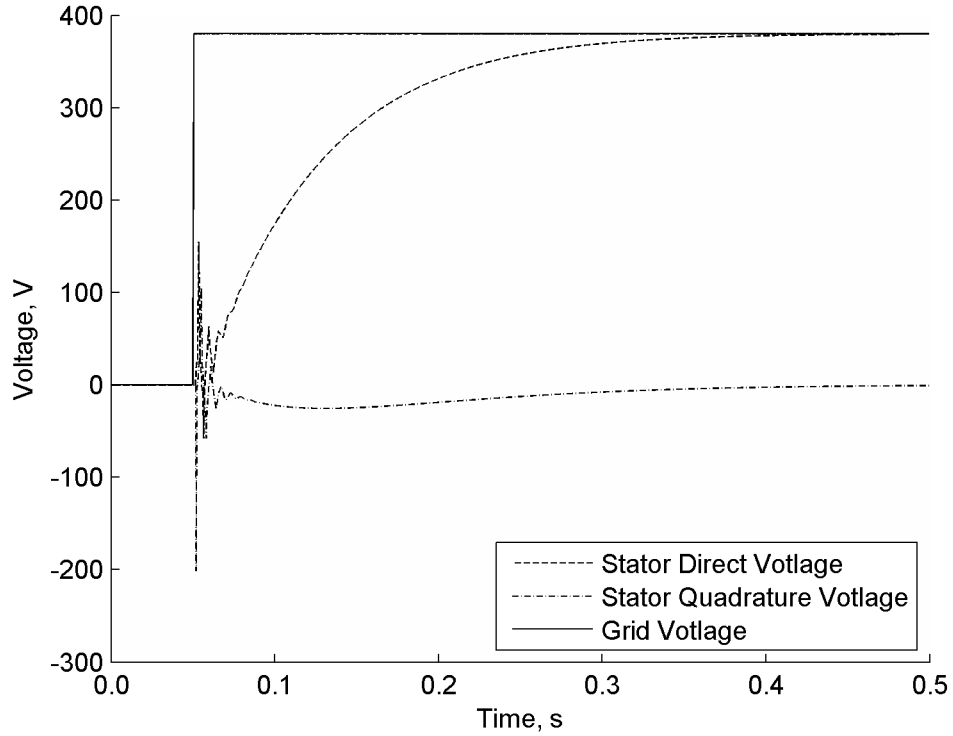

Fig. 2.10 Simulated grid, stator direct and quadrature voltages during synchronization at 1325 RPM

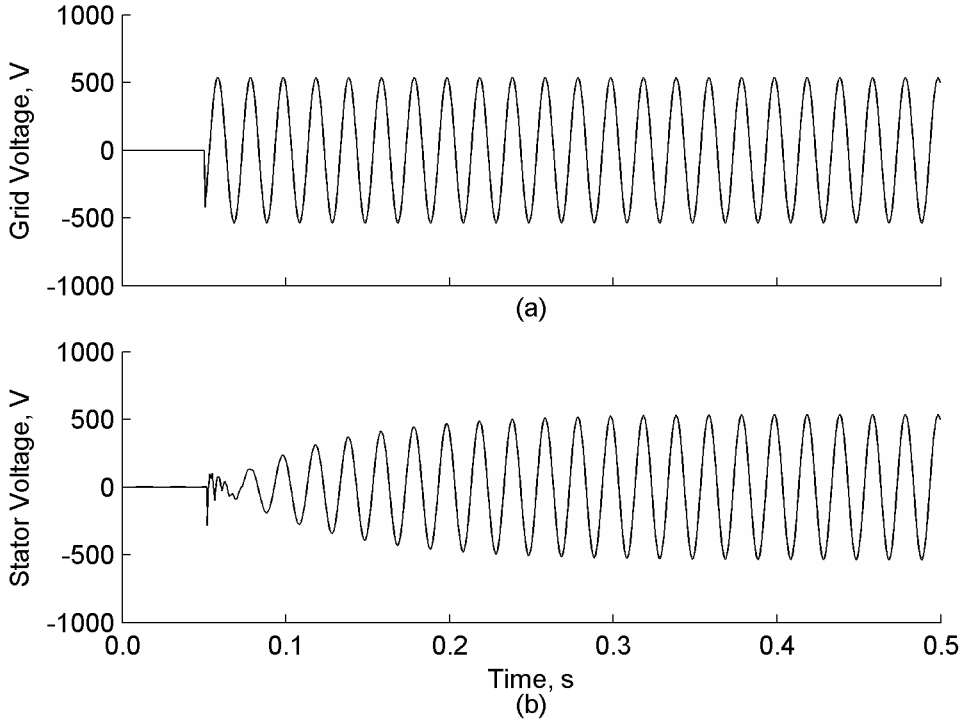

Fig. 2.11 Simulated line-to-line voltages during synchronization at 1686 RPM (a) Grid, (b) Stator

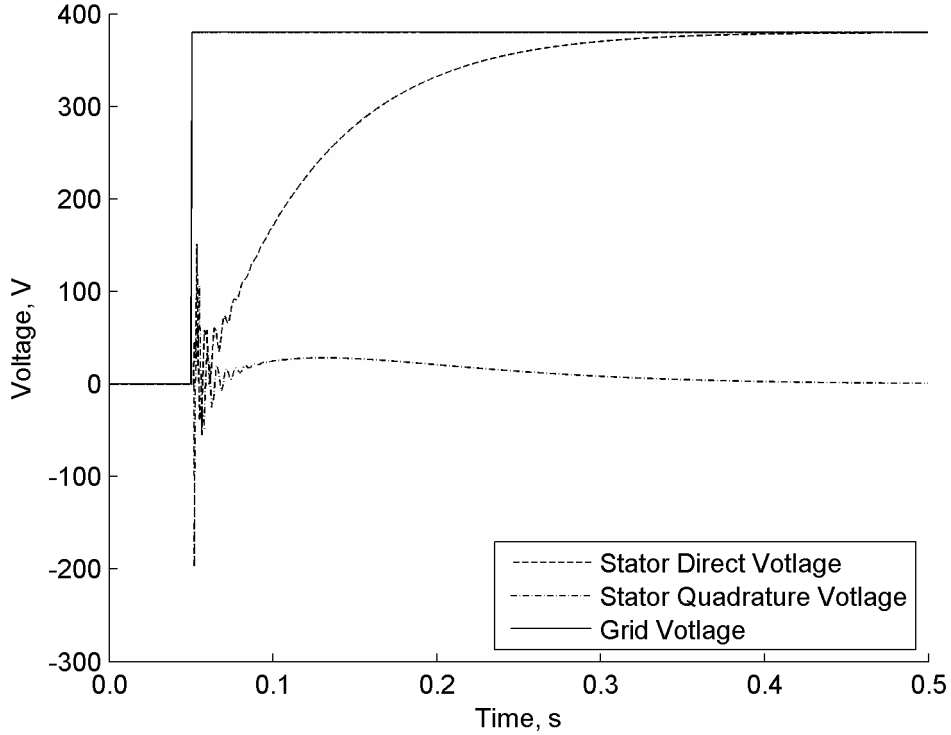

Fig. 2.12 Simulated grid, stator direct and quadrature voltages during synchronization at 1686 RPM

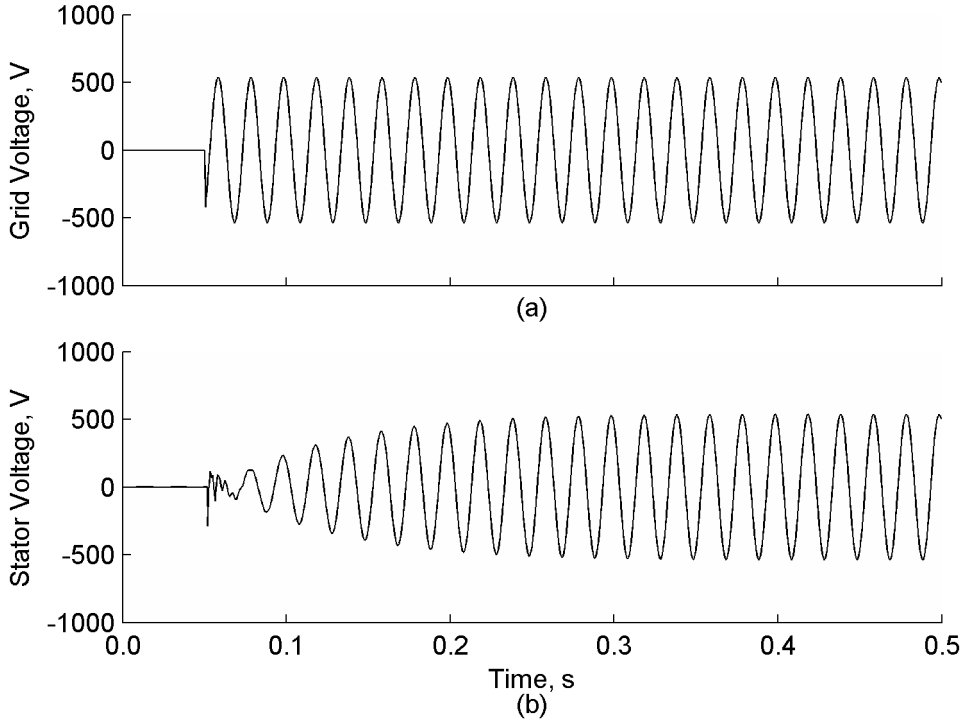

Fig. 2.13 Simulated line-to-line voltages during synchronization at 1800 RPM (a) Grid, (b) Stator

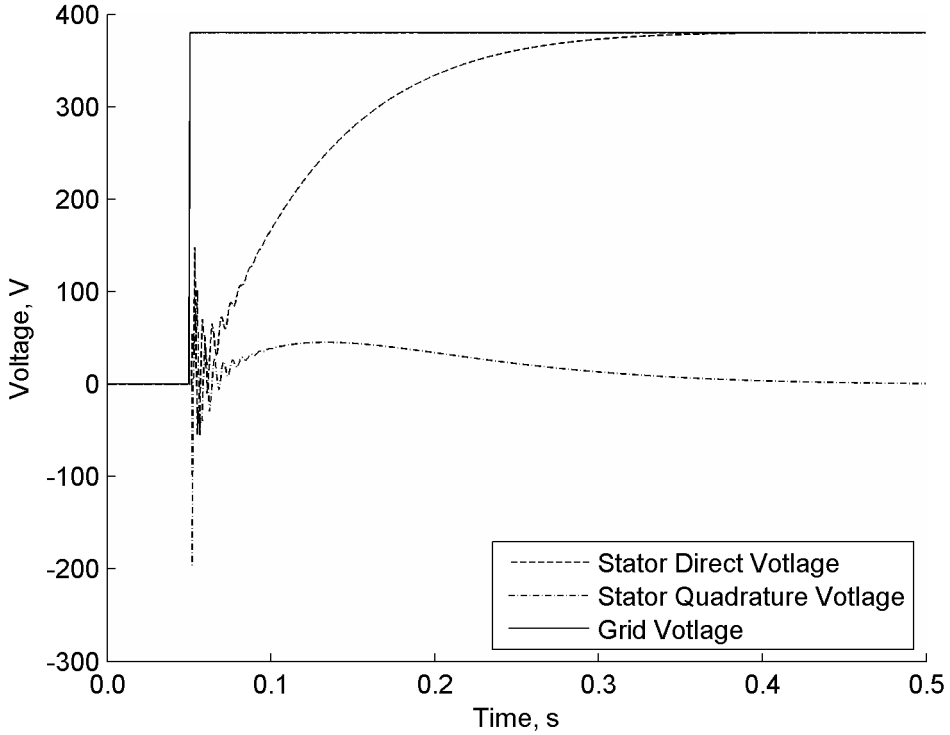

Fig. 2.14 Simulated grid, stator direct and quadrature voltages during synchronization at 1800 RPM

2.7 Practical Consideration on Stator Voltage Acquisition

As SVM is implemented in the control scheme, it operates at a constant switching frequency and hence is able to offer a controller with very little low frequency switching harmonics. However, in SVM and other pulse-width modulation methods, the output voltages of the converter require rapid switching between either the DC link voltage or zero in every switching cycle. The rotor voltage is thus comprised of a high frequency component, which is about the switching frequency, and a low frequency component near zero frequency in the synchronous reference frame. The effects of high frequency component of the rotor voltage on the stator voltage can be evaluated from the transfer equation between them. Substituting (2.24) and (2.25) into the Laplace equation of (2.10) yields

$$v_{sx}(s) = \left(sv_{rx}'(s) - \omega_s v_{ry}'(s)\right)\frac{L_m}{s(L_m + L_{r\sigma}) + R_r} \tag{2.45}$$

$$v_{sy}(s) = \left(sv_{ry}'(s) + \omega_s v_{rx}'(s)\right)\frac{L_m}{s(L_m + L_{r\sigma}) + R_r}. \tag{2.46}$$

Substitution of $j\infty$ to s gives the high frequency characteristics:

$$v_{sx}(j\infty)/v_{rx}'(j\infty) = L_m/(L_m + L_{r\sigma}) \tag{2.47}$$

$$v_{sy}(j\infty)/v_{ry}'(j\infty) = L_m/(L_m + L_{r\sigma}) \tag{2.48}$$

Since the leakage inductance is much smaller than the magnetizing inductance, (2.47) and (2.48) are near unity. Therefore, the stator voltage will contain high frequency components of the rotor voltage. The phenomenon is studied using computer simulation as shown in Fig. 2.15, where a space-vector modulated three-phase sine wave is applied to the rotor winding. The stator voltage is seen to contain both high frequency and low frequency components. The amplitude of the high frequency component is comparable to those of the low frequency components.

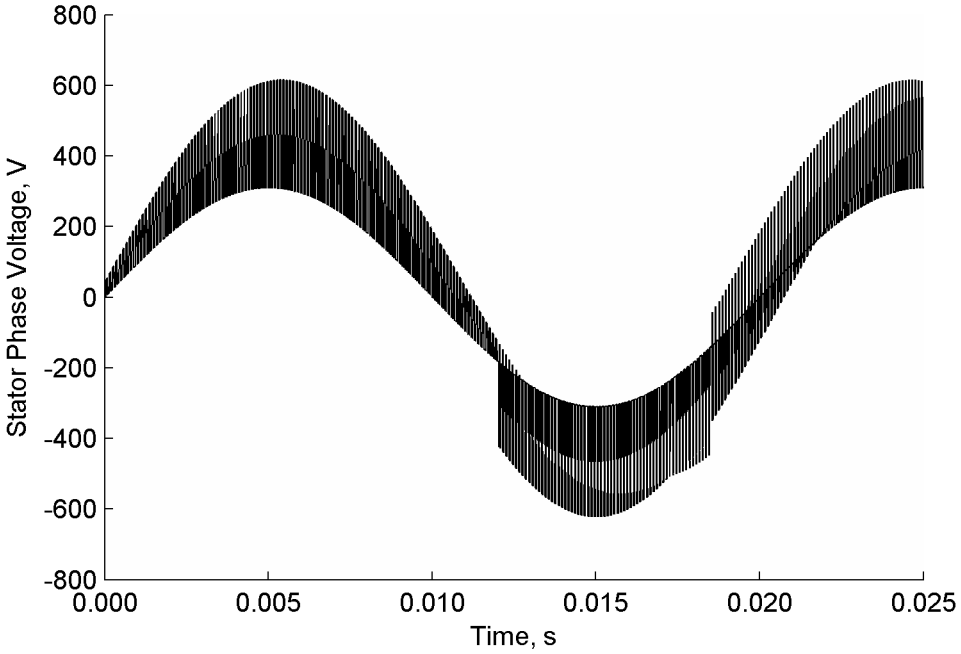

Fig. 2.15 Induced stator voltage with switching rotor voltage

Unlike the rotor currents, the harmonics in the stator voltage cannot be eliminated by employing synchronous sampling technique, which is commonly used in current sensing algorithms for motor drives, because the stator voltage is always at the extremes due to the presence of high frequency components. To eliminate these harmonics, high frequency capacitors are attached to the stator winding terminals because the capacitors and leakage inductances of DFIG behave as a low pass filter, which has a high attenuation to high frequency induced voltages, but not to the low frequency components. The capacitor must have a small contribution to reactive power, in comparison with the reactive power of the DFIG, in order to avoid excessive phase shifts in the stator voltage.

2.8 Experimental Setup

A test rig as shown in Fig. 2.16 is built to verify the proposed control scheme. The speed of the DFIG is regulated by adjusting the voltage applied to the coupled DC machine. The sensors attenuate and convert the voltages into low voltage analogue signals. The dSpace DS1104 is a prototyping card, which acquires signals from the sensors and the encoder and processes them with the proposed algorithm implemented with Matlalb/Simulink at a rate of 2 kHz, which is much higher than the closed-loop bandwidth to provide satisfactory approximation between the continuous-time and discrete-time designs. The card then generates the SVM pattern at 10 kHz for the rotor converter, which controls and switches the voltage applied to the rotor windings accordingly. The card, together with a personal computer, also forms a user interface for control and data acquisition.

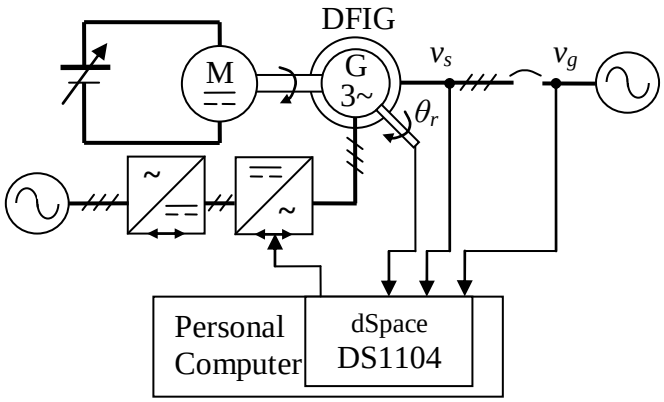

Fig. 2.16 Experimental setup

2.9 Experimental Results

The grid and stator voltages during synchronization at a rotor speed 1325 RPM are shown in Fig. 2.17 and Fig. 2.18. The stator voltage follows the grid voltage as the grid voltage is applied at 0.05 s. They are synchronized at 0.35 s with equal

amplitude, phase and frequency. Even with the presence of high frequency harmonics, the stator direct voltage follows the grid voltage and the quadrature voltage is reduced to zero after the starting transient has lapsed. Similarly, the stator voltage is synchronized to the grid voltage at the rotor speed of 1686 RPM, as shown in Fig. 2.19 and Fig. 2.20.

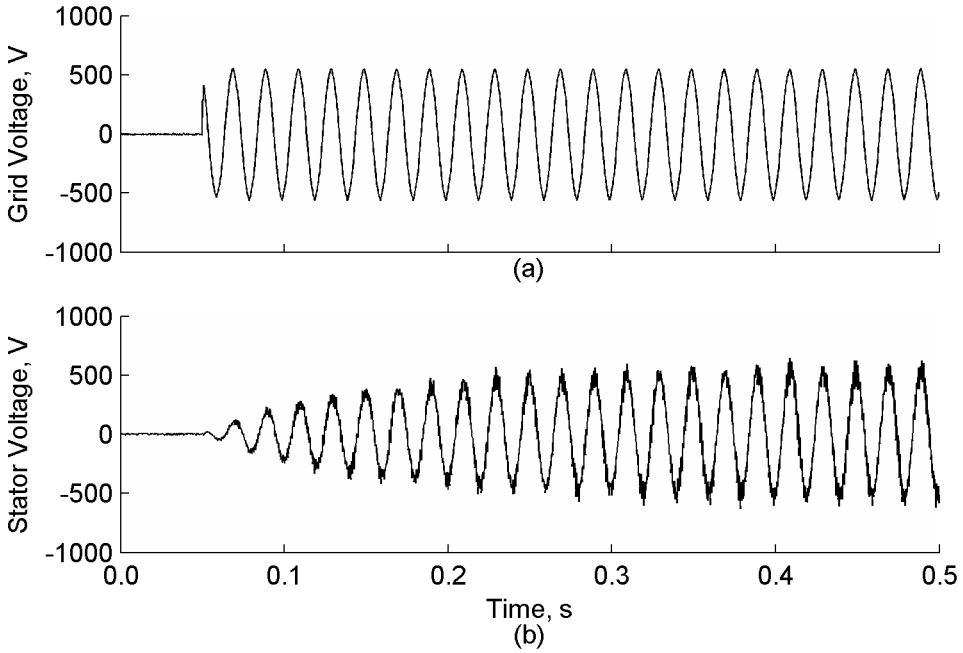

Fig. 2.17 Line-to-line voltages during synchronization at 1325 RPM

(a) Grid, (b) Stator

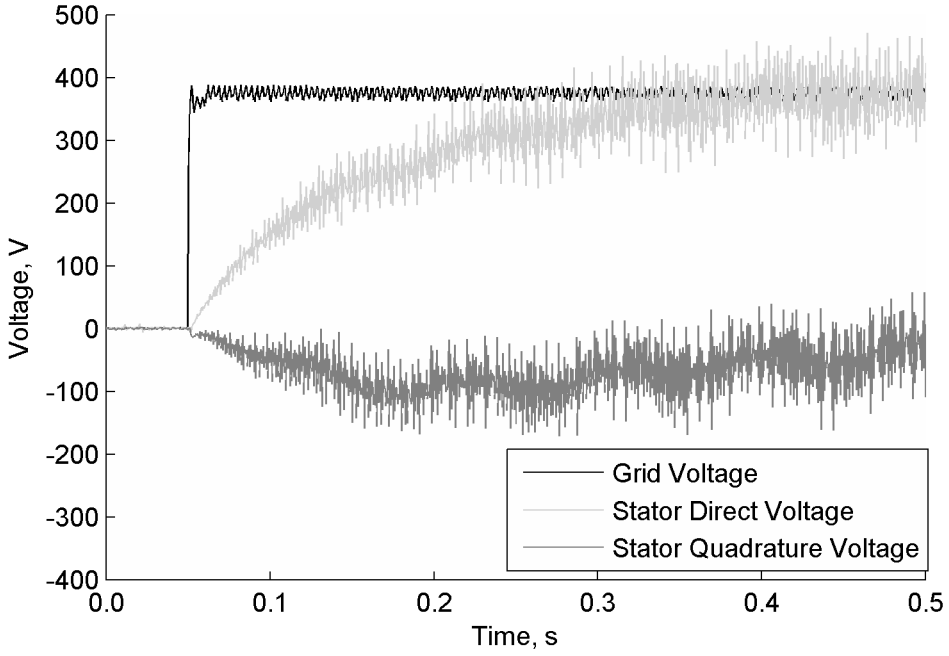

Fig. 2.18 Grid, stator direct and stator quadrature voltages during synchronization at 1325 RPM

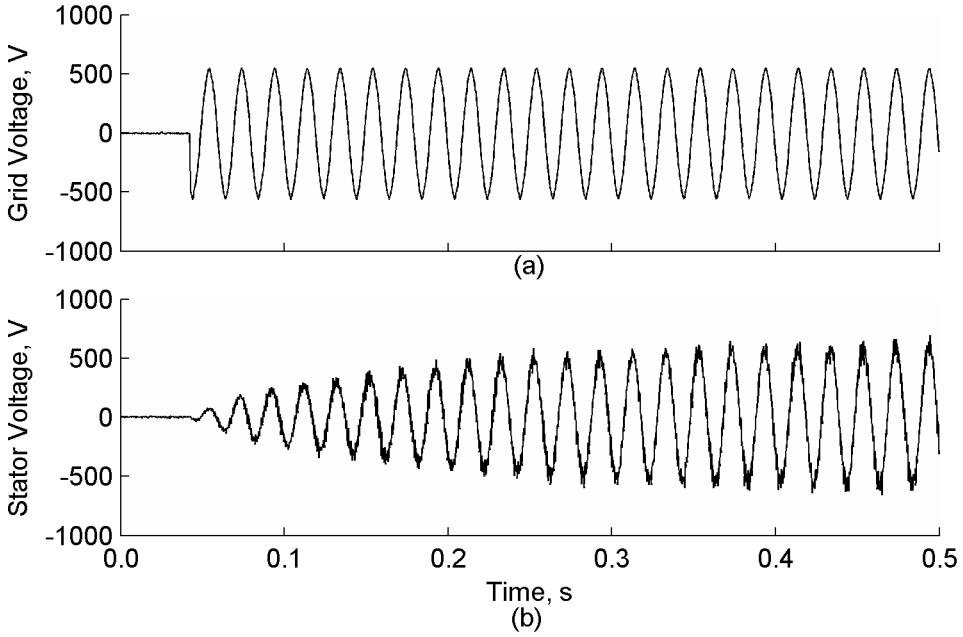

Fig. 2.19 Line-to-line voltages during synchronization at 1686 RPM

(a) Grid, (b) Stator

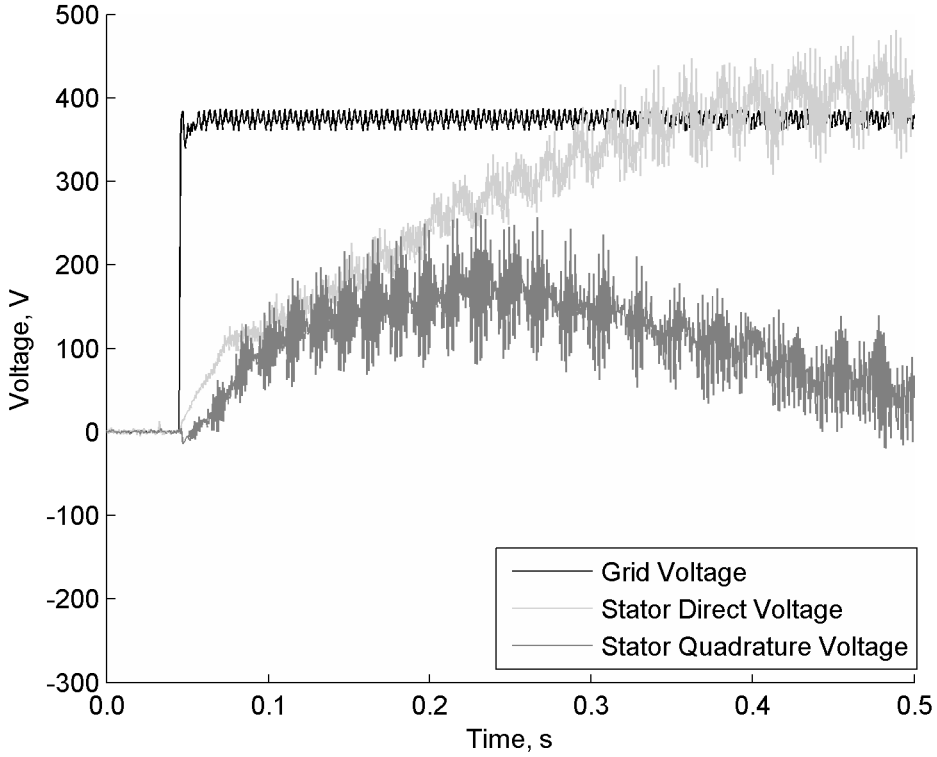

Fig. 2.20 Grid, stator direct and stator quadrature voltages during synchronization at 1686 RPM

To evaluate the harmonic contents of the stator voltage, the line-to-line stator voltage spectrum is recorded as shown in Fig. 2.21 and Fig. 2.22. The DFIG is operated at a rotor speed of 1325 RPM and the grid voltage is 380 V. The dominant peak frequency is at the grid frequency of 50 Hz, the second dominant frequency is at 1 kHz, half of the sampling frequency. The distortions are very small, and should have insignificant interferences to the generation equipments. The frequency spectrum is similar for the DFIG operating at a rotor speed of 1686 RPM.

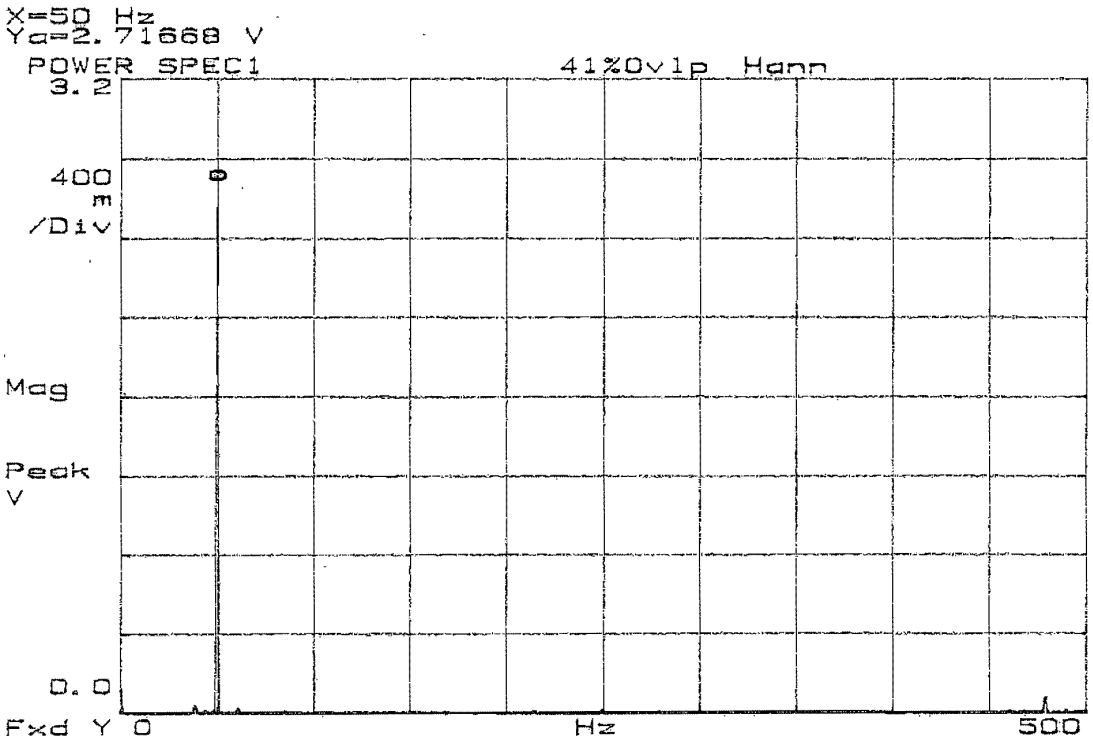

Fig. 2.21 Frequency spectrum of the stator voltage (frequency span: 500 Hz, probe gain: 200 V/V)

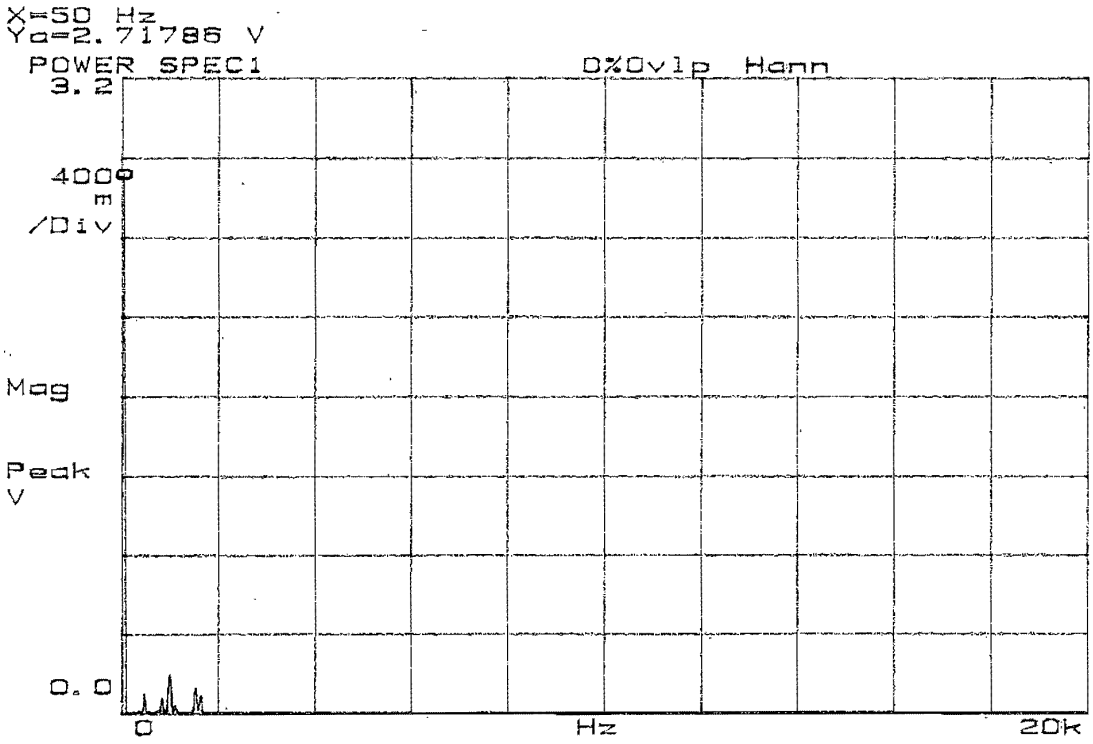

Fig. 2.22 Frequency spectrum of the stator voltage (frequency span: 20 kHz, probe gain: 200 V/V)

2.10 Summary

The chapter presents a single-loop direct voltage control scheme for the synchronization of the DFIG to the power grid. The derivation of control strategy from first principles is reported. Comparison with the cascaded scheme is given to highlight the significance of the proposed scheme that are, namely, simple control loop design, low demand on computational power, and constant switching frequency to avoid low frequency switching harmonic distortion. Consideration in respect to practical implementation is also made to address possible errors arising from switching harmonics. Simulation results are provided to validate the control algorithm and to demonstrate the good performance of the proposed algorithm under different operating speeds. Experimental results, showing good conformance with the simulation results, prove that the algorithm also performs reliably in a practical environment, even with the presence of environmental and measurement noises and disturbances. The results show that the proposed scheme is an effective algorithm to synchronize the DFIG output to the grid system rapidly over a wide speed range.

3 Direct Torque Control in Grids with Balanced Voltage

3.1 Introduction

In this chapter, DTC-SVM for DFIGs is proposed to control the operation of DFIGs for electric power generation. The scheme controls the torque and reactive power production by processing the feedback variables directly. Being a direct control scheme, the proposed scheme has a simpler structure when compared to the conventional FOC method as shown in Fig. 3.1 [33]. Furthermore, the proposed scheme does not inherit the drawbacks of other direct control schemes, such as the hysteresis switching operation of DTC shown in Fig. 3.2 [39, 40], and the feedback of part of the power generated as in DPC [46, 47].

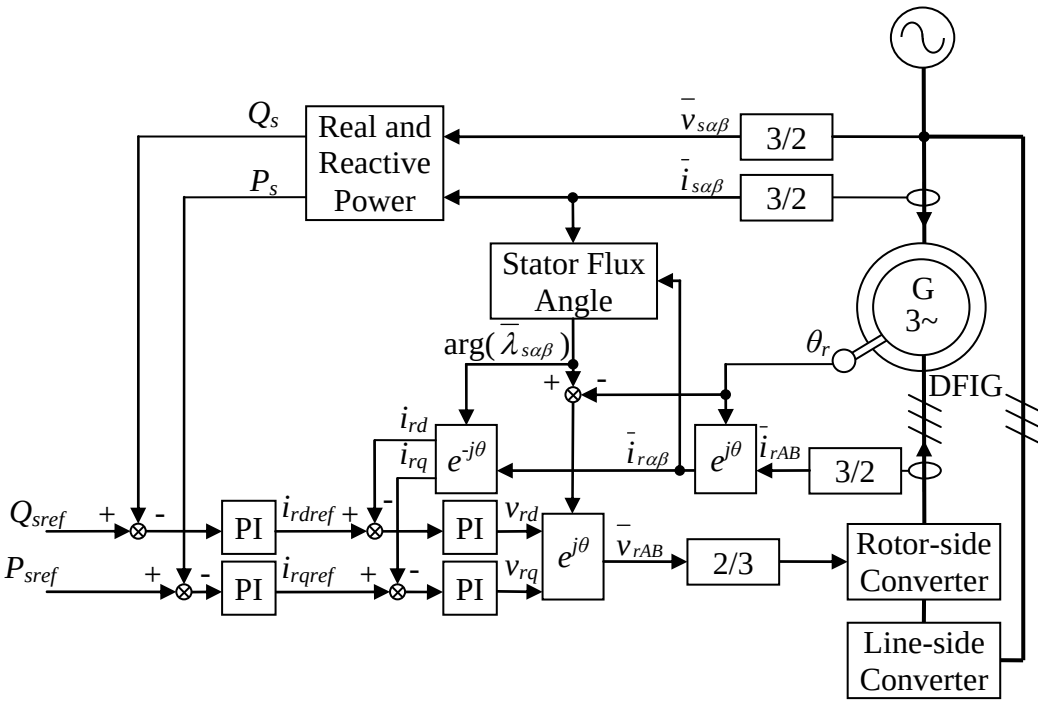

Fig. 3.1 Stator field oriented control of DFIG

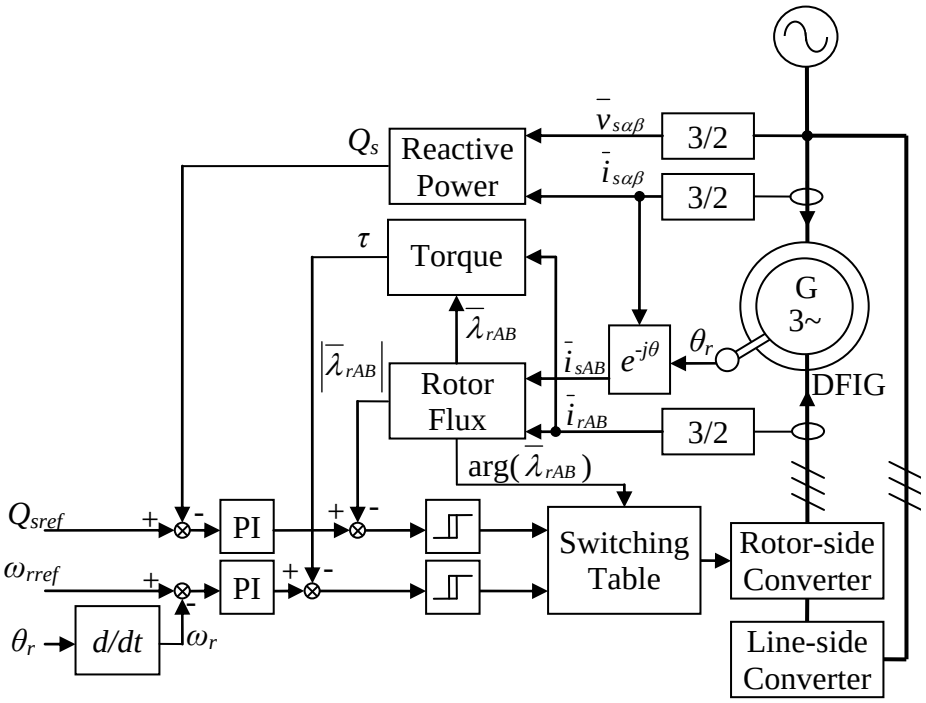

Fig. 3.2 Direct torque control of DFIG

3.2 Mathematical Model

The topology of DFIG during power generation is shown in Fig. 3.3, which is similar to Fig. 2.1 but with the stator winding of the DFIG directly connected to the grid and the stator current acquired. The currents and voltages are transformed to complex variables with (2.1) to (2.6). The stator flux can be obtained from the stator and rotor currents:

$$\bar{\lambda}_{s\alpha\beta} = (L_{s\sigma} + L_m)\bar{i}_{s\alpha\beta} + L_m \bar{i}_{rAB} \exp(jp\theta_r) \tag{3.1}$$

The rotor current is than transformed to the stator flux reference frame with Park transformation:

$$\bar{i}_{rdq} = \bar{i}_{rAB} \exp\left(-j\left(\arg\left(\bar{\lambda}_{s\alpha\beta}\right) - p\theta_r\right)\right) \tag{3.2}$$

Similarly, the stator current in the stator flux reference frame is derived with

$$\bar{i}_{sdq} = \bar{i}_{s\alpha\beta} \exp\left(- j \arg\left(\bar{\lambda}_{s\alpha\beta}\right)\right). \tag{3.3}$$

With the same transformations on the stator and rotor voltages, the following equations describe the operation of DFIG during power generation, in the stator flux reference frame.

$$\bar{v}_{sdq} = R_s \bar{i}_{sdq} + \frac{d\bar{\lambda}_{sdq}}{dt} + j\omega_s \bar{\lambda}_{sdq} \tag{3.4}$$

$$\bar{v}_{rdq} = R_r \bar{i}_{rdq} + \frac{d\bar{\lambda}_{rdq}}{dt} + j(\omega_s - p\omega_r)\bar{\lambda}_{rdq} \tag{3.5}$$

$$\bar{\lambda}_{sdq} = \left|\bar{\lambda}_{sdq}\right| = (L_{s\sigma} + L_m)\bar{i}_{sdq} + L_m \bar{i}_{rdq} \tag{3.6}$$

$$\bar{\lambda}_{rdq} = L_m \bar{i}_{sdq} + (L_{r\sigma} + L_m)\bar{i}_{rdq} \tag{3.7}$$

$$\tau = -p \frac{L_m}{L_{s\sigma} + L_m} \left|\bar{\lambda}_{sdq}\right| i_{rq} \tag{3.8}$$

$$Q_s = \frac{\omega_s \left|\bar{\lambda}_{sdq}\right|}{L_{s\sigma} + L_m} (\left|\bar{\lambda}_{sdq}\right| - L_m i_{rd}) \tag{3.9}$$

The corresponding equivalent circuit is shown in Fig. 3.4.

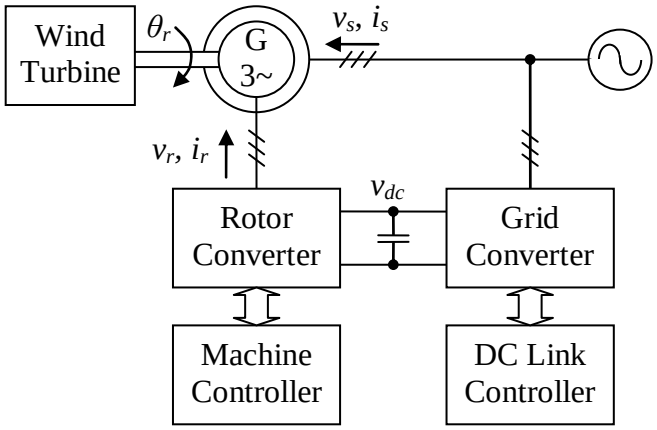

Fig. 3.3 Topology of DFIG during power generation

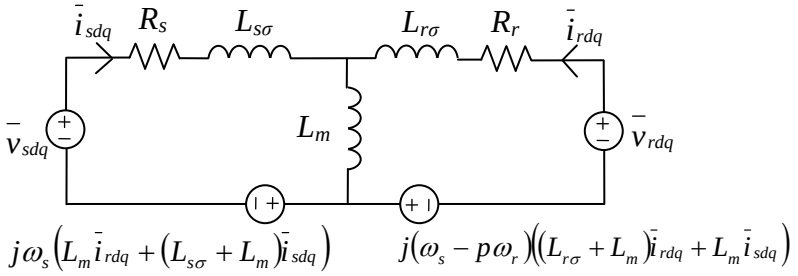

Fig. 3.4 Equivalent circuit of DFIG in the stator flux reference frame

3.3 Control of DFIG

The proposed control scheme of DFIG is shown in Fig. 3.5

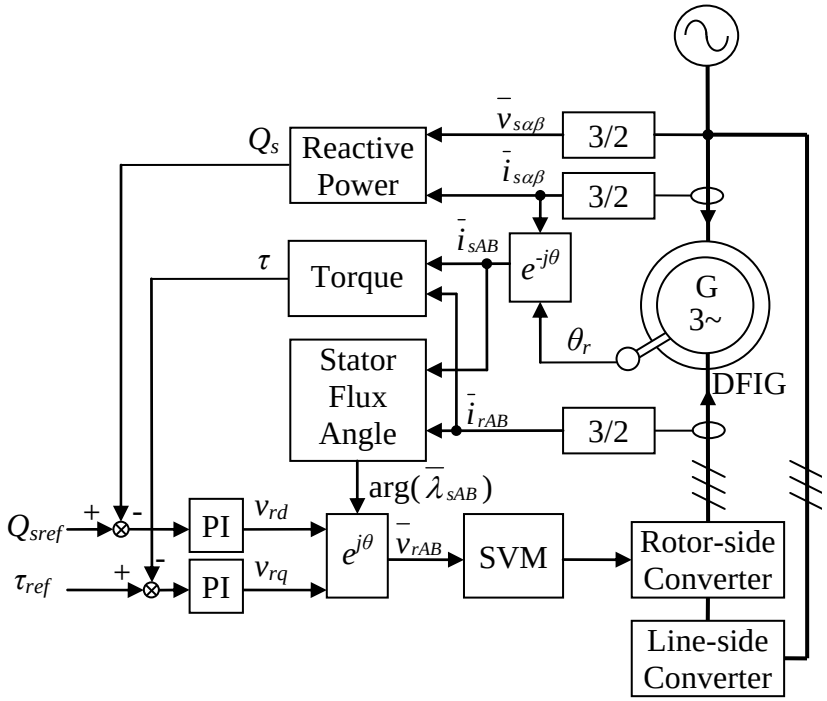

Fig. 3.5 DTC-SVM scheme of DFIG system

The scheme is a vector control scheme composing of a reactive power control loop and a torque loop. The reactive power is regulated by comparing the reference reactive power Q_{sref} with the stator reactive power to control the real part of the rotor voltage v_{rd} in the stator flux frame, which is aligned with the stator flux appropriately. Similarly, the torque is controlled by comparing the reference torque τ_{ref} with the generator torque so as to control the imaginary part of the rotor voltage v_{rq}. The rotor voltage in the rotor coordinate is derived from the corresponding voltage in the stator flux frame using inverse Park transformation. SVM is used to synthesize the output rotor voltage from the rotor converter. The reference torque is derived from the measured generator speed to provide a tracking on the maximum power and to limit the output power if the output runs into the danger of exceeding its rated power.

To allow proper design of the proportional-integral (PI) controllers, the transfer equations among the feedback variables, the torque and the reactive power, as well as the output variables, the rotor voltages, have to be established.

3.3.1 Torque Control

(3.8) shows that the torque is a scaled product of the stator flux and the imaginary part of the rotor current. In the stator reference frame, the stator flux can be represented as

$$\bar{\lambda}_{s\alpha\beta} = \int (\bar{v}_{s\alpha\beta} - R_s \bar{i}_{s\alpha\beta}) dt \,. \tag{3.10}$$

With the generator data as given in the Appendices, it is found that the product of the stator resistance and current is about 4% of the stator voltage at rated condition. Therefore, as indicated in (3.10), the stator flux is largely dominated by the stator voltage and will be assumed constant in the following analysis. Moreover, as the stator winding is directly connected to the grid, the stator voltage and hence the stator flux cannot be controlled by the rotor converter. In other words, the torque can only be controlled with the imaginary part of the rotor current.

In the stator flux reference frame, expressing the rotor flux with the stator flux by substituting (3.6) into (3.7), one obtains:

$$\bar{\lambda}_{rdq} = \bar{\lambda}_{sdq} - L_{s\sigma} \bar{i}_{sdq} + L_{r\sigma} \bar{i}_{rdq} \tag{3.11}$$

Substituting (3.11) into (3.5) gives

$$\bar{v}_{rdq} = R_r \bar{i}_{rdq} + \frac{d(\bar{\lambda}_{sdq} - L_{s\sigma}\bar{i}_{sdq} + L_{r\sigma}\bar{i}_{rdq})}{dt} + j(\omega_s - p\omega_r)(\bar{\lambda}_{sdq} - L_{s\sigma}\bar{i}_{sdq} + L_{r\sigma}\bar{i}_{rdq}) \tag{3.12}$$

The last term is considered as a feed forward term, in which the difference in speeds is limited to 20% of the synchronous speed of the machine. The feed forward term can be interpreted as a negligibly small disturbance which can be compensated by the controller, because of the small speed difference [67]. As for the second term, the stator flux is constant and hence the derivative of the stator flux would be zero. Consequently, (3.12) becomes

$$\bar{v}_{rdq} = R_r \bar{i}_{rdq} + \frac{d(-L_{s\sigma}\bar{i}_{sdq} + L_{r\sigma}\bar{i}_{rdq})}{dt}. \tag{3.13}$$

Differentiating (3.6) with respect to time and rearranging the terms yields

$$\frac{d\bar{i}_{sdq}}{dt} = -\frac{L_m}{(L_{s\sigma} + L_m)}\frac{d\bar{i}_{rdq}}{dt}. \tag{3.14}$$

Substitution of (3.14) into (3.13) gives

$$\bar{v}_{rdq} = R_r \bar{i}_{rdq} + \frac{d}{dt}\left(\left(\frac{L_{s\sigma}L_m}{L_{s\sigma} + L_m} + L_{r\sigma}\right)\bar{i}_{rdq}\right). \tag{3.15}$$

Let $L_{rk} = L_{s\sigma}L_m/(L_{s\sigma}+L_m)+L_{r\sigma}$, the transfer equations relating the real and imaginary rotor currents and the rotor voltages become

$$i_{rd}(s) = \frac{1}{R_r + sL_{rk}} v_{rd}(s) \tag{3.16}$$

and

$$i_{rq}(s) = \frac{1}{R_r + sL_{rk}} v_{rq}(s) . \tag{3.17}$$

(3.16) and (3.17) indicate that the real and imaginary rotor voltages are controlling the real and imaginary rotor currents independently. However, if the rotor current is selected alongside with the stator flux to form the control loops as in FOC, a relatively complex coordinate transformation on the rotor current must be performed. To avoid the need for such transformation, it is proposed that the torque is to be used to form the control loop. Substituting (3.17) into the Laplace form of (3.8), the torque can be expressed as

$$\tau(s) = -\frac{pL_m \left|\overline{\lambda}_{sdq}\right|}{(L_{s\sigma} + L_m)(R_r + sL_{rk})} v_{rq}(s) . \tag{3.18}$$

As the dynamics between the imaginary part of the rotor voltage and the torque is established with (3.18), the proportional-integral controller can be designed. The controller is described with the following equation

$$v_{rq} = K_p \left((\tau_{ref} - \tau) + \frac{1}{T_i} \int (\tau_{ref} - \tau) dt \right) + v_{rq}(0) , \tag{3.19}$$

where $v_{rq}(0)$ is the initial value of the output voltage which is zero as the transfer equation between the torque and the imaginary rotor voltage has no offset. To obtain a first order closed-loop response with a time constant T_{cl}, the parameters of the controller are assigned as

$$K_p = \left(L_{s\sigma} + L_{r\sigma}(\frac{L_{s\sigma}}{L_m} + 1) \right) \frac{-1}{\left|\bar{\lambda}_{sdq}\right| p T_{cl}} \tag{3.20}$$

$$T_i = \left(\frac{L_{s\sigma} L_m}{L_{s\sigma} + L_m} + L_{r\sigma} \right) \frac{1}{R_r}. \tag{3.21}$$

The instantaneous torque is calculated, without Park transformation to the stator flux frame, as the scaled cross product of the stator and rotor currents:

$$\tau = pL_m \left(i_{sB} i_{rA} - i_{sA} i_{rB} \right) \tag{3.22}$$

3.3.2 Reactive Power Control

Substitution of (3.16) to the Laplace form of (3.9) gives

$$Q_s(s) = \frac{\omega_s \left|\bar{\lambda}_{sdq}\right|}{L_{s\sigma} + L_m} \left(\left|\bar{\lambda}_{sdq}\right| - \frac{L_m}{R_r + sL_{rk}} v_{rd}(s) \right). \tag{3.23}$$

Equation (3.23) indicates that the stator reactive power is composed of a constant part and a variable part. Since the integral action of the proportional-integral controller compensates for the constant part of the reactive power, the dynamics between the reactive power and the rotor voltage would rely on the coefficient of the imaginary rotor voltage only. Hence, the parameters of the proportional-integral controller can be derived. The implementation of the controller is similar to (3.19), with the following parameters:

$$K_p = \left(L_{s\sigma} + L_{r\sigma}(\frac{L_{s\sigma}}{L_m} + 1) \right) \frac{-1}{\left|\bar{\lambda}_{sdq}\right| \omega_s T_{cl}} \tag{3.24}$$

$$T_i = \left(\frac{L_{s\sigma} L_m}{L_{s\sigma} + L_m} + L_{r\sigma} \right) \frac{1}{R_r} \tag{3.25}$$

The imaginary rotor voltage in (3.19) is replaced by the real rotor voltage, while the torque is replaced by the reactive power.

To have a smooth transition from synchronization to power generation, the initial real rotor voltage $v_{rd}(0)$ must be assigned first. Since the reactive power during the transition must be zero, the initial real rotor voltage is deduced by calculating the real rotor voltage corresponding to zero reactive power at steady state. Substituting $s = 0$ and $Q_s(0) = 0$ VAR into (3.23), one has

$$v_{rd}(0) = \frac{R_r}{L_m}\left|\bar{\lambda}_{sdq}\right|. \tag{3.26}$$

As similar to torque computation, the instantaneous reactive power can be efficiently computed from

$$Q_s = v_{s\beta} i_{s\alpha} - v_{s\alpha} i_{s\beta} \tag{3.27}$$

3.4 Simulation Results

The proposed control scheme of DFIG with the parameters given in the Appendices is simulated in Matlab/Simulink for different operating conditions. The total inertia of the turbine and generator is 0.292 kgm^2. The closed-loop time constants of both the reactive power loop and the torque loop are 5 ms. The wind speed is 8 m/s. The turbine characteristics are given in Fig. 1.2. In this simulation, the torque command is manually input instead of being derived from the generator speed so as to test the performance of the torque control.

The responses to a torque step from 0 Nm to -10 Nm at the simulation time of 0.1 s are shown in Fig. 3.6. It is observed that a step change in the reference torque is tracked by the generator quickly. The torque and reactive power are settled within 0.05 s. Oscillations in the reactive power, when the step change in torque is applied, come from the cross coupling of the feed forward term in (3.12) and changes in stator flux. It can be seen that oscillations in the reactive power are compensated by the controller and it settles to a steady value as the torque stops changing. Even though the generator decelerates from super-synchronous speed to sub-synchronous speed, as the magnitude of the generator torque is larger than that of the turbine after the torque step is applied, the generator torque and reactive power remain roughly the same at the reference levels. The DFIG generates power continuously subsequent to the application of the step change in torque.

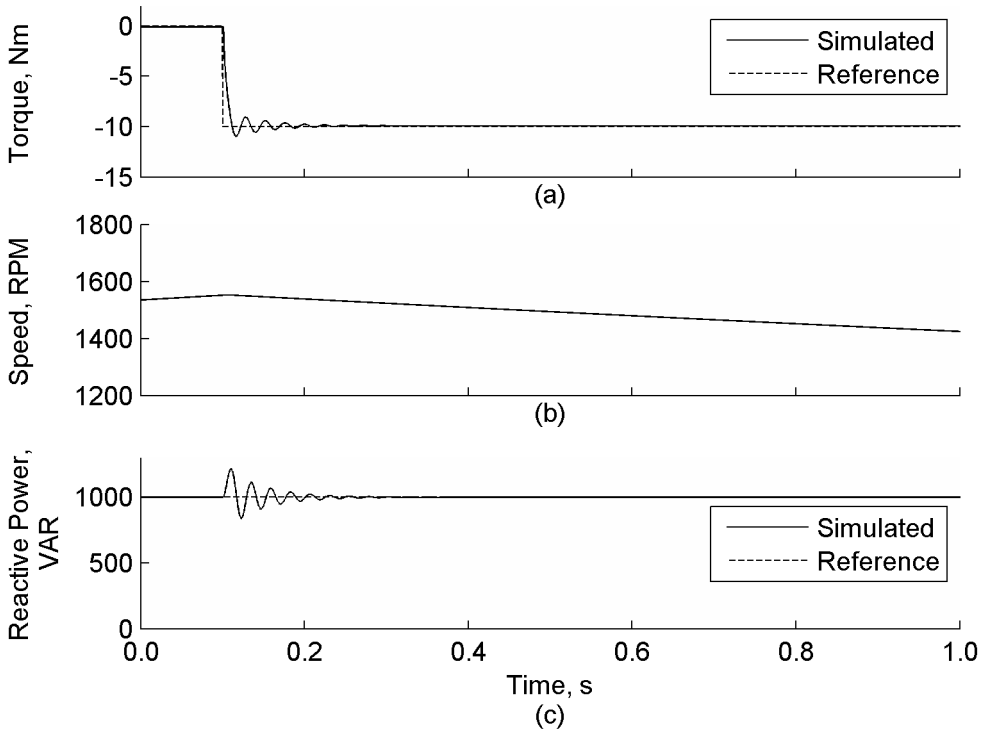

Fig. 3.6 Simulated responses to a step change in the torque reference value

(a) Torque, (b) Speed, (c) Stator reactive power

The speed and torque responses to a step change in the reactive power reference, from 500 VAR to 1000 VAR at a generator speed of 1600 RPM, are shown in Fig. 3.7. The reactive power follows the change in the reference and reaches a steady state within about 0.05 s. The torque oscillations introduced by the step change in reactive power are dampened by the controller. The simulation results are very similar for other speeds within +/- 20 % of the synchronous speed.

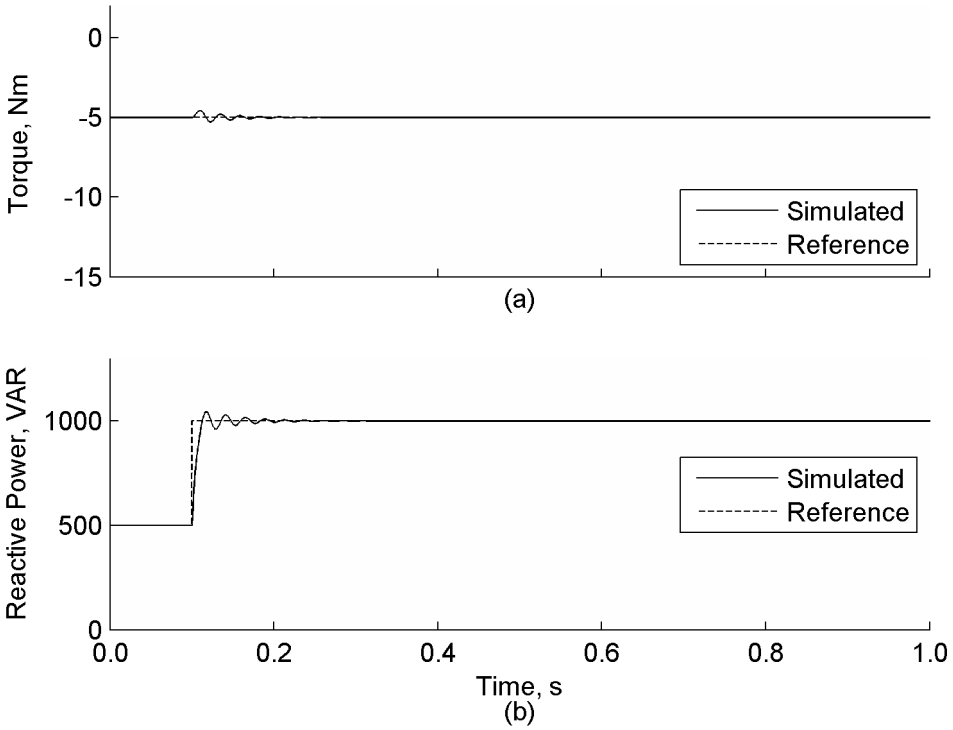

Fig. 3.7 Simulated responses to a step change in the reactive power reference

(a) Torque, (b) Stator reactive power

As the thermal insulation class of the DFIG is class B, the operating temperature of the DFIG is 130 °C [68]. Since the temperature coefficient of copper is 0.39 $\%K^{-1}$ at 20 °C, the winding resistance may vary by 42.9 % over the operating temperature. To investigate the effects of possible model mismatches, which may arise from the variations in the operating temperature, on the system performance,

the parameters of the controller such as the rotor resistance, leakage and magnetizing inductances are varied. Step changes in the reactive power demand with different controller parameters are simulated with the responses plotted in Fig. 3.8, the DFIG is operated at -5 Nm, 1600 RPM throughout the simulation. Although the step responses vary as the parameters change, they converge to the reference value after the transients. Therefore, the algorithm is robust against parameter variations.

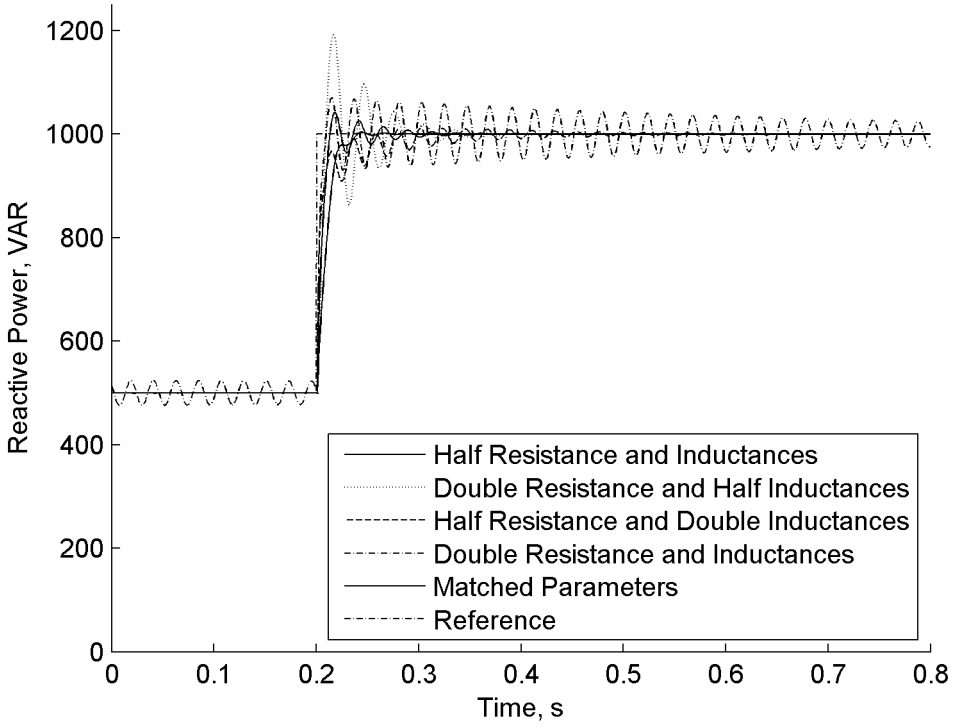

Fig. 3.8 Simulated responses to changes in the reactive power reference with different parameters

3.5 Experimental Results

The experimental setup is shown in Fig. 3.9, which is similar to Fig. 2.16. However, in the setup shown in Fig. 3.9, the stator winding of the DFIG is connected to the grid directly and the stator current is sampled, together with the signals from the rotor current, stator voltage and the encoder, to control the operation of the

DFIG. The closed-loop time constant is 5 ms, which is much higher than the sampling period to give a close approximation between the continuous-time and discrete-time designs.

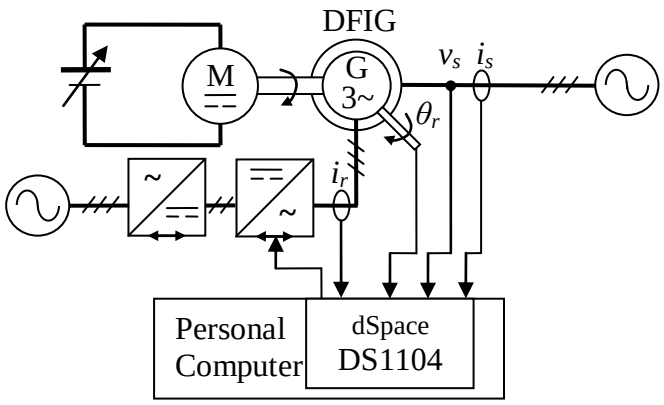

Fig. 3.9 Experimental setup

The measured torque and the stator reactive power, in response to a step change in the reference torque, at the time 0.1 s, are shown in Fig. 3.10. The simulated responses with the experimental parameters and DC motor characteristics are also plotted for comparison. The corresponding rotor and stator currents are also shown in Fig. 3.11. The torque reaches the new reference of -10 Nm within 0.05 s. The cross coupling between the torque and the reactive power is quickly compensated. Even the generator slows down from 1680 RPM to 1420 RPM in 0.4 s after the step is applied, the reactive power and the torque are observed to be following the reference values, and the generator delivers energy continuously. The experimental responses are similar to the simulated responses, showing that the experimental results and the theoretical derivations are coherent. One may notice that the deceleration of the generator in the experiment is much faster than that in the simulation shown in Fig. 3.6 because the combined inertia of the generator and DC motor used in the experiment is lower than that of the turbine and the generator in

the simulation. It also confirms that the turbine characteristic does not affect the control of the reactive power and torque of the DFIG.

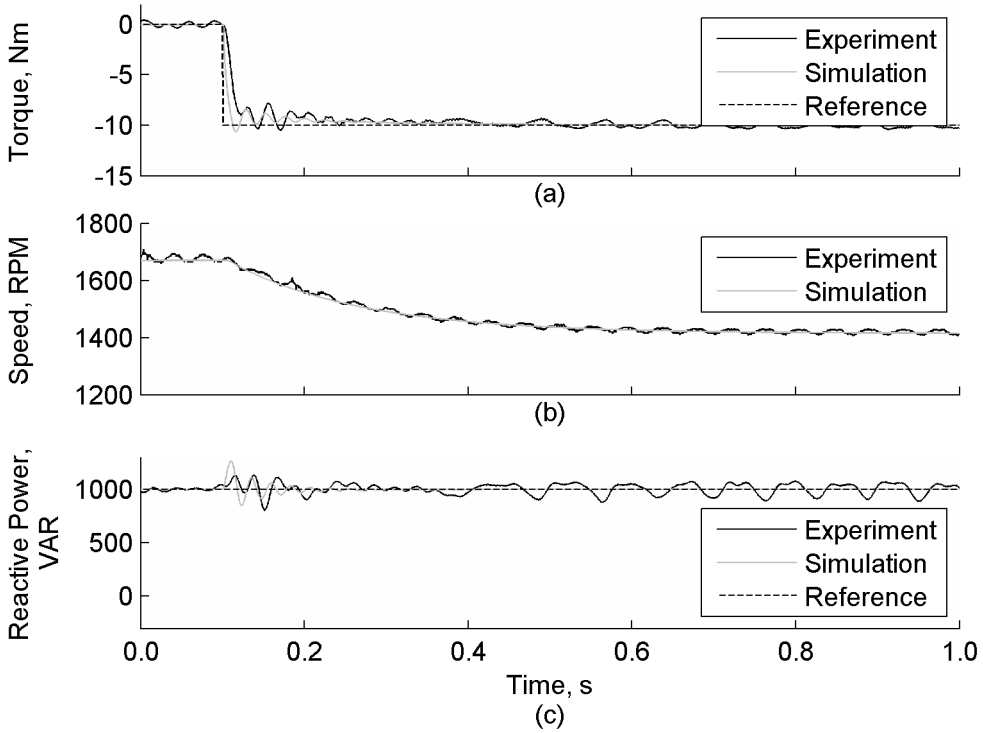

Fig. 3.10 Responses to a step change in the torque reference

(a) Torque, (b) Speed, (c) Stator reactive power

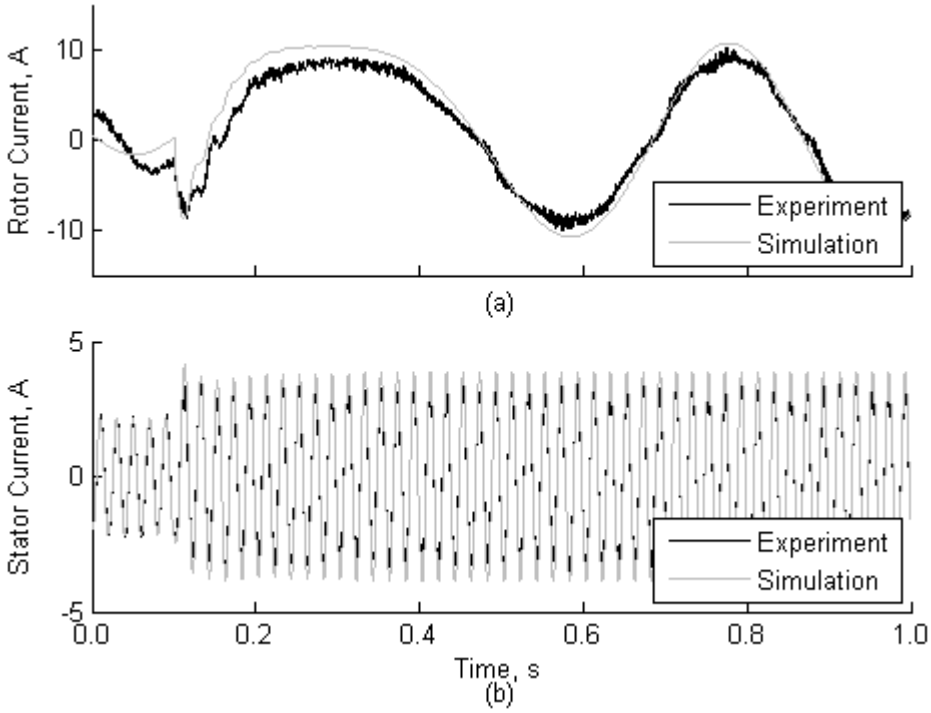

Fig. 3.11 Responses to a step change in the torque reference

(a) Rotor current, (b) Stator current

In Fig. 3.12 and Fig. 3.13, a step change in the reference reactive power is introduced with a generator speed of 1600 RPM. The reactive power follows the step and reaches a plateau in 0.05 s. The torque remains unchanged throughout the period. The experimental results are also in agreement with the simulation results.

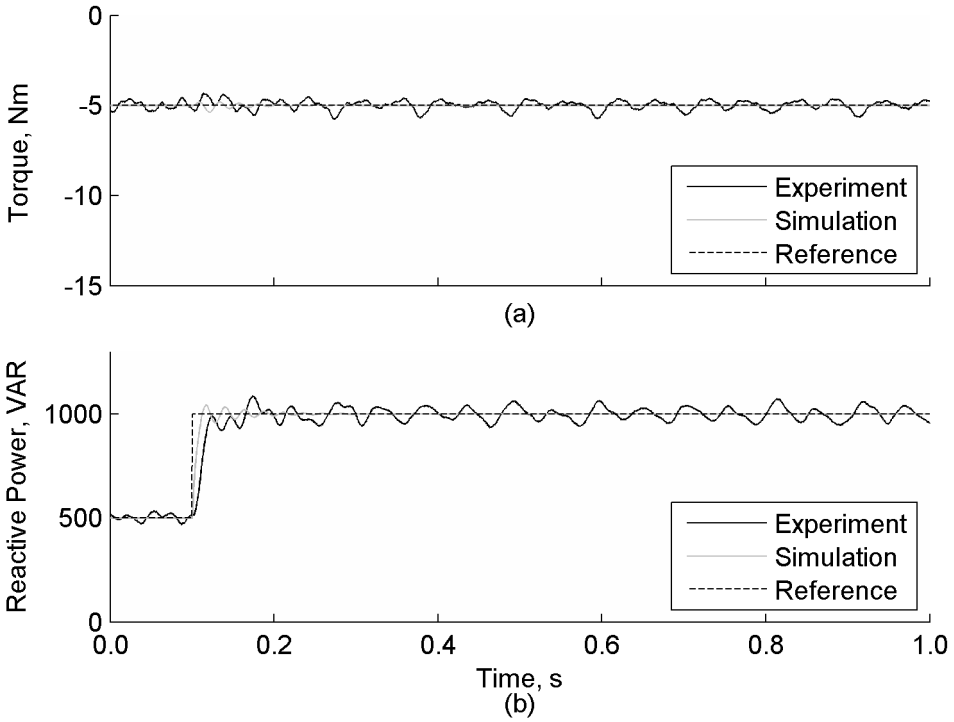

Fig. 3.12 Responses to a step change in the reactive power reference

(a) Torque, (b) Stator reactive power

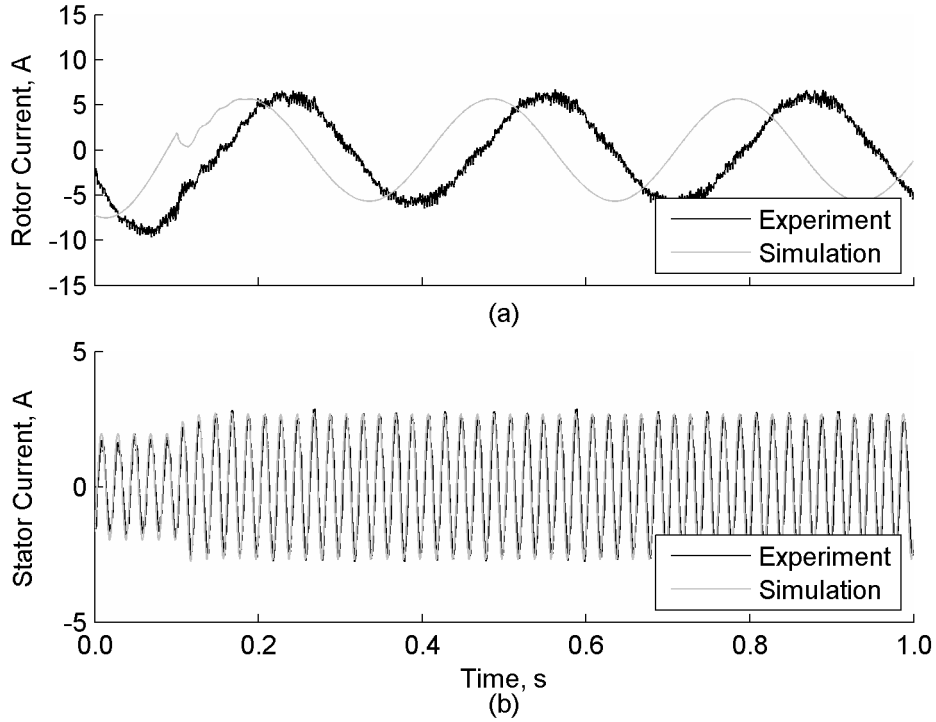

Fig. 3.13 Responses to a step change in the reactive power reference

(a) Rotor current, (b) Stator current

The frequency spectrum of the rotor line-to-line voltage of the DFIG operating with a torque of -10 Nm and a reactive power of 1000 VAR at 1438 RPM are shown in Fig. 3.14 and Fig. 3.15. The dominant frequencies of the rotor voltage are 2.5 Hz and 10 kHz, which are the slip frequency and the switching frequency respectively. The constant frequency employed in the proposed DTC-SVM scheme does not introduce low frequency sub-harmonics, which are common in conventional DTC schemes. The corresponding spectrum of the rotor current is shown in Fig. 3.16 and Fig. 3.17. The rotor current has a single dominant frequency at the slip frequency. No component at the switching frequency is observed. Similarly, the stator current has a dominant frequency at the grid frequency of 50 Hz, as shown in Fig. 3.18 and Fig. 3.19.

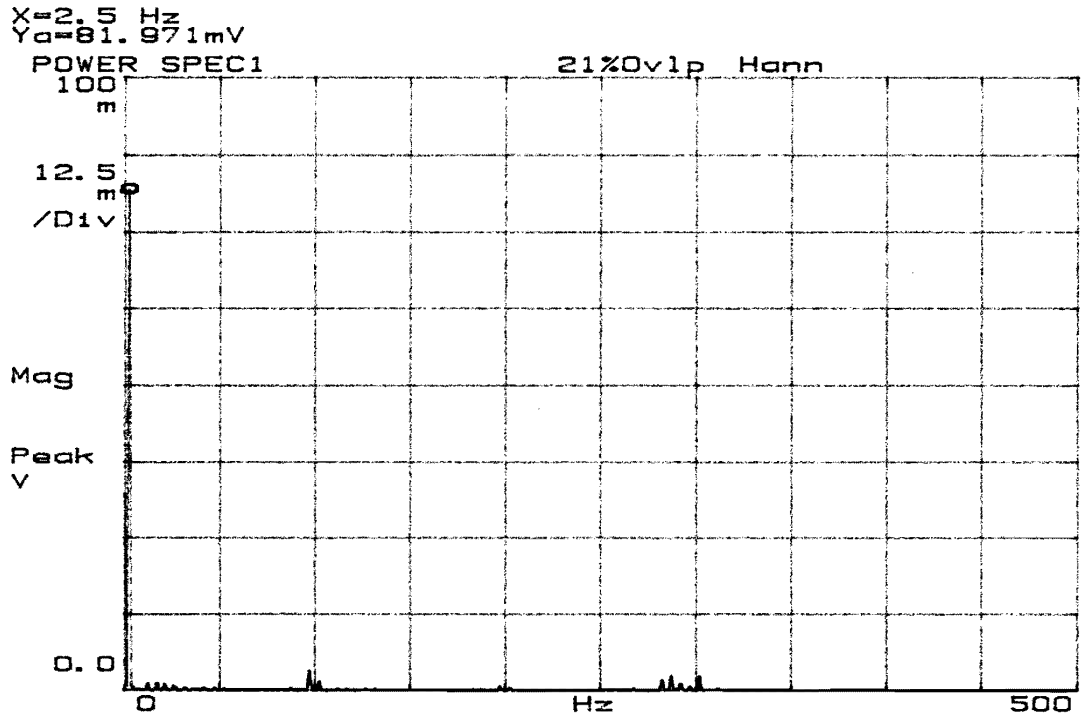

Fig. 3.14 Frequency spectrum of the rotor line-voltage

(frequency span: 500 Hz, probe gain: 200 V/V)

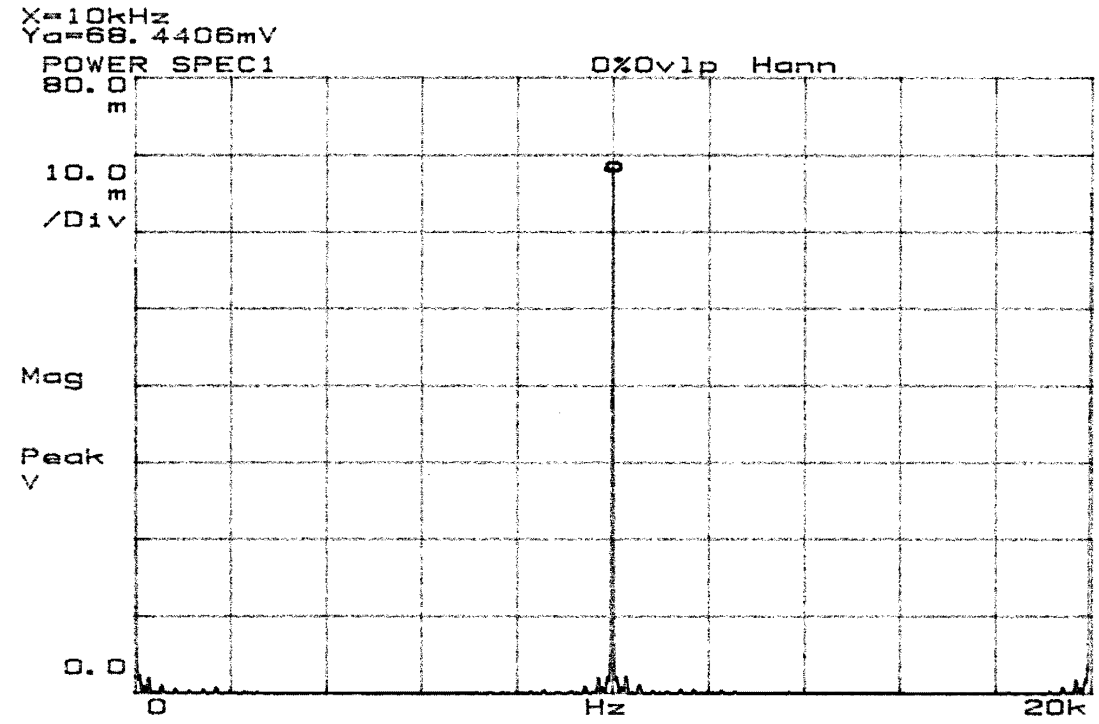

Fig. 3.15 Frequency spectrum of the rotor line-voltage

(frequency span: 20 kHz, probe gain: 200 V/V)

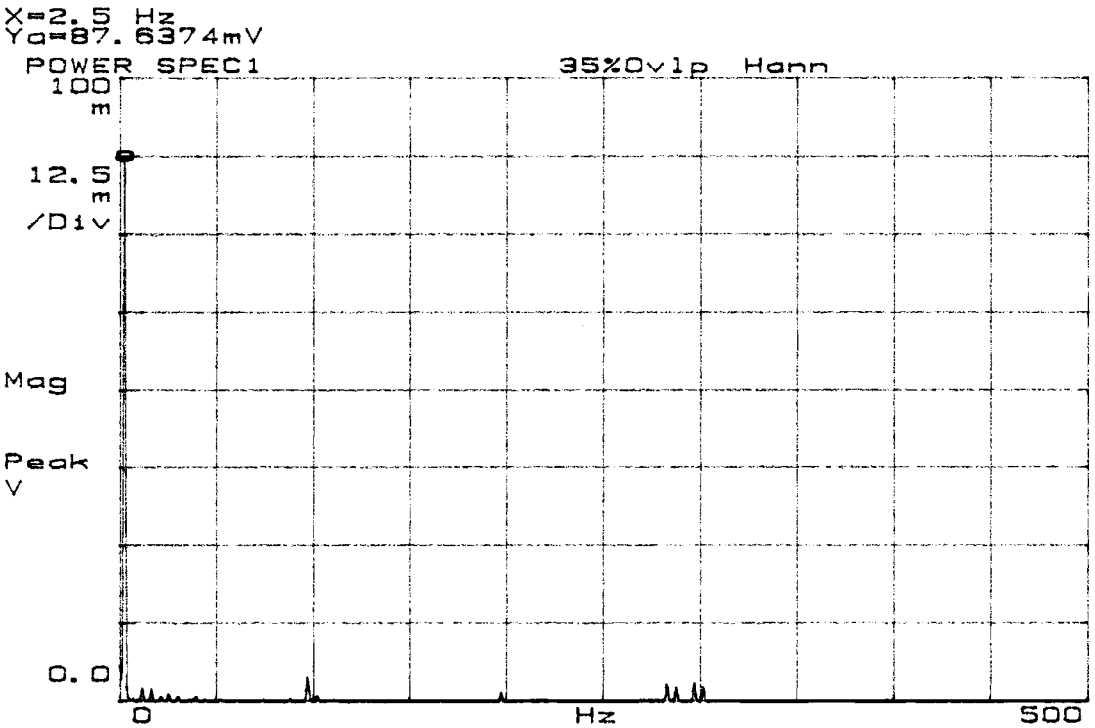

Fig. 3.16 Frequency spectrum of the rotor current

(frequency span: 500 Hz, probe gain: 100 A/V)

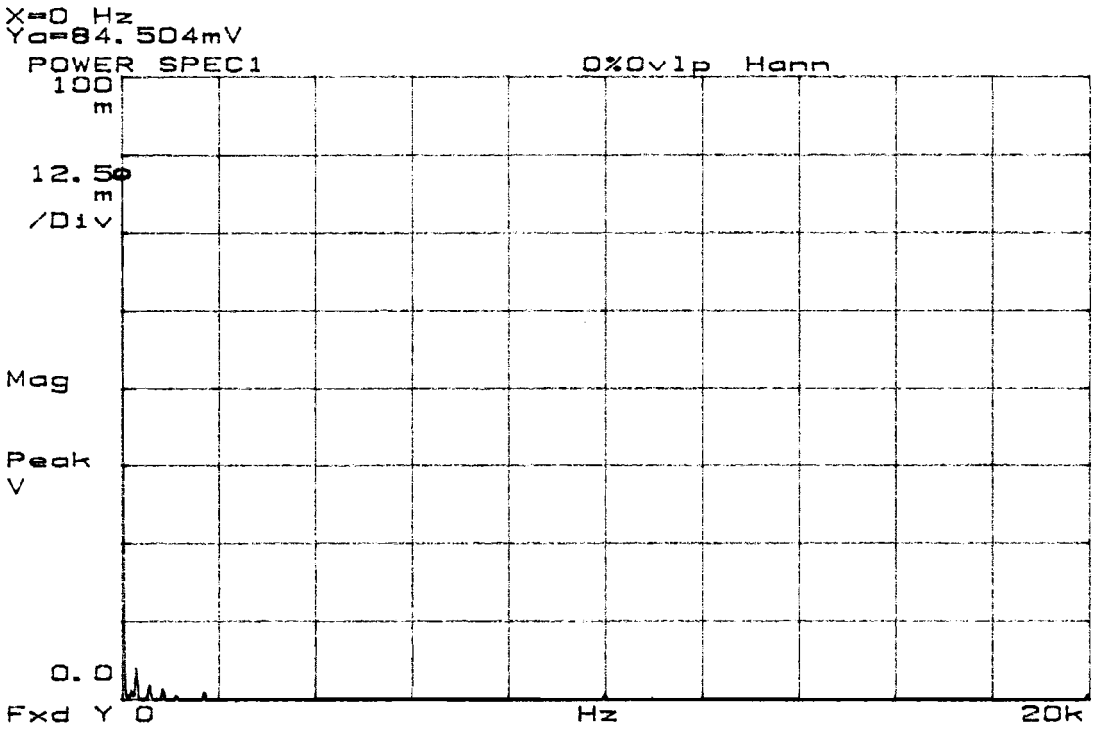

Fig. 3.17 Frequency spectrum of the rotor current

(frequency span: 20 kHz, probe gain: 100 A/V)

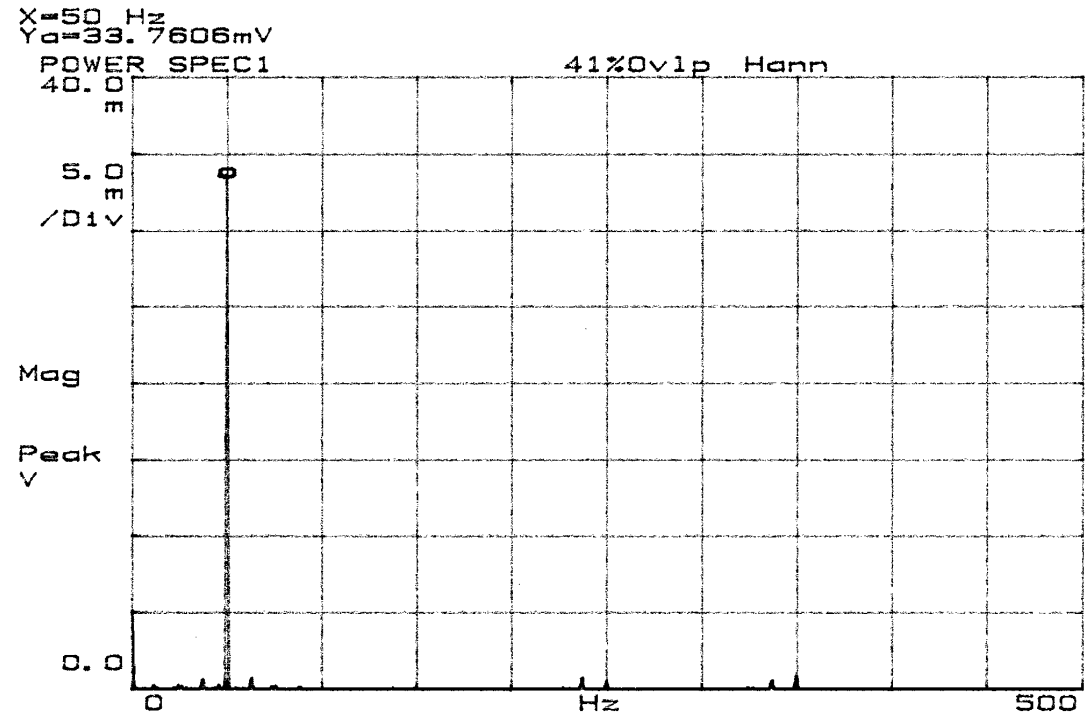

Fig. 3.18 Frequency spectrum of the stator current

(frequency span: 500 Hz, probe gain: 100 A/V)

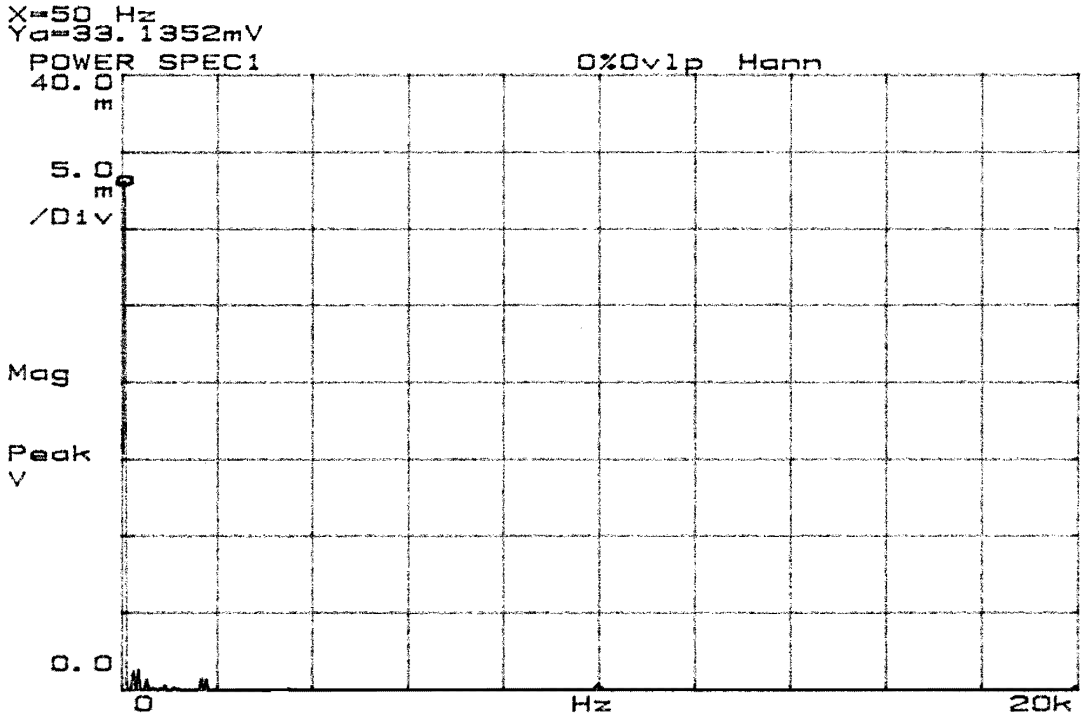

Fig. 3.19 Frequency spectrum of the stator current

(frequency span: 20 kHz, probe gain: 100 A/V)

3.6 Summary

A DTC-SVM control scheme for DFIG has been proposed. The scheme has a simple structure because of the elimination of the decoupled current control loops and the doing away of the coordinate transformation. Fast response time is obtained from the simple structure and direct feedback of the control variables with the proposed algorithm. In contrast with DTC scheme, the proposed DTC-SVM employs a constant switching frequency, and hence the generated harmonics and the switching loss are easily predictable. As DTC-SVM also allows independent control of its torque and reactive power throughout the operating speed range, stall control and optimal power control of the wind turbine can be realized readily. Simulation and experimental results show that DTC-SVM is reliable and practical for industrial applications.

4 Direct Torque Control in Grids with Balanced Voltage and High Source Impedances

4.1 Introduction

In this chapter, DTC-SVM for DFIGs in grids with considerable source impedances is investigated. The effects of source impedance on the control and operation of DFIGs are minimized with the proposed algorithm so as to increase the robustness of the system. Derivations of the controller structure and the parameters with internal model control (IMC) design method are discussed. The robustness of the system against parameter variations and comparison with existing algorithm are reported to highlight the significance of the proposed algorithm.

4.2 Mathematical Model

The structure of the DFIG system is similar to that in Fig. 3.3, but with the presence of the source impedance contributed by the power transmission components such as transmission lines and transformers, as shown in Fig. 4.1.

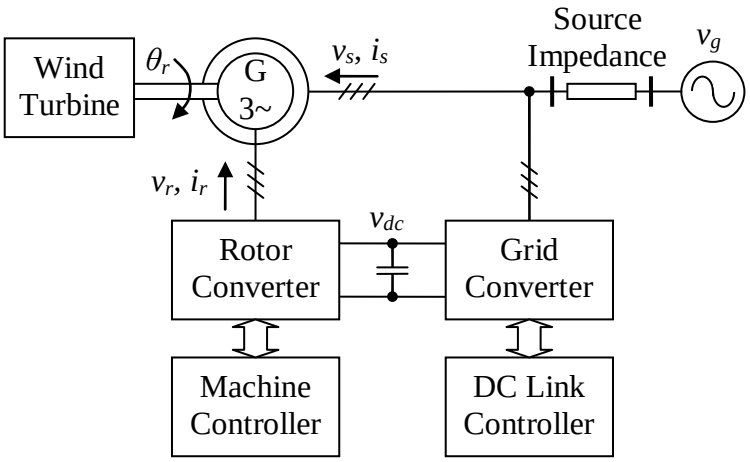

Fig. 4.1 Topology of DFIG during power generation with source impedance

(3.4)–(3.9) are also valid for DFIG with source impedance. To approximate the stator voltage variation, the following equation is included in the mathematical model [69]:

$$\left|\bar{v}_{g\alpha\beta}\right| - \left|\bar{v}_{s\alpha\beta}\right| = \frac{R_g P_s + \omega_s L_g Q_s}{\left|\bar{v}_{g\alpha\beta}\right|} \tag{4.1}$$

The effect of the rotor real power is excluded from (4.1) because the rotor power is only a fraction of the stator output power [6], and the effect of the real power on the voltage difference is much smaller than that due to the reactive power.

4.3 Control Strategy

The overall control structure is shown in Fig. 4.2. The reactive power, torque and the stator flux are processed by the IMC controller to generate the command rotor voltage, which is transformed into the rotor coordinates and modulated as switching voltage with SVM.

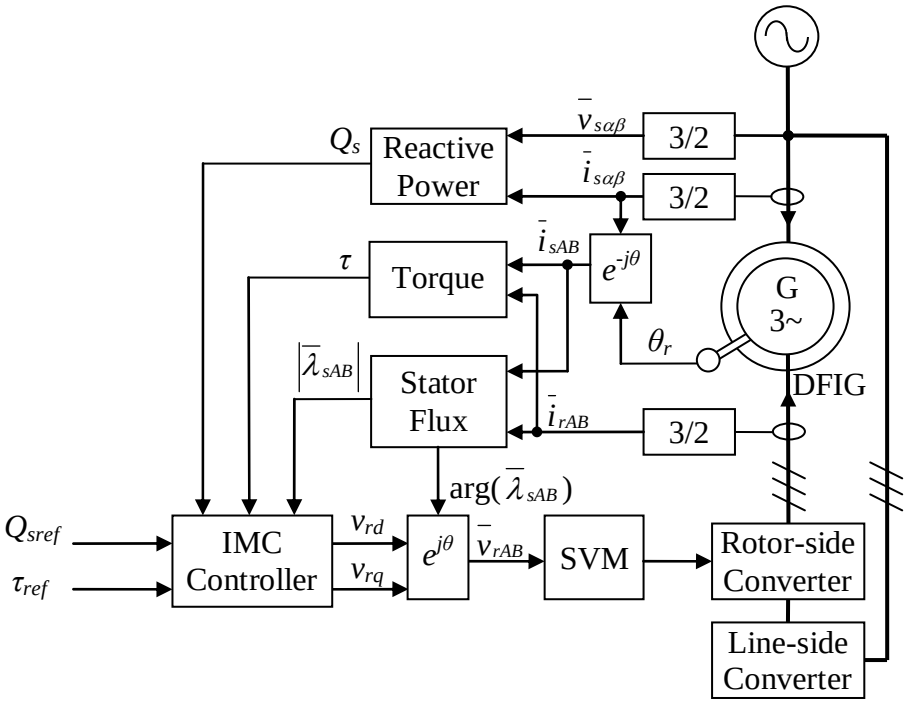

Fig. 4.2 Overall control structure

The IMC [70] structure of the DFIG is shown in Fig. 4.3, where $\boldsymbol{G}(s)$ is the model of the DFIG in the form of

$$\begin{pmatrix} Q_s(s) \\ \tau(s) \end{pmatrix} = \boldsymbol{G}(s) \begin{pmatrix} v_{rd}(s) \\ v_{rq}(s) \end{pmatrix}. \tag{4.2}$$

The differences between the measured and the estimated torque and reactive power are computed and compared with the reference inputs to act on the controller. The controller then computes the rotor voltages accordingly. If the internal model is the exact model of the DFIG, the difference between the estimated and the real torque and reactive power will be zero. Consequently, the feedback path to the controller will be zero and the system becomes an open-loop system. If the controller is the inverse of the DFIG model, the outputs will follow the inputs immediately. However, as the controller may generate over-reacted rotor voltage commands at

high frequencies, a low-pass filter is incorporated into the controller to filter out the noises. The DFIG transfer equations are derived from the generator characteristics so as to have a correct internal model of the DFIG and the controller is then designed accordingly.

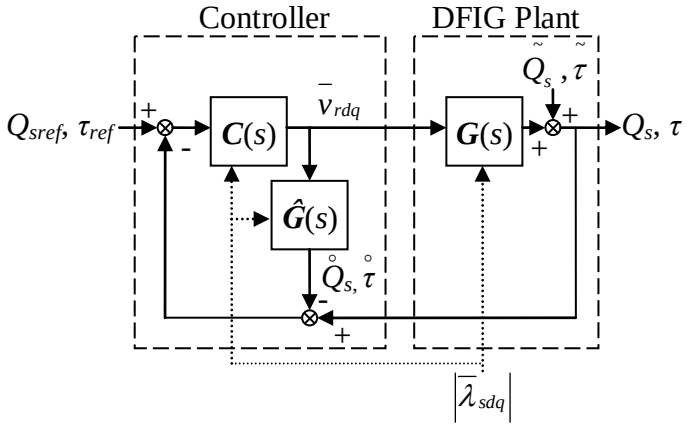

Fig. 4.3 Internal model control structure of DFIG

4.3.1 DFIG Transfer Equation

As the stator flux is a time integral of the stator voltage as shown in (3.10), the stator flux will not change abruptly, and it can be assumed to be constant in the quasi-steady-state [71]. Hence, in the stator flux reference frame, the stator voltage can be approximated with the stator flux and the synchronous frequency as

$$\bar{v}_{sdq} \approx j\left|\bar{\lambda}_{sdq}\right|\omega_s . \tag{4.3}$$

Perturbation of the rotor and stator currents in (3.6) yields the following equation:

$$\delta\bar{i}_{sdq} = -\frac{L_m}{(L_{s\sigma} + L_m)}\delta\bar{i}_{rdq} \tag{4.4}$$

For a small change in the rotor flux, (3.11) becomes

$$\delta\bar{\lambda}_{rdq} = -L_{s\sigma}\delta\bar{i}_{sdq} + L_{r\sigma}\delta\bar{i}_{rdq}\,. \tag{4.5}$$

Substituting (4.4) for the stator current term, (4.5) becomes

$$\delta\bar{\lambda}_{rdq} = L_{rk}\delta\bar{i}_{rdq}\,. \tag{4.6}$$

Substitution of (4.6) into the perturbed form of (3.5) gives the following system of Laplace equation:

$$\begin{pmatrix}\delta v_{rd}(s)\\ \delta v_{rq}(s)\end{pmatrix} = \begin{pmatrix} R_r + sL_{rk} & -L_{rk}(\omega_s - p\omega_r)\\ L_{rk}(\omega_s - p\omega_r) & R_r + sL_{rk}\end{pmatrix}\begin{pmatrix}\delta i_{rd}(s)\\ \delta i_{rq}(s)\end{pmatrix} \tag{4.7}$$

The torque and the quadrature rotor current can be expressed explicitly from (3.8) to become

$$i_{rq} = -\frac{L_{s\sigma} + L_m}{pL_m\left|\bar{\lambda}_{sdq}\right|}\tau\,. \tag{4.8}$$

The equation for the stator reactive power in (3.9) can be rearranged as

$$i_{rd} = \frac{\left|\bar{\lambda}_{sdq}\right|}{L_m} - \frac{L_{s\sigma} + L_m}{\omega_s L_m\left|\bar{\lambda}_{sdq}\right|}Q_s\,. \tag{4.9}$$

Perturbation of the current and reactive power in (4.9) yields

$$\delta i_{rd} = -\frac{L_{s\sigma} + L_m}{\omega_s L_m\left|\bar{\lambda}_{sdq}\right|}\delta Q_s\,. \tag{4.10}$$

Substitution of (4.10) and the perturbed form of (4.8) into (4.7) gives

$$\begin{pmatrix} \delta v_{rd}(s) \\ \delta v_{rq}(s) \end{pmatrix} = -\frac{L_{s\sigma} + L_m}{L_m \left| \overline{\lambda}_{sdq} \right|} \begin{pmatrix} R_r + sL_{rk} & -L_{rk}(\omega_s - p\omega_r) \\ L_{rk}(\omega_s - p\omega_r) & R_r + sL_{rk} \end{pmatrix} \begin{pmatrix} \delta Q_s(s)/\omega_s \\ \delta\tau(s)/p \end{pmatrix}. \quad (4.11)$$

Hence, the inverse of the internal model of the DFIG becomes

$$\hat{\boldsymbol{G}}(s)^{-1} = -\frac{L_{s\sigma} + L_m}{L_m \left| \overline{\lambda}_{sdq} \right|} \begin{pmatrix} (R_r + sL_{rk})/\omega_s & -L_{rk}(\omega_s - p\omega_r)/p \\ L_{rk}(\omega_s - p\omega_r)/\omega_s & (R_r + sL_{rk})/p \end{pmatrix}. \quad (4.12)$$

(4.12) can be decomposed into

$$\hat{\boldsymbol{G}}(s)^{-1} = \boldsymbol{D}(s) + \boldsymbol{W}(s). \quad (4.13)$$

The diagonal component and the off-diagonal component are as shown below:

$$\boldsymbol{D}(s) = -\frac{L_{s\sigma} + L_m}{L_m \left| \overline{\lambda}_{sdq} \right|} \begin{pmatrix} (R_r + sL_{rk})/\omega_s & 0 \\ 0 & (R_r + sL_{rk})/p \end{pmatrix} \quad (4.14)$$

$$\boldsymbol{W}(s) = -\frac{L_{s\sigma} + L_m}{L_m \left| \overline{\lambda}_{sdq} \right|} \begin{pmatrix} 0 & -L_{rk}(\omega_s - p\omega_r)/p \\ L_{rk}(\omega_s - p\omega_r)/\omega_s & 0 \end{pmatrix} \quad (4.15)$$

4.3.2 Internal Model Controller

To identify appropriate control pairs between the inputs and outputs, the RGA for the transfer equation has to be evaluated. The RGA of (4.12) at zero frequency is

$$\frac{1}{R_r^{\,2} + (\omega_s - p\omega_r)^2 L_{rk}^{\,2}} \begin{pmatrix} R_r^{\,2} & (\omega_s - p\omega_r)^2 L_{rk}^{\,2} \\ (\omega_s - p\omega_r)^2 L_{rk}^{\,2} & R_r^{\,2} \end{pmatrix}. \quad (4.16)$$

Since most DFIGs operate at around their synchronous frequencies [10], the product of the rotor speed and number of pole pairs may be close to the synchronous speed, and the difference between them are nearly zero if this is the case. Therefore, the RGA may become an identity matrix in the normal speed range of DFIG. The RGA, which is evaluated as an identity matrix, indicates that real part of the rotor voltage interacts closely with the reactive power, while the imaginary part of the rotor voltage interacts closely with the torque. As a result, the reactive power should be regulated by controlling the real part of the rotor voltage, and the torque is controlled by altering the imaginary part of the rotor voltage.

As mentioned in section 4.3, the internal model controller is comprised of the inverse of the internal model and a low pass filter as

$$\boldsymbol{C}(s) = \boldsymbol{L}(s)\hat{\boldsymbol{G}}(s)^{-1}, \tag{4.17}$$

where the number of poles of the low pass filter should be larger than or equal to the number of zeros minus the number of poles of the inverse of the internal model for the controller to be practically realizable. Since the inverse of the internal model is a multi-input multi-output matrix and the off-diagonal elements of the RGA may approach zero, the off-diagonal component of the inverse of the transfer matrix is to be compensated as a feed-forward term to reduce the complexity of the controller. The controller design hence involves the diagonal terms only. As the diagonal terms include first-order zeros, the minimum order of the filter will be one. In other words,

$$\boldsymbol{L}(s) = \frac{1}{sT_{cl}+1}\begin{pmatrix} 1 & 0 \\ 0 & 1 \end{pmatrix}. \tag{4.18}$$

4.3.3 Realization of the Controller

Practical implementation of the IMC involves computations for the internal model and the controller as shown in Fig. 4.3, and it can be reduced to a simpler form as shown in Fig. 4.4. $\boldsymbol{F}(s)$ can be described with

$$\boldsymbol{F}(s)=\left(\boldsymbol{I}-\boldsymbol{C}(s)\boldsymbol{D}(s)^{-1}\right)^{-1}\boldsymbol{C}(s). \tag{4.19}$$

Substitution of (4.14), (4.17) and (4.18) to (4.19) yields

$$\boldsymbol{F}(s)=-\frac{1}{sT_{cl}}(R_r+sL_{rk})\frac{L_{s\sigma}+L_m}{L_m\left|\overline{\lambda}_{sdq}\right|}\begin{pmatrix}1/\omega_s & 0\\ 0 & 1/p\end{pmatrix}, \tag{4.20}$$

which is a first order transfer equation and can be realized with a general proportional-integral controller. Even the stator flux is assumed constant in the quasi-steady state, it will change as the grid voltage varies and the power flow between the DFIG and the grid varies. Therefore, adjustments to the proportional part of (4.20) have to be made according to the magnitude of the stator flux, as calculated from the following equation:

$$\left|\overline{\lambda}_{sdq}\right|=\sqrt{\left((L_{s\sigma}+L_m)i_{sA}+L_m i_{rA}\right)^2+\left((L_{s\sigma}+L_m)i_{sB}+L_m i_{rB}\right)^2} \tag{4.21}$$

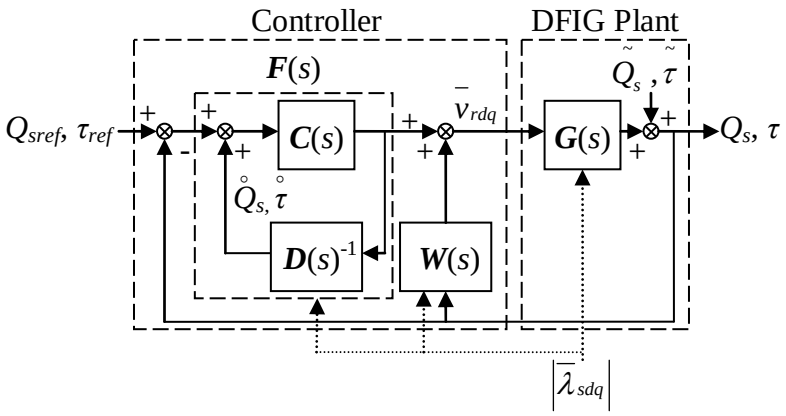

Fig. 4.4 Internal model control structure for realization

4.3.4 Disturbance Rejection

The supply voltage with disturbances can be expressed as $v_{sd} + \tilde{v}_{sd}$ and $v_{sq} + \tilde{v}_{sq}$. The stator currents with disturbances will be $i_{sd} + \tilde{i}_{sd}$ and $i_{sq} + \tilde{i}_{sq}$. The stator reactive power can be expressed as

$$Q_s + \tilde{Q}_s = \left(v_{sq} + \tilde{v}_{sq}\right)\left(i_{sd} + \tilde{i}_{sd}\right) - \left(v_{sd} + \tilde{v}_{sd}\right)\left(i_{sq} + \tilde{i}_{sq}\right). \tag{4.22}$$

By ignoring the product between the disturbance terms, which should be small, the disturbance in the reactive power becomes

$$\tilde{Q}_s = \left(v_{sq}\,\tilde{i}_{sd} + i_{sd}\,\tilde{v}_{sq}\right) - \left(v_{sd}\,\tilde{i}_{sq} + i_{sq}\,\tilde{v}_{sd}\right). \tag{4.23}$$

Therefore, the disturbance in the supply voltage and the stator current will become disturbance in the reactive power. With reference to Fig. 4.4, if the feed-forward term $\boldsymbol{W}(s)$ completely compensates the off diagonal term in $\boldsymbol{G}(s)^{-1}$ and

the gain of the controller is correctly adjusted in conjunction with the stator flux, the transfer function between the reactive power and its disturbance becomes

$$\frac{Q_s}{\tilde{Q}_s} = \frac{s}{s + 1/T_{cl}}. \tag{4.24}$$

As a result, the DC components of the disturbance will be completely rejected, but the attenuation of the disturbance will decrease as the frequency increases. Since the reactive disturbance will be of finite amplitude and will not be amplified by the control loops, the DFIG will be stable regardless of the influence due to the disturbances.

Similarly, the torque disturbance can be expressed as

$$\tilde{\tau} = pL_m\left(\left(i_{sq}\,\tilde{i}_{rd} + i_{rd}\,\tilde{i}_{sq}\right) - \left(i_{sd}\,\tilde{i}_{rq} + i_{rq}\,\tilde{i}_{sd}\right)\right). \tag{4.25}$$

As the control loop design for the torque is similar to that for the reactive power, the performance of the controller in rejecting the torque disturbances will be the same.

4.3.5 Comparison with Existing Control Algorithm

In contrast to the FOC approaches employed in [32, 33], the proposed algorithm is comprised of a reactive power control loop and a torque control loop; whereas the FOC requires two current control loops for the currents in parallel and perpendicular to the stator flux, and there are also two outer loops in FOC to individually regulate the real and reactive power. The response time of FOC is relatively long, because the

outer power loops must have a settling time longer than that of the inner current loop to ensure the overall control loop is stable [72]. For instance, the current loop settling time in [33] is tuned to 40 ms; while the settling time of the outer power loop is tuned to 70 ms, and this explains why it is commented as ‘a slower power control loop’ in [32]. Furthermore, in the proposed algorithm, only two coordinate transformations are needed; one to change the stator current to the rotor reference frame for stator flux and torque calculation, and another one to change the rotor voltage command from the stator flux reference frame to the rotor reference frame. However, in FOC [33], two additional transformations are required: one to align the rotor current to the flux frame, and another one to align the stator current to the flux frame for the computation of real and reactive power. The proposed single loop approach could have disturbance rejection that is comparable with that of the inner loop of FOC, if the closed-loop setting time is tuned to be the same as that in the inner loop of the FOC. This is because the disturbance rejection is mainly related to the closed-loop settling time [70]. Another feature of FOC, which is to impose a current limit, can also be realized in the proposed algorithm as the generator power limit can be derived from the current limit [33].

As for DTC [39], even though it utilizes feedbacks of torque and flux to eliminate the need for coordinate transformation, it still needs one transformation to calculate the rotor flux. DTC also possesses an outer control loop to regulate the reactive power, while the proposed algorithm requires a single loop to control the reactive power. Besides, both DTC and DPC [43, 46] suffer from similar drawbacks of hysteresis control, such as variable switching frequencies, current and torque distortions from the sector changes in the rotor voltage, and the need for a high

sampling frequency with limited steady state accuracy [42]. However, these undesirable features are eliminated in the proposed algorithm because of the use of constant switching frequency.

In DPC with constant switching frequency [47], deadbeat controller instead of hysteresis controller is used, and the stator real and reactive powers are used as feedback variables. The stator power, which can be measured easily, is a fraction of the full output power of the DFIG, whereas the remaining fraction of the full output power will flow between the DFIG and the grid through the rotor winding and the power electronics converters. However, to control the speed of the generator, the generator torque or the full output power by the DFIG has to be controlled, instead of the stator power alone, because the speed of the DFIG is dependent on the net torque difference between the turbine and the DFIG, or the power difference between them, divided by the turbine speed. As the conventional control algorithm of DFIG uses the stator output power, which is a fraction of the full output power, as the feedback signal, whereas the feedback signal of the proposed algorithm is the generator torque, which is readily computed using measured currents and inductance, it is obvious that the proposed algorithm is simpler for speed control in terms of implementation.

4.4 Simulations Results

A simulation environment in Matlab/Simulink is set up with the parameters as given in the Appendices. The designed closed-loop bandwidth is 200 Hz. The per-phase source inductance of 0.0497 H, or 15.6 Ω at 50 Hz, in the experimental setup is much larger than that in real practice so as to test the operation of the DFIG

in extreme conditions. In Fig. 4.5, the generator operates initially at 600 VAR, 1400 RPM and generates a torque of -4 Nm, while the grid voltage is 380 V and the stator voltage is 350 V. Subsequent to a step change in the reactive power reference to 1000 VAR at 0.2 s, the reactive power reaches the reference within 0.02 s with an overshoot of 40 VAR. The torque oscillates slightly with an amplitude of 0.15 Nm. During the same period, the voltage drops to 330 V, due to an increase in the voltage drop across the transmission line because of changes in the reactive power. It can be seen in the figure that the transients are over at the simulation time of 0.25 s and the system reaches a new state of equilibrium. The overshoot and the torque oscillations are attributed to changes in the stator flux, which are compensated by the controller. The speed is constant at 1400 RPM throughout the simulation.

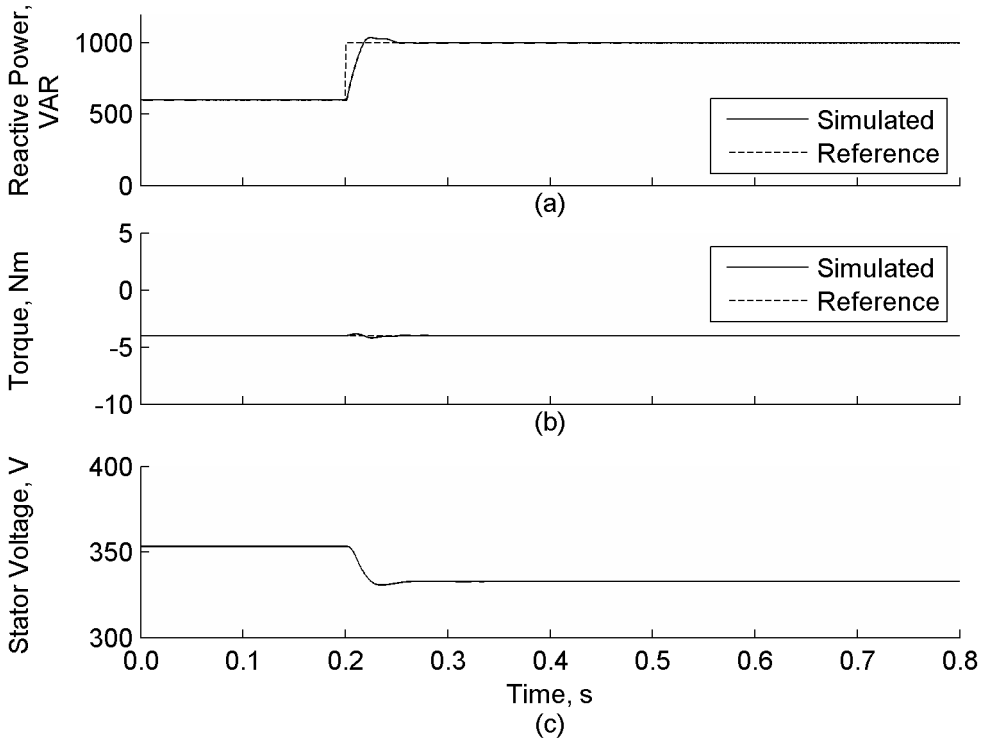

Fig. 4.5 Simulated responses to a change in the reactive power reference

(a) Reactive power, (b) Torque, (c) Stator voltage

The effects of a step change in the torque are shown in Fig. 4.6. From start to 0.2 s, the torque is 0 Nm, and the generator accelerates as the turbine supplies power to the generator. At 0.2 s, the torque reference decreases from 0 Nm to -8 Nm. Oscillations with an amplitude of 72 VAR are present in the reactive power while the torque undershoots the reference level. From 0.2 s to 1.0 s, even the rotor speed decreases from 1530 RPM to 1480 RPM, it can be seen that the reactive power and torque are remaining at their respective references. Unlike the simulation for the case that studies a change in the reactive power reference, the stator voltage in this simulation stays at 340 V, as there is no change in the reactive power.

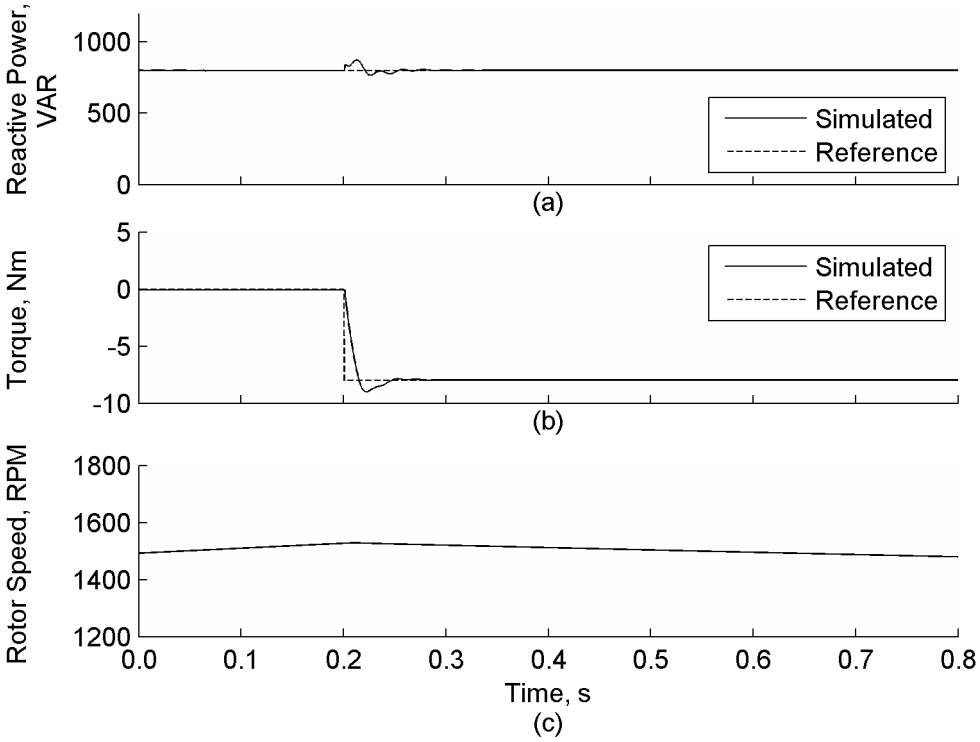

Fig. 4.6 Simulated responses to a change in the torque reference

(a) Reactive power, (b) Torque, (c) Rotor Speed

To investigate the effects of model mismatch, which may arise from the variations in the operating temperature, on the system performance, the parameters

of the controller such as the rotor resistance, leakage and magnetizing inductances are varied. By assuming that the feed-forward term $\boldsymbol{W}(s)$ in (4.13) perfectly matches the plant parameters, the transfer equation between the stator reactive power and the direct rotor voltage becomes

$$G_Q^{-1}(s) = \frac{v_{rd}(s)}{Q_s(s)} = -\frac{(L_{s\sigma} + L_m)(R_r + sL_{rk})}{L_m \left|\overline{\lambda}_{sdq}\right| \omega_s}. \tag{4.26}$$

If the controller $\boldsymbol{F}(s)$ in (4.20) is designed with mismatched parameters, the mismatched controller $F_Q(s)'$ for the stator reactive power control is

$$F_Q(s)' = \frac{v_{rd}(s)}{Q_{sref}(s) - Q_s(s)} = -\frac{1}{sT_{cl}}(R_r' + sL_{rk}')\frac{L_{s\sigma}' + L_m'}{L_m' \left|\overline{\lambda}_{sdq}'\right| \omega_s}. \tag{4.27}$$

Further assume that the magnetizing inductance is much larger than the leakage inductances, the product of the controller and the plant transfer equations becomes

$$G_Q(s)F_Q(s)' = \frac{(R_r' + sL_{rk}')\left|\overline{\lambda}_{sdq}\right|}{sT_{cl}(R_r + sL_{rk})\left|\overline{\lambda}_{sdq}'\right|}. \tag{4.28}$$

The corresponding closed-loop transfer equation is

$$\frac{Q_s(s)}{Q_{sref}(s)} = \frac{G_Q(s)F_Q(s)'}{1 + G_Q(s)F_Q(s)'} = \frac{(R_r' + sL_{rk}')\left|\overline{\lambda}_{sdq}\right|}{sT_{cl}(R_r + sL_{rk})\left|\overline{\lambda}_{sdq}'\right| + (R_r' + sL_{rk}')\left|\overline{\lambda}_{sdq}\right|}. \tag{4.29}$$

As the real part of the roots of (4.29) is negative for positive parameters, the system is always stable, despite the parameter mismatch may generate over-damped or under-damped transient step responses.

Step changes in the reactive power demand with different controller parameters are simulated with the responses plotted in Fig. 4.7. The DFIG is operated at -4 Nm, 1400 RPM. With parameters of both the resistance and inductances being halved or doubled, the step responses of the controller are similar to those with matched parameters, and there are unnoticeable changes in the rise times.

This is because the time constant of the controller is the same as that of the DFIG, hence the variations affect the closed-loop bandwidth only. With the parameters of double resistance and half inductances, the step change introduces a 220 VAR overshoot of the reactive power with oscillations at 30 Hz; while an under-damped response is obtained with parameters having half resistance and double inductances. The changes in shape of the responses are arising from a shift in the location of the zero contributed by the controller. For all controller parameters, the reactive power reaches the reference value within 0.3 s after a step change in the reference at the simulation time of 0.2 s. The torque oscillations and stator voltage changes during the reactive power transients are similar to those in Fig. 4.5. The effects of model mismatches on the torque step responses are similar to those on the reactive power step responses, and will not be repeated here. As the DFIG has stable operation even with large variations in the controller parameters, the control algorithm is robust with respect to plant model mismatches.

The effects of source impedance on the system stability and dynamics are shown in Fig. 4.8. Despite the source impedance varies from 0.0497 H to 0 H, and the stator voltage fluctuates because of the variation in the source impedance, the dynamics response to step changes in the reactive power are similar.

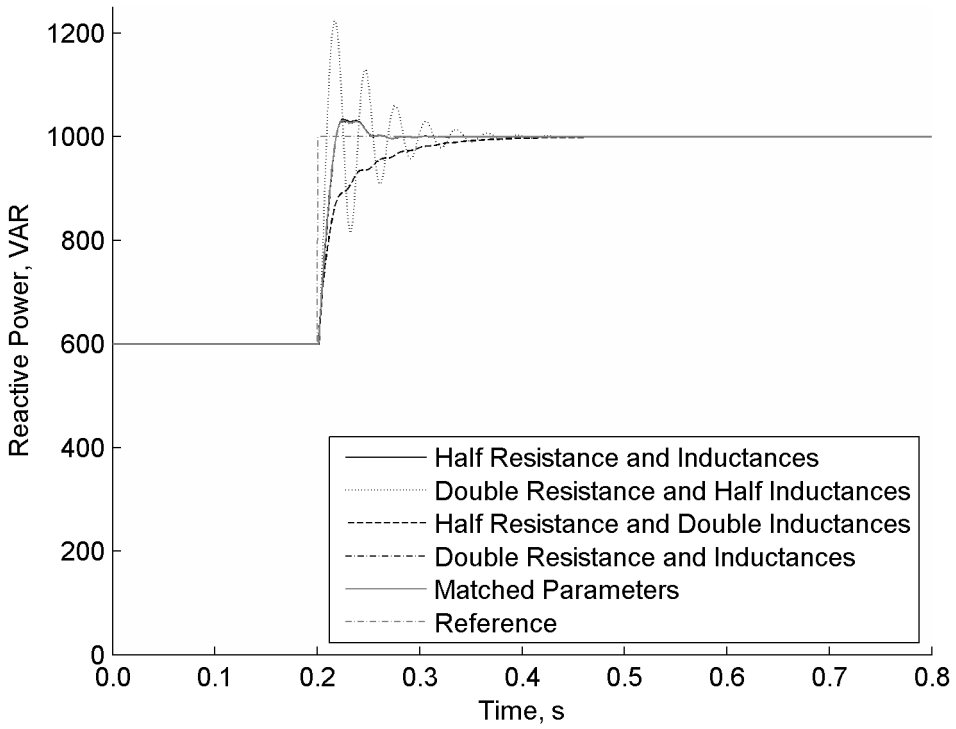

Fig. 4.7 Simulated responses to changes in the reactive power reference with different parameters

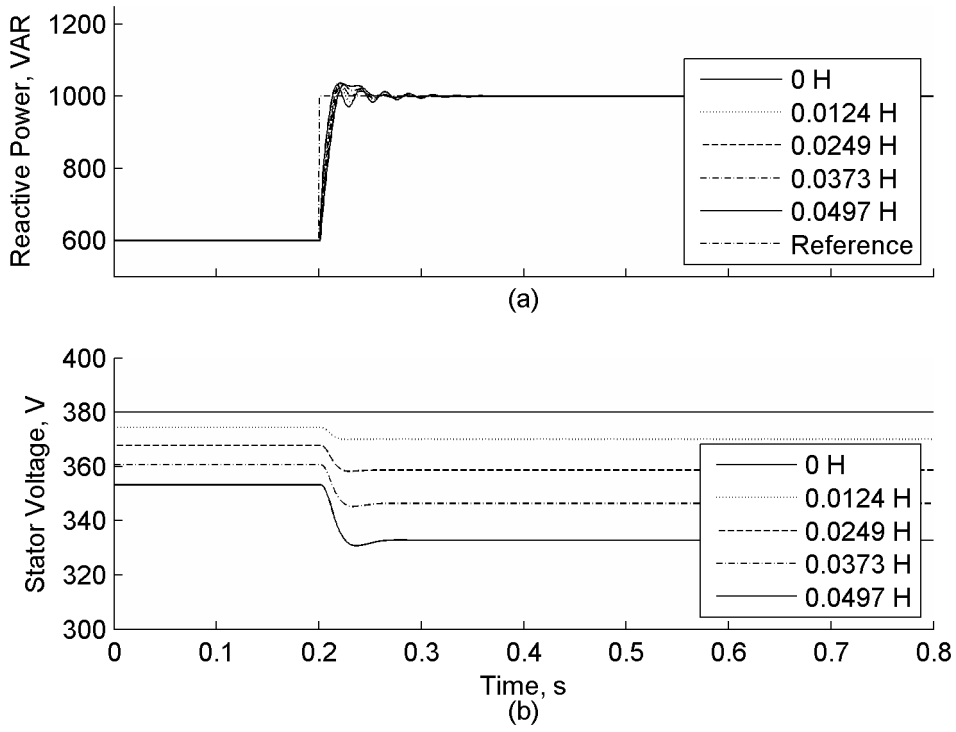

Fig. 4.8 Simulated responses to changes in the reactive power reference with different source impedance

4.5 Experimental Results

The experimental setup is similar to the setup in Fig. 3.9, but with an inductor connected between the DFIG and the grid to emulate the source impedance of the grid as shown in Fig. 4.9.

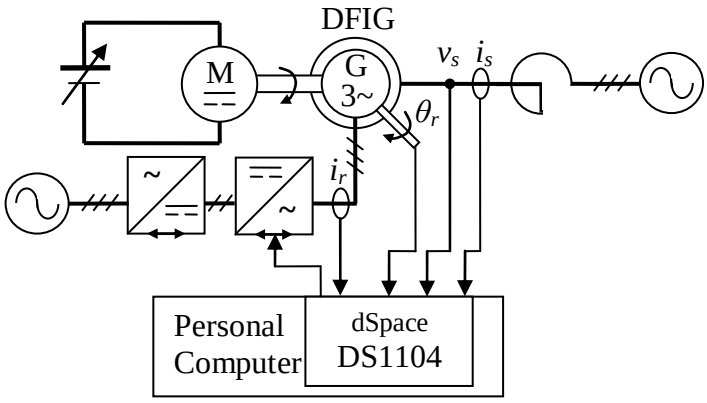

Fig. 4.9 Experimental setup

The reactive power, torque and stator voltage responses subjected to a step change in reactive power are shown in Fig. 4.10, whereas computer simulation with the experimental settings are also shown for references. The corresponding current waveforms are shown in Fig. 4.11. The rotor speed is 1430 RPM. The initial reactive power reference and the torque reference are 600 VAR and -4 Nm respectively. The reactive power reference increases from 600 VAR to 1000 VAR at the time 0.2 s. The reactive power follows the change and reaches the reference at the time 0.23 s without noticeable overshoot. Even the stator voltage is reduced from its initial value of 360 V to 340 V as the reactive power demand changes, the torque remains at -4 Nm. Despite the torque and reactive power ripples, which are attributed to the flexible mechanical coupling linking the DC motor and the DFIG, the experimental and simulation results are matched.

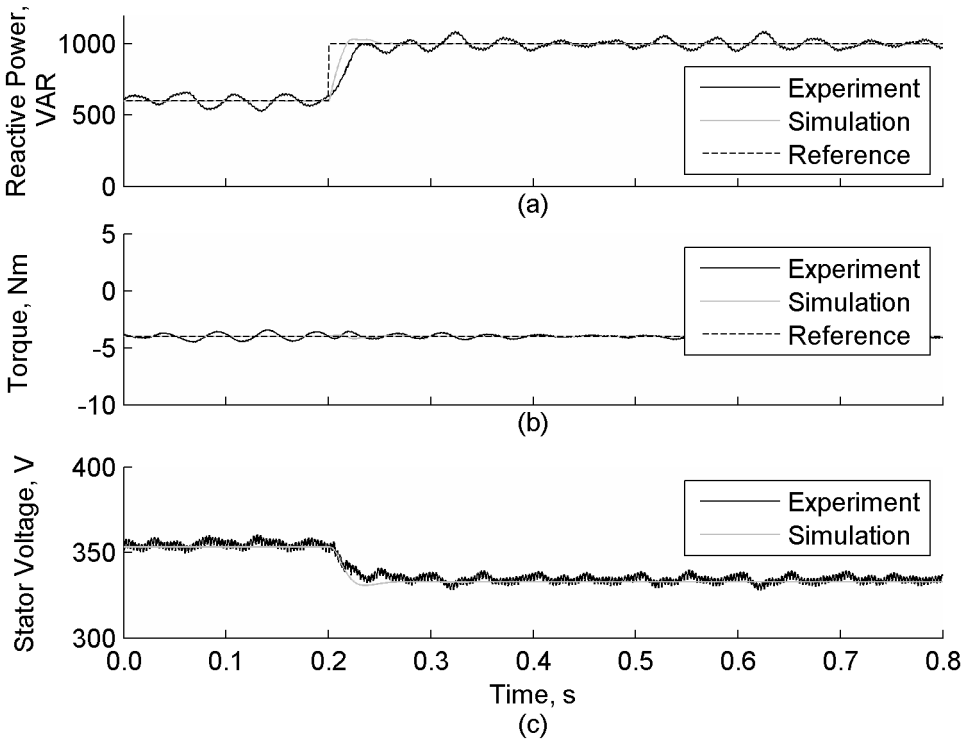

Fig. 4.10 Step responses to a change in the reactive power reference

(a) Reactive power, (b) Torque, (c) Stator voltage

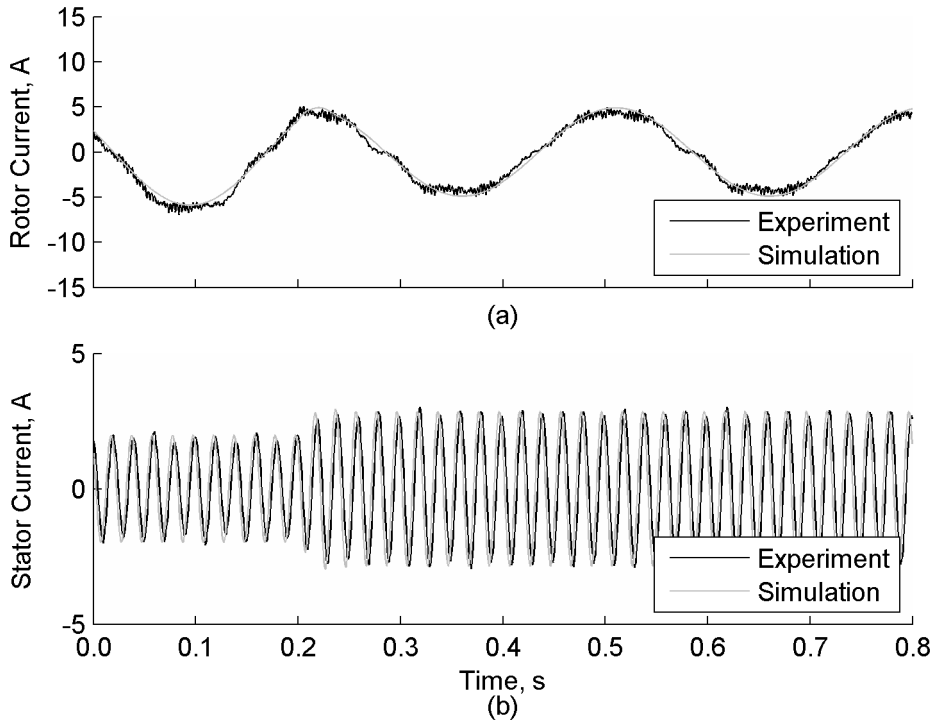

Fig. 4.11 Step responses to a change in the reactive power reference

(a) Rotor current, (b) Stator current

To study the torque step response, a step change in the torque reference from 0 Nm to -8 Nm is applied at the time 0.2 s as shown in Fig. 4.12, with current waveforms shown in Fig. 4.13. The stator voltage is constant at 350 V because the reactive power remains unchanged at 800 VAR. The generator torque tracks the reference torque quickly and settles at the time 0.23 s. The speed of the DFIG decreases gradually from 1600 RPM to 1400 RPM as the magnitude of the torque increases, until the motoring torque of the DC motor is equal to the generator torque at the time 0.53 s. The simulation results with the DC generator characteristics are similar to the experimental results. The deceleration of the DFIG is more rapid than that in the computer simulation as shown in Fig. 4.6, because of the low inertia of the DFIG and the DC motor, as compared with the inertia of a realistic wind turbine in the simulation. It shows that the algorithm is independent of the turbine characteristics. Despite the rapid deceleration, the torque and the reactive power reach the references from the time of 0.24 s onwards. The change in ripple frequencies of the reactive power further confirms that they are from the mechanical coupling. It is because as the speed decreases, the ripple frequencies decrease and the magnitudes increase, which are characteristic features arising from mechanical oscillations due to coupling. The principle behind is that the stator and rotor current harmonics are dependent on the slip. Hence, the speed of the DFIG, which is dependent on the slip, affects the current harmonics as well [73]. It is worth noting that the harmonics and the speed ripples cause beating in the stator current which gives rise to fluctuations in the torque and reactive power [74]. The torque and reactive power spectra show that the magnitudes of the ripples are less than 2% of the zero frequency components.

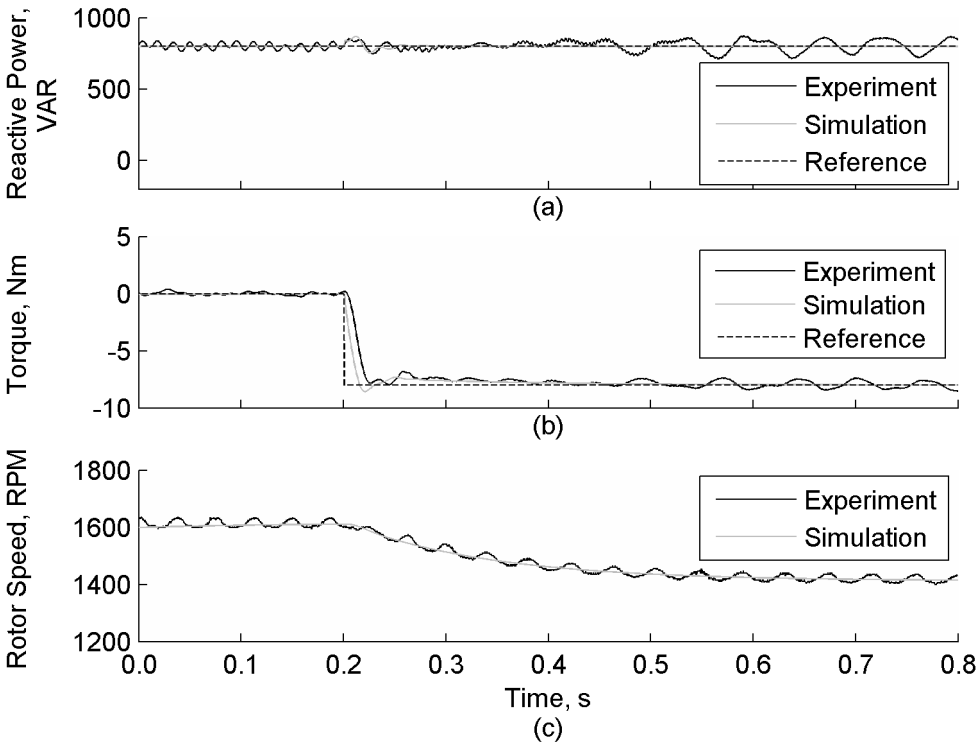

Fig. 4.12 Step responses to a change in the torque reference

(a) Reactive power, (b) Torque, (c) Rotor Speed

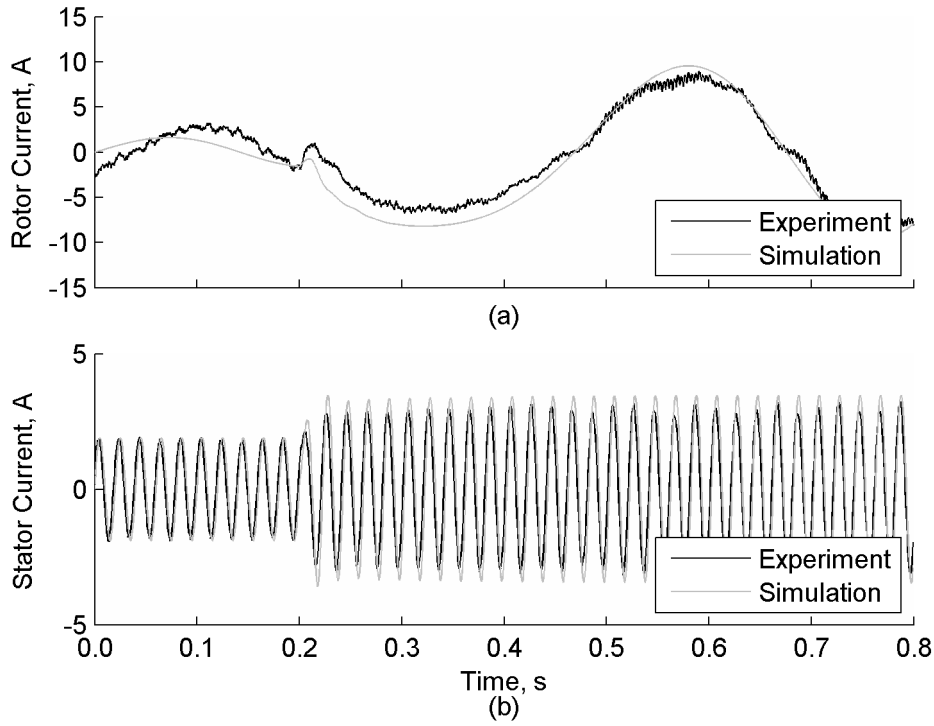

Fig. 4.13 Step responses to a change in the torque reference

(a) Rotor current, (b) Stator current

Fig. 4.14 to Fig. 4.17 show the frequency spectra of the stator and rotor currents when the DFIG operates at 1419 RPM, -8 Nm, and 800 VAR. For the stator current, the dominating current component is at the operating frequency of the grid; whereas for the rotor current, the most prominent component is at the slip frequency of 2.5 Hz. The unique peak frequencies in the spectra imply low harmonic distortions generated by the DFIG. The corresponding waveforms of the phase A currents are plotted in Fig. 4.18. No noticeable switching current ripples are found in the spectra of both currents. The shape distortion of the fundamental components of the rotor current is from the non-linear magnetizing characteristic of the DFIG. Comparing the experimental waveforms with the simulation waveforms from DTC [39] with ideal supply voltage and DFIG characteristics, the current harmonic distortions from the experimental results is lower than that from DTC, and is of lower frequency. It is because the distortions in the experiment are from non-ideal characteristics in a realistic situation, while those in DTC simulation are contributed by the hysteresis switching of the controller.

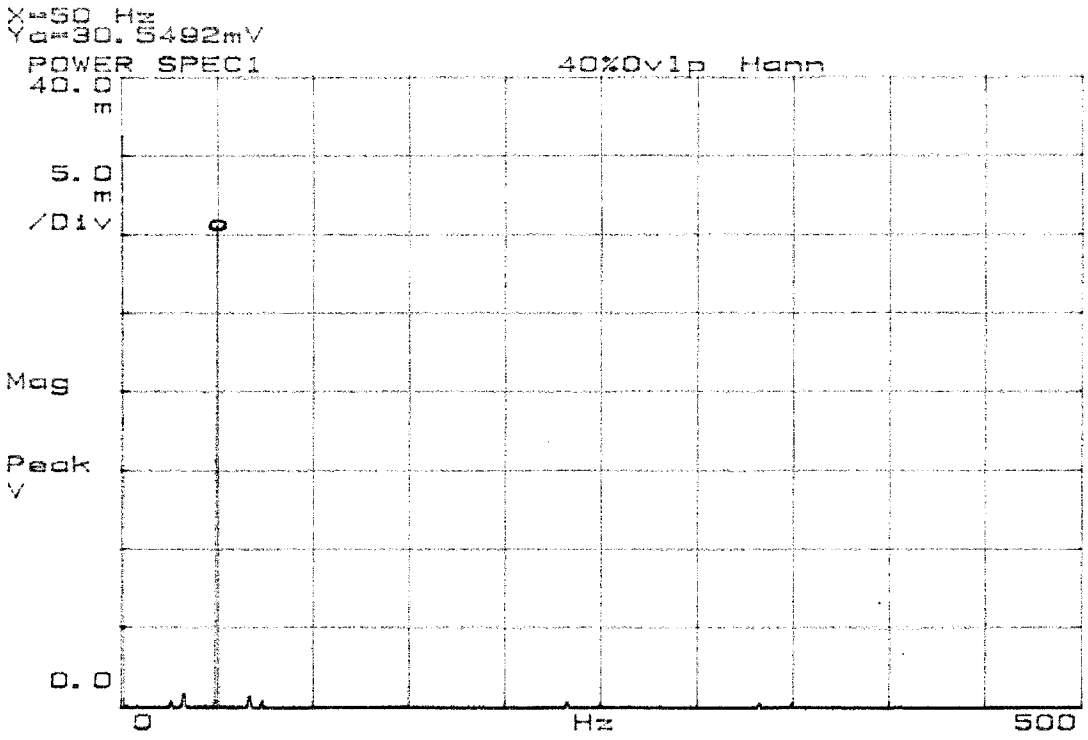

Fig. 4.14 Frequency spectrum of the stator current (frequency span: 500 Hz, probe gain: 100 A/V)

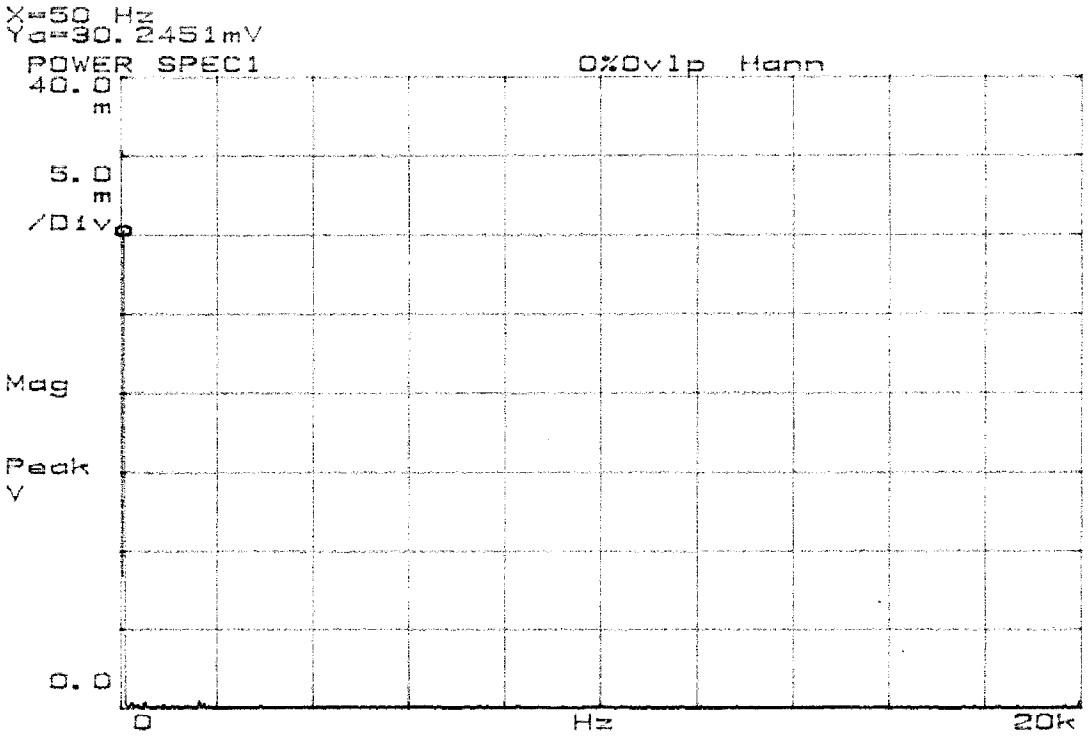

Fig. 4.15 Frequency spectrum of the stator current (frequency span: 20 kHz, probe gain: 100 A/V)

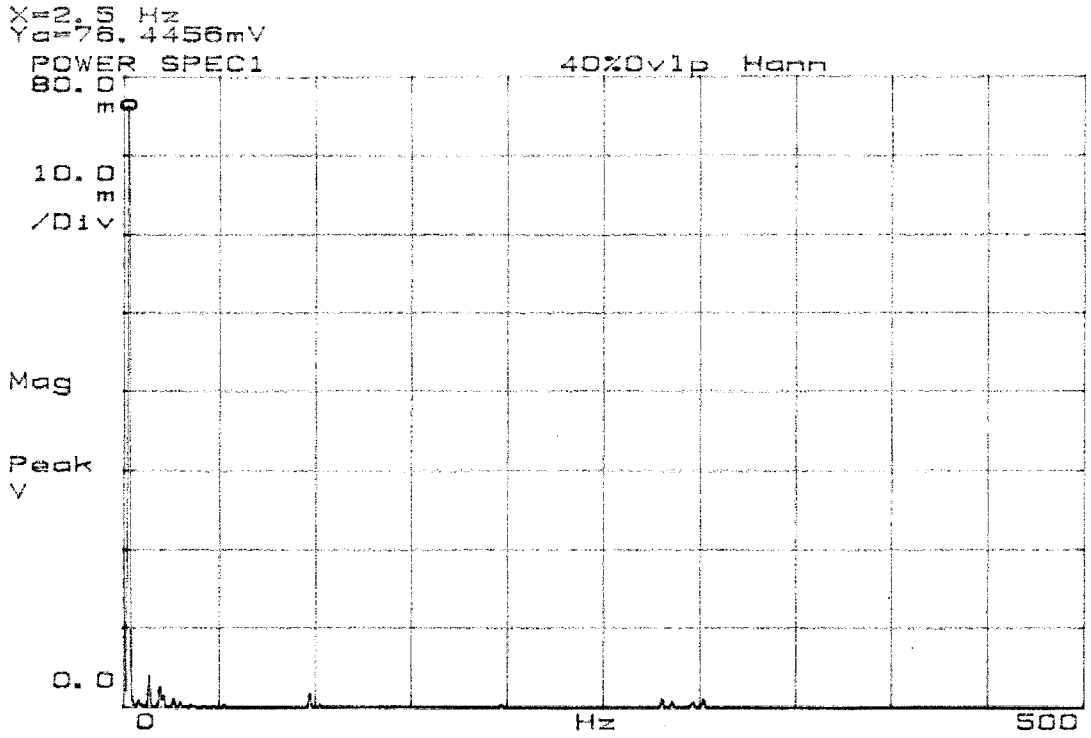

Fig. 4.16 Frequency spectrum of the rotor current (frequency span: 500 Hz, probe gain: 100 A/V)

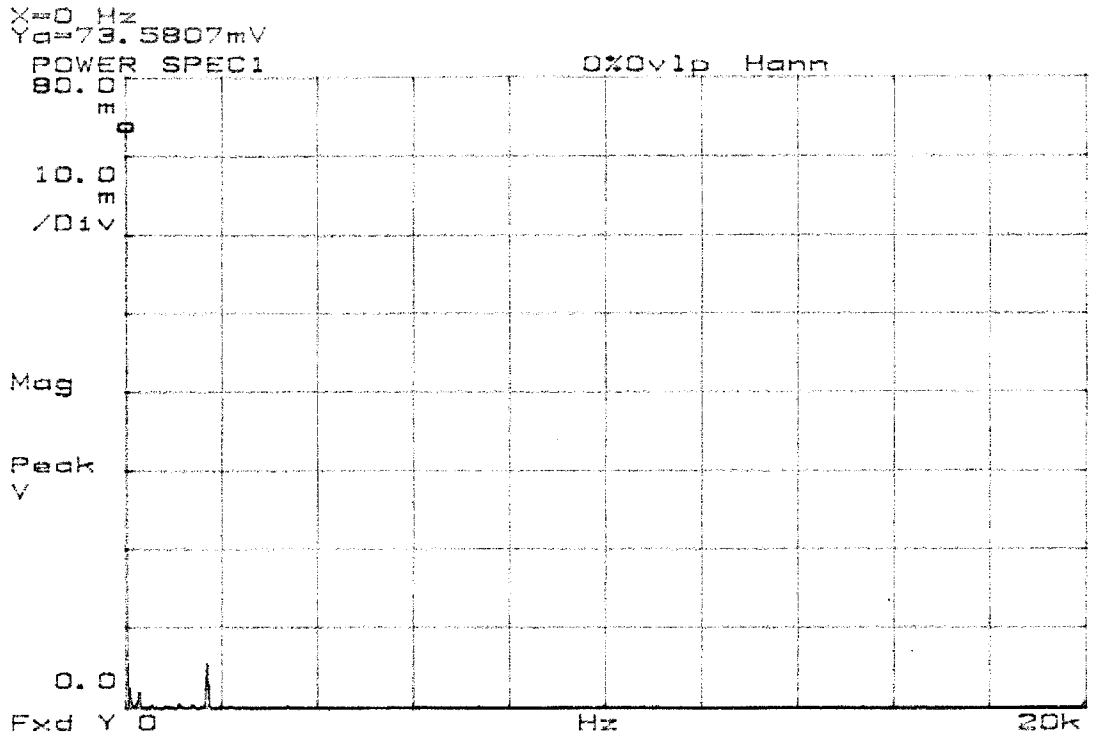

Fig. 4.17 Frequency spectrum of the rotor current (frequency span: 20 kHz, probe gain: 100 A/V)

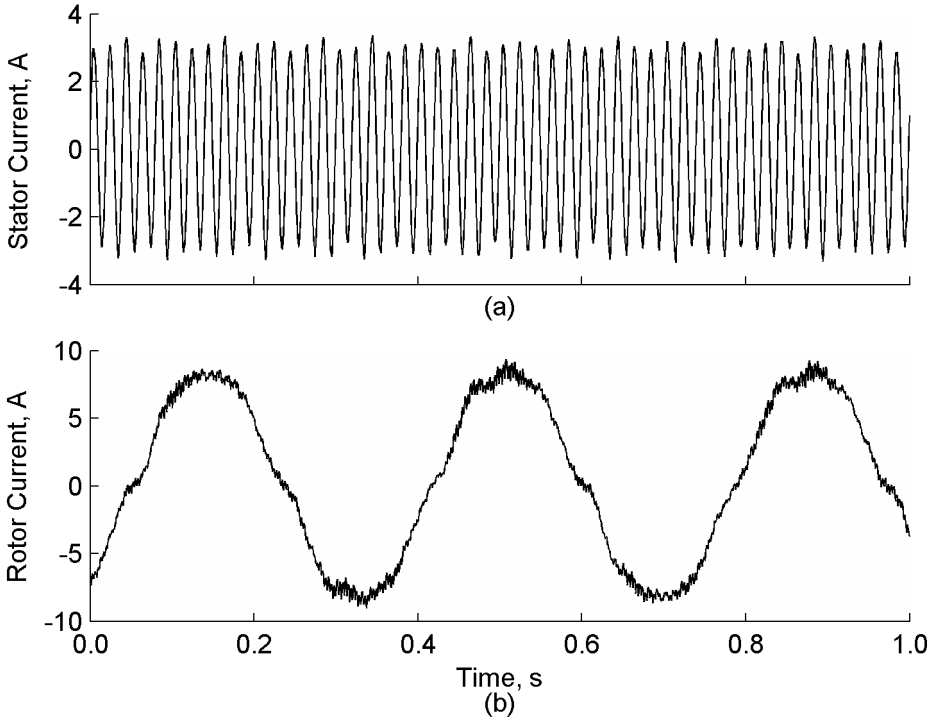

Fig. 4.18 Waveforms of the measured phase A currents

(a) Stator, (b) Rotor

4.6 Summary

The torque and reactive power control algorithm for DFIG has been presented. The algorithm makes use of direct feedback and control of torque and reactive power. Since only one control loop is necessary for each control variable, the tuning is simpler than those of the multi-loop design. Furthermore, a reduction in the number of control loops reduces the response time and computational requirements of the DFIG system. The internal model control method provides an in-depth knowledge based on the operation of the DFIG and forms the basis of tuning. Comparison with existing algorithms shows that the proposed algorithm does not inherit drawbacks of either of them. The computer simulation verifies that the algorithm is capable of independently controlling the torque and reactive power, even in the presence of large source impedance and changes in rotor speed. The

robustness of the algorithm is verified as the DFIG operates stably despite there are large variations in the controller parameters. Experimental data have a high degree of conformance with those obtained from simulations and theoretical derivations. The mechanical oscillations as observed in the experiment do not affect the performance of the algorithm either. The low distortions in the rotor and stator currents indicate that the switching operation of the converter does not introduce switching harmonics to the grid, therefore no harmonic filters are required.

5 Direct Torque Control in Grids with Unbalanced Voltage

5.1 Introduction

In this chapter, torque and reactive power controls for both positive and negative sequence components of DFIG are developed to formulate a direct control scheme. As the positive and negative sequence components of the torque and reactive power are extracted and independently regulated, the scheme can realise different objectives, such as minimization of reactive power and torque ripples, or minimization of stator real power ripples.

5.2 Mathematical Model

As the neutral point of the DFIG is not connected to the external grid, the zero sequence component in the stator voltage will not affect the operation of the DFIG and hence will not be considered in the following analysis. With the Clark transformation defined in (2.4)–(2.6), in the stator reference frame, the unbalanced stator voltage includes a positive sequence vector and a negative sequence vector:

$$\bar{v}_{s\alpha\beta} = \bar{v}_{s+\alpha\beta} + \bar{v}_{s-\alpha\beta}, \tag{5.1}$$

whereas the sequence components are defined as complex values rotating in opposite directions:

$$\bar{v}_{s+\alpha\beta} = \bar{v}_{s+} e^{j\omega_s t} \tag{5.2}$$

$$\bar{v}_{s-\alpha\beta} = \bar{v}_{s-} e^{-j\omega_s t} \tag{5.3}$$

As the stator flux is essentially a time integral of the stator voltage as shown in (3.10), the stator flux in the stator reference frame can also be expressed as the sum of two rotating vectors:

$$\bar{\lambda}_{s\alpha\beta} = \bar{\lambda}_{s+\alpha\beta} + \bar{\lambda}_{s-\alpha\beta} \tag{5.4}$$

A stator current is assumed to possess both positive and negative sequence components as shown in the following equation:

$$\bar{i}_{s\alpha\beta} = \bar{i}_{s+\alpha\beta} + \bar{i}_{s-\alpha\beta} \tag{5.5}$$

In the positive sequence stator flux reference frame, the following space vector equations describe the relationship among the positive sequence variables:

$$\bar{\lambda}_{s+dq} = \left|\bar{\lambda}_{s+dq}\right| = \left(L_{s\sigma} + L_m\right)\bar{i}_{s+dq} + L_m \bar{i}_{r+dq} \tag{5.6}$$

$$\bar{\lambda}_{r+dq} = L_m \bar{i}_{s+dq} + \left(L_{r\sigma} + L_m\right)\bar{i}_{r+dq} \tag{5.7}$$

$$\bar{v}_{s+dq} = R_s \bar{i}_{s+dq} + \frac{d\bar{\lambda}_{s+dq}}{dt} + j\omega_s \bar{\lambda}_{s+dq} \tag{5.8}$$

$$\bar{v}_{r+dq} = R_r \bar{i}_{r+dq} + \frac{d\bar{\lambda}_{r+dq}}{dt} + j\left(\omega_s - p\omega_r\right)\bar{\lambda}_{r+dq} \tag{5.9}$$

The equivalent circuit is shown in Fig. 5.1.

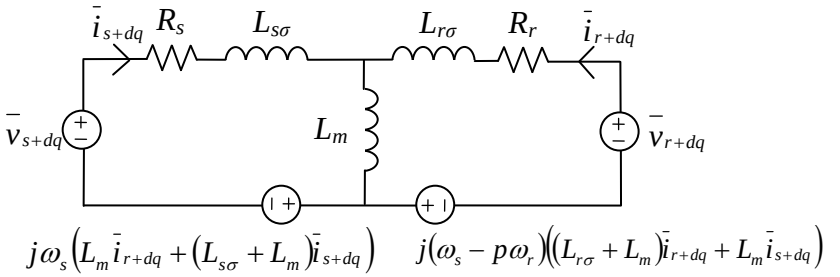

Fig. 5.1 Positive sequence equivalent circuit of DFIG in the flux reference frame

Equations (5.6) and (5.7) are also valid for the negative sequence current and flux in the negative sequence stator flux reference frame. However, the voltage equations in the negative sequence frame are different from those of their positive sequence counterparts because the positive and negative sequence frames are rotating in opposite directions:

$$\bar{v}_{s-dq}=R_s\bar{i}_{s-dq}+\frac{d\bar{\lambda}_{s-dq}}{dt}-j\omega_s\bar{\lambda}_{s-dq} \tag{5.10}$$

$$\bar{v}_{r-dq}=R_r\bar{i}_{r-dq}+\frac{d\bar{\lambda}_{r-dq}}{dt}+j\left(-\omega_s-p\omega_r\right)\bar{\lambda}_{r-dq} \tag{5.11}$$

The equivalent circuit is shown in Fig. 5.2.

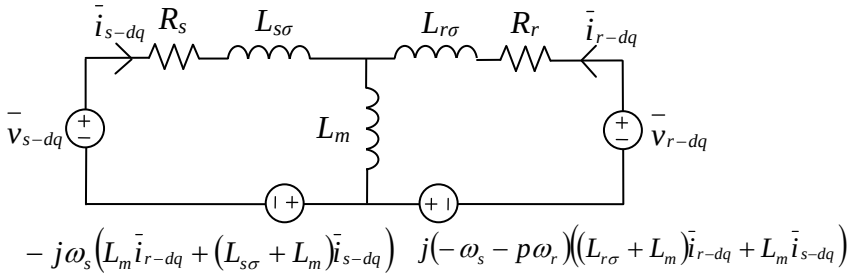

Fig. 5.2 Negative sequence equivalent circuit of DFIG in the flux reference frame

The stator side apparent power can be expressed as the product of the stator voltage and the conjugate of the stator current:

$$\bar{S}_s = \bar{v}_{s\alpha\beta}\bar{i}^*_{s\alpha\beta} = \bar{v}_{s+}\bar{i}^*_{s+} + \bar{v}_{s-}\bar{i}^*_{s-} + \bar{v}_{s-}\bar{i}^*_{s+}e^{-j2\omega_s t} + \bar{v}_{s+}\bar{i}^*_{s-}e^{j2\omega_s t} \tag{5.12}$$

Alternatively, substituting the voltage and currents by their respective flux reference frame counterparts gives

$$\bar{S}_s = \bar{v}_{s+dq}\bar{i}^*_{s+dq} + \bar{v}_{s-dq}\bar{i}^*_{s-dq} + \bar{v}_{s-dq}\bar{i}^*_{s+dq}e^{-j2\omega_s t}e^{j\angle\lambda_{s+-}} + \bar{v}_{s+dq}\bar{i}^*_{s-dq}e^{j2\omega_s t}e^{-j\angle\lambda_{s+-}}, \tag{5.13}$$

where $\angle\lambda_{s+-}$ is the difference in argument between the negative and positive sequence components of the stator flux:

$$\angle\lambda_{s+-} = \arg(\bar{\lambda}_{s-}) - \arg(\bar{\lambda}_{s+}) \tag{5.14}$$

The electromagnetic torque is the cross product of the stator flux and the stator current:

$$\begin{aligned}\tau &= -\mathrm{Im}\left(\bar{\lambda}_{s\alpha\beta}\bar{i}^*_{s\alpha\beta}\right)p \\ &= -\mathrm{Im}\left(\bar{\lambda}_{s+}\bar{i}^*_{s+} + \bar{\lambda}_{s-}\bar{i}^*_{s-} + \bar{\lambda}_{s-}\bar{i}^*_{s+}e^{-j2\omega_s t} + \bar{\lambda}_{s+}\bar{i}^*_{s-}e^{j2\omega_s t}\right)p\end{aligned} \tag{5.15}$$

Expressing (5.15) with the stator flux frame variables yields

$$\begin{aligned}\tau = -\mathrm{Im}(&\bar{\lambda}_{s+dq}\bar{i}^*_{s+dq} + \bar{\lambda}_{s-dq}\bar{i}^*_{s-dq} + \\ &\bar{\lambda}_{s-dq}\bar{i}^*_{s+dq}e^{-j2\omega_s t}e^{j\angle\lambda_{s+-}} + \bar{\lambda}_{s+dq}\bar{i}^*_{s-dq}e^{j2\omega_s t}e^{-j\angle\lambda_{s+-}})\,p\end{aligned}. \tag{5.16}$$

5.3 Controller Design

Similar to the control objective of DFIG controllers in balanced grids in Chapter 3 and Chapter 4, the most common and primary control objective of DFIG controller in an unbalanced grid is to regulate the stator reactive power and torque. The second objective is to minimize ripples in the stator real power, reactive power, or torque arising from unbalance in the grid voltage. As indicated in (5.12) and (5.15), terms having complex exponents contribute to ripples at twice synchronous frequency in both power and torque. Coefficients of the complex exponent terms in (5.12) and (5.15) comprise of the positive sequence and negative sequence components of stator voltage, stator flux, and stator current. As the positive sequence current is related to the primary objective, the controller can only minimize the power or torque ripples by regulating the negative sequence stator current [63].

For both positive and negative sequence components, in their respective stator flux reference frames, the stator flux has real parts only. By assuming that the products of the stator currents and resistances are small in (5.8) and (5.10), when compared to other terms, the stator voltages have imaginary parts only at steady state:

$$\bar{v}_{s+dq} = j\omega_s \left|\bar{\lambda}_{s+dq}\right| \tag{5.17}$$

$$\bar{v}_{s-dq} = -j\omega_s \left|\bar{\lambda}_{s-dq}\right| \tag{5.18}$$

A positive sequence reactive power Q_{s+} is defined as

$$Q_{s+} = \mathrm{Im}\left(\bar{v}_{s+dq}\bar{i}^{*}_{s+dq}\right). \tag{5.19}$$

It can alternatively be defined in terms of the stator frame variables as

$$Q_{s+} = \mathrm{Im}\left(\bar{v}_{s+\alpha\beta}\,\bar{i}^{*}_{s+\alpha\beta}\right). \tag{5.20}$$

Substituting (5.17) into (5.19), the positive sequence reactive power becomes

$$Q_{s+} = \omega_s \left|\bar{\lambda}_{s+dq}\right| i_{s+d}\,. \tag{5.21}$$

A positive sequence torque is defined as the cross product of the stator flux and current:

$$\tau_{+} = -\mathrm{Im}\left(\bar{\lambda}_{s+dq}\,\bar{i}^{*}_{s+dq}\right)p\,, \tag{5.22}$$

which is equivalent to

$$\tau_{+} = -\mathrm{Im}\left(\bar{\lambda}_{s+\alpha\beta}\,\bar{i}^{*}_{s+\alpha\beta}\right)p\,. \tag{5.23}$$

As the stator flux in *per se* reference frame has real part only, the torque can be derived as

$$\tau_{+} = p\left|\bar{\lambda}_{s+dq}\right| i_{s+q}\,. \tag{5.24}$$

Similarly, by defining a negative sequence stator reactive power Q_{s-} as

$$Q_{s-} = \mathrm{Im}\left(\bar{v}_{s-dq}\,\bar{i}^{*}_{s-dq}\right), \tag{5.25}$$

or equivalently,

$$Q_{s-} = \mathrm{Im}\left(\bar{v}_{s-\alpha\beta}\,\bar{i}^{*}_{s-\alpha\beta}\right), \tag{5.26}$$

then by substituting (5.18) into (5.25), the negative sequence stator reactive power becomes

$$Q_{s-} = -\omega_s \left|\bar{\lambda}_{s-dq}\right| i_{s-d} \,. \tag{5.27}$$

Moreover, the negative sequence torque can be defined as

$$\tau_{-} = -\mathrm{Im}\left(\bar{\lambda}_{s-\alpha\beta}\,\bar{i}^{*}_{s-\alpha\beta}\right)p = -\mathrm{Im}\left(\bar{\lambda}_{s-dq}\,\bar{i}^{*}_{s-dq}\right)p \,, \tag{5.28}$$

which can be derived as

$$\tau_{-} = p\left|\bar{\lambda}_{s-dq}\right| i_{s-q} \,. \tag{5.29}$$

As the real and imaginary parts of the stator currents are proportional to the stator reactive powers and torques, the second objective of minimizing the stator real power, reactive power, or the torque ripples can be realized by regulating the negative sequence stator reactive power and torque.

Fig. 5.3 shows the overall control system of the DFIG. Park transformation is performed on the rotor current to change the rotor current from the rotor reference frame to the stator reference frame. The positive and negative sequence components of the stator voltage, stator current, and rotor current are then extracted for the computation of the positive and negative sequence reactive power, torque, and flux angle. The reactive power and torque are compared with their reference values, whereas the negative sequence reference values are derived from the positive

sequence reference values and the ratio of the magnitude of the positive sequence flux to the magnitude of the negative sequence flux. The proportional-integral controllers and the integral controllers are used to compute the required rotor voltages from the differences between feedback and reference values. The sum of the positive and negative sequence voltages is modulated with SVM to act on the rotor winding.

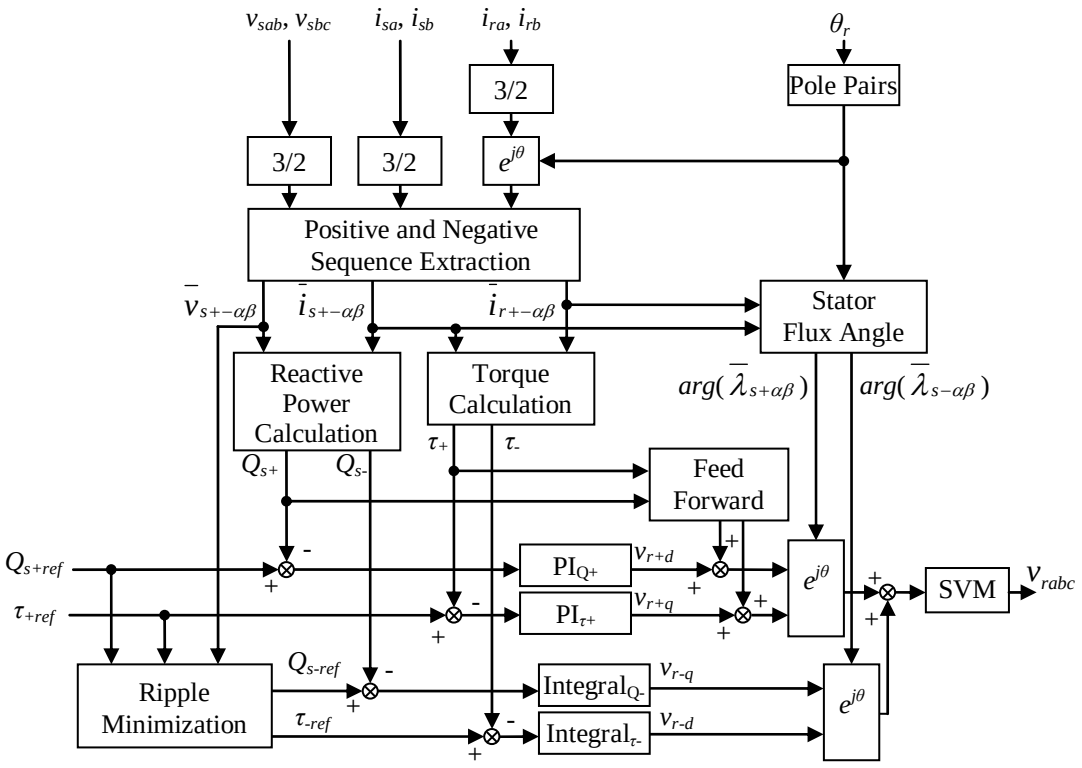

Fig. 5.3 Direct torque control system for DFIG with voltage unbalance

5.3.1 Ripple Minimization

Terms with exponents in (5.16) contribute to torque ripples from the negative sequence components. The torque ripples τ_{ripple} can be expressed as

$$\tau_{ripple} = -\mathrm{Im}(\bar{\lambda}_{s-dq}\bar{i}^{*}_{s+dq}e^{-j2\omega_s t}e^{j\angle\lambda_{s+-}} + \bar{\lambda}_{s+dq}\bar{i}^{*}_{s-dq}e^{j2\omega_s t}e^{-j\angle\lambda_{s+-}})\,p\,. \qquad (5.30)$$

Expanding the exponents, the torque ripple terms become

$$\begin{aligned}\tau_{ripple} = -(&\left|\overline{\lambda}_{s-dq}\right| i_{s+d} \sin\left(-2\omega_s t + \angle\lambda_{s+-}\right) + \left|\overline{\lambda}_{s+dq}\right| i_{s-d} \sin\left(2\omega_s t - \angle\lambda_{s+-}\right) \\ &- \left|\overline{\lambda}_{s-dq}\right| i_{s+q} \cos\left(-2\omega_s t + \angle\lambda_{s+-}\right) - \left|\overline{\lambda}_{s+dq}\right| i_{s-q} \cos\left(2\omega_s t - \angle\lambda_{s+-}\right))\, p\end{aligned} . \quad (5.31)$$

There are no ripples if i) the coefficients of the first two terms are equal, and ii) the coefficients of the last two terms are equal in magnitude and opposite in sign. Equating the coefficients of the first two terms of (5.31) yields

$$\left|\overline{\lambda}_{s-dq}\right| i_{s+d} = \left|\overline{\lambda}_{s+dq}\right| i_{s-d} . \quad (5.32)$$

Multiplying both sides with the positive sequence stator flux, negative sequence stator flux, and the synchronous frequency, and rearranging, (5.32) becomes

$$\omega_s \left|\overline{\lambda}_{s+dq}\right| i_{s+d} = \left(\left|\overline{\lambda}_{s+dq}\right| / \left|\overline{\lambda}_{s-dq}\right|\right)^2 \omega_s \left|\overline{\lambda}_{s-dq}\right| i_{s-d} . \quad (5.33)$$

Substitutions of (5.21) and (5.27) into (5.33) gives

$$Q_{s+} = -\left(\left|\overline{\lambda}_{s+dq}\right| / \left|\overline{\lambda}_{s-dq}\right|\right)^2 Q_{s-} . \quad (5.34)$$

By defining a negative sequence ratio n_{+-} as the ratio of the magnitude of the negative sequence flux to the magnitude of the positive sequence flux

$$n_{+-} = \frac{\left|\overline{\lambda}_{s-dq}\right|}{\left|\overline{\lambda}_{s+dq}\right|}, \quad (5.35)$$

the required negative sequence reactive power becomes

$$Q_{s-} = -n_{+-}^2 Q_{s+} . \tag{5.36}$$

If the coefficients of the last two terms of (5.31) have the same magnitude, but opposite in sign, they become

$$\left|\overline{\lambda}_{s-dq}\right| i_{s+q} = -\left|\overline{\lambda}_{s+dq}\right| i_{s-q} . \tag{5.37}$$

Multiplying both sides with the positive sequence stator flux, negative sequence stator flux, and the number of pole pairs, (5.37) becomes

$$p\left|\overline{\lambda}_{s+dq}\right| i_{s+q} = -\left(\left|\overline{\lambda}_{s+dq}\right| / \left|\overline{\lambda}_{s-dq}\right|\right)^2 p\left|\overline{\lambda}_{s-dq}\right| i_{s-q} . \tag{5.38}$$

Substituting (5.24), (5.29), and (5.35) into (5.38), the relationship between the negative and positive sequence torque for minimal torque ripples becomes

$$\tau_- = -n_{+-}^2 \tau_+ . \tag{5.39}$$

Therefore, (5.36) and (5.39) define the conditions for minimal torque ripples from unbalanced voltage.

As for the reactive power ripples $Q_{s\ ripple}$, they can be expressed as the imaginary parts of the last two terms of (5.13):

$$Q_{s\ ripple} = \mathrm{Im}\left(\overline{v}_{s-dq}\, \overline{i}_{s+dq}^{*} e^{-j2\omega_s t} e^{j\angle\lambda_{s+-}} + \overline{v}_{s+dq}\, \overline{i}_{s-dq}^{*} e^{j2\omega_s t} e^{-j\angle\lambda_{s+-}}\right) \tag{5.40}$$

Substituting (5.17) and (5.18) into (5.40) and expanding, the reactive power ripples become

$$Q_{s\,ripple} = \omega_s(-\left|\bar{\lambda}_{s-dq}\right| i_{s+q} \sin(-2\omega_s t + \angle\lambda_{s+-}) + \left|\bar{\lambda}_{s+dq}\right| i_{s-q} \sin(2\omega_s t - \angle\lambda_{s+-}) \\ -\left|\bar{\lambda}_{s-dq}\right| i_{s+d} \cos(-2\omega_s t + \angle\lambda_{s+-}) + \left|\bar{\lambda}_{s+dq}\right| i_{s-d} \cos(2\omega_s t - \angle\lambda_{s+-})) \quad (5.41)$$

To obtain no ripples, the coefficients of the first two terms of (5.41) should be equal, which is the same as (5.37), and the coefficients of the last two terms of (5.41) should be equal but with opposite sign, which is equivalent to (5.32). Therefore, the conditions for minimal reactive power ripples are the same as the conditions for minimal torque ripples, as given in (5.36) and (5.39).

Similarly, the expression for the stator real power ripples $P_{s\,ripple}$ is the real parts of the last two terms of (5.13):

$$P_{s\,ripple} = \mathrm{Re}\left(\bar{v}_{s-dq}\bar{i}^{*}_{s+dq}e^{-j2\omega_s t}e^{j\angle\lambda_{s+-}} + \bar{v}_{s+dq}\bar{i}^{*}_{s-dq}e^{j2\omega_s t}e^{-j\angle\lambda_{s+-}}\right) \quad (5.42)$$

Replacing the stator voltages with (5.17)and (5.18), (5.42) becomes

$$P_{s\,ripple} = \omega_s(\left|\bar{\lambda}_{s-dq}\right| i_{s+d} \sin(-2\omega_s t + \angle\lambda_{s+-}) - \left|\bar{\lambda}_{s+dq}\right| i_{s-d} \sin(2\omega_s t - \angle\lambda_{s+-}) \\ -\left|\bar{\lambda}_{s-dq}\right| i_{s+q} \cos(-2\omega_s t + \angle\lambda_{s+-}) + \left|\bar{\lambda}_{s+dq}\right| i_{s-q} \cos(2\omega_s t - \angle\lambda_{s+-})) \quad . \quad (5.43)$$

For minimal stator real power ripples, the following two conditions have to be fulfilled:

$$\left|\bar{\lambda}_{s-dq}\right| i_{s+d} = -\left|\bar{\lambda}_{s+dq}\right| i_{s-d} \quad (5.44)$$

$$\left|\bar{\lambda}_{s-dq}\right| i_{s+q} = \left|\bar{\lambda}_{s+dq}\right| i_{s-q} \quad (5.45)$$

As (5.44) and (5.45) are similar to (5.32) and (5.37) respectively, but with opposite signs on their right hand sides, the following conditions for minimal stator real power ripples can be similarly derived:

$$Q_{s-} = n_{+-}^2 Q_{s+} \tag{5.46}$$

$$\tau_{-} = n_{+-}^2 \tau_{+} \tag{5.47}$$

5.3.2 Positive and Negative Sequence Extraction

The positive and negative sequence components of the stator voltage, stator and rotor currents have to be extracted for the subsequent computation of the positive sequence and negative sequence stator reactive power, torque and flux. The extraction method is based on [75], but without the need to have harmonic and zero sequence detections. To perform the sequence component extraction, the stator voltage defined in (5.1) is firstly delayed for one-fourth of the fundamental period:

$$\bar{v}_{s\alpha\beta 90} = \bar{v}_{s+} e^{j\omega_s (t-\pi/2\omega_s)} + \bar{v}_{s-} e^{-j\omega_s (t-\pi/2\omega_s)} \tag{5.48}$$

The sum of the original stator voltage and the product of the delayed voltage and *j* becomes

$$\bar{v}_{s\alpha\beta} + j\bar{v}_{s\alpha\beta 90} = \left(\bar{v}_{s+} e^{j\omega_s t} + \bar{v}_{s-} e^{-j\omega_s t}\right) + j\left(\bar{v}_{s+} e^{j\omega_s (t-\pi/2\omega_s)} + \bar{v}_{s-} e^{-j\omega_s (t-\pi/2\omega_s)}\right), \tag{5.49}$$

which can be simplified and rearranged to yield the instantaneous positive sequence stator voltage:

$$\bar{v}_{s+\alpha\beta} = \left(\bar{v}_{s\alpha\beta} + j\bar{v}_{s\alpha\beta 90}\right)/2 \tag{5.50}$$

Hence, the positive sequence stator voltage component rotating in the stator frame can be computed from the instantaneous and delayed stator voltages. Similarly, the difference between the original stator voltage and the product of the delayed voltage and *j* becomes

$$\bar{v}_{s\alpha\beta} - j\bar{v}_{s\alpha\beta 90} = \left(\bar{v}_{s+}e^{j\omega_s t} + \bar{v}_{s-}e^{-j\omega_s t}\right) - j\left(\bar{v}_{s+}e^{j\omega_s (t-\pi/2\omega_s)} + \bar{v}_{s-}e^{-j\omega_s (t-\pi/2\omega_s)}\right). \quad (5.51)$$

Simplifying (5.51) gives the instantaneous negative sequence stator voltage:

$$\bar{v}_{s-\alpha\beta} = \left(\bar{v}_{s\alpha\beta} - j\bar{v}_{s\alpha\beta 90}\right)/2 \quad (5.52)$$

The scheme shown in Fig. 5.4 is used to extract the positive and negative components of the stator voltage. The scheme is also applied to the stator and rotor currents in the stator frame.

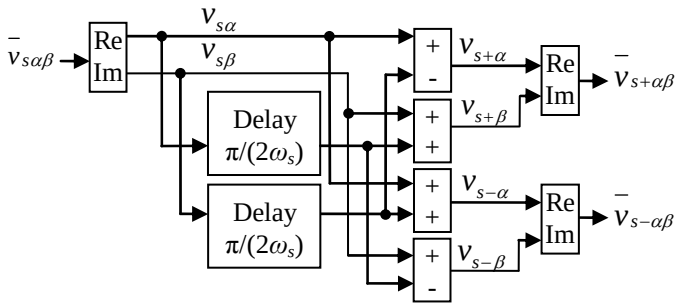

Fig. 5.4 Extraction of positive and negative sequence components

5.3.3 Control of Sequence Components

As equations governing the positive sequence components, as shown in (5.6)–(5.9), (5.19) and (5.24), are the same as (3.4)–(3.9), the control strategy developed in Chapter 4 can be used to control the positive sequence component reactive power and torque. However, the control of the negative sequence

components is different from that of the positive sequence components. With the derivation of the transfer equation similar to that shown in section 4.3.1, the following equation for the negative sequence components can be obtained:

$$\begin{pmatrix} \delta v_{rd-}(s) \\ \delta v_{rq-}(s) \end{pmatrix} = \frac{L_{s\sigma} + L_m}{L_m \left| \bar{\lambda}_{s-dq} \right|} \begin{pmatrix} \dfrac{R_r + sL_{rk}}{\omega_s} & -\dfrac{L_{rk}(\omega_s + p\omega_r)}{p} \\ -\dfrac{L_{rk}(\omega_s + p\omega_r)}{\omega_s} & -\dfrac{R_r + sL_{rk}}{p} \end{pmatrix} \begin{pmatrix} \delta Q_{s-}(s) \\ \delta \tau_{-}(s) \end{pmatrix} \quad (5.53)$$

The corresponding RGA at zero frequency is

$$\frac{1}{R_r^{\,2} + (\omega_s + p\omega_r)^2 L_{rk}^{\,2}} \begin{pmatrix} R_r^{\,2} & (\omega_s + p\omega_r)^2 L_{rk}^{\,2} \\ (\omega_s + p\omega_r)^2 L_{rk}^{\,2} & R_r^{\,2} \end{pmatrix}. \quad (5.54)$$

Substituting the parameters as listed in the Appendices into (5.54), the numerical result of the RGA is computed for the DFIG operating at synchronous frequency as

$$\begin{pmatrix} 0.0381 & 0.9619 \\ 0.9619 & 0.0381 \end{pmatrix}. \quad (5.55)$$

Similar results would be obtained if the DFIG operates at other rotor speeds in the vicinity of the synchronous frequency. Unlike the RGA for the positive sequence components, the off-diagonal elements are much larger than the diagonal elements for negative sequence components. It implies that the negative sequence reactive power interacts closely with the imaginary part of the negative sequence rotor voltage, while the negative sequence torque and the real part of the negative sequence rotor voltage are strongly correlated. Therefore, the negative sequence reactive power should be controlled by the imaginary part of the negative sequence

rotor voltage, and the torque should be controlled by the real part of the rotor voltage. As the off diagonal elements in (5.53) have no transient terms, the integral controllers implemented in accordance to (5.56) and (5.57) would give rise to first order closed-loop step responses.

$$v_{r-q} = -\frac{L_{rk}\left(\omega_s + p\omega_r\right)\left(L_{s\sigma} + L_m\right)}{L_m\left|\overline{\lambda}_{s-dq}\right|\omega_s T_{cl}}\int\left(Q_{s-ref} - Q_{s-}\right)dt \tag{5.56}$$

$$v_{r-d} = -\frac{L_{rk}\left(\omega_s + p\omega_r\right)\left(L_{s\sigma} + L_m\right)}{L_m\left|\overline{\lambda}_{s-dq}\right|pT_{cl}}\int\left(\tau_{-ref} - \tau_{-}\right)dt \tag{5.57}$$

(5.26) and (5.28) are used to compute the negative sequence reactive power and torque from the voltage, current and flux in the stator reference frame.

5.4 Simulation Results

The proposed scheme is simulated with Matlab/Simulink. The DFIG, with parameters as listed in the Appendices, operates at 1400 RPM with phase A and phase B voltages at the nominal values. The phase C voltage is reduced to introduce an unbalanced three-phase voltage source with a negative sequence ratio of 0.1. The closed-loop time constant of the control loops is 0.05 s. The simulation results with torque and reactive power ripple minimization are shown in Fig. 5.5. The reference torque and reactive power are the values of the positive sequence references, while the measured values are the instantaneous values calculated with (5.12) and (5.15). Throughout the simulation, the torque remains at the reference value of -4 Nm with no ripples. The average value of the stator real power is -580 W and the amplitude of the power ripples at twice synchronous frequency is 232 W from the simulation time of 0 s to 0.5 s. The reactive power follows the step change in the reactive power

reference from 1000 VAR to 600 VAR at the simulation time of 0.5 s. The reactive power possesses no ripples in the simulation. As indicated in (5.21) and (5.27), the reactive power is dependent on the real part of the stator current, which contributes to the stator real power ripples as the first two terms in (5.43). Therefore, the amplitude of the stator real power ripple is reduced from 232 W to 171 W when the reactive power decreases from 1000 VAR to 600 VAR.

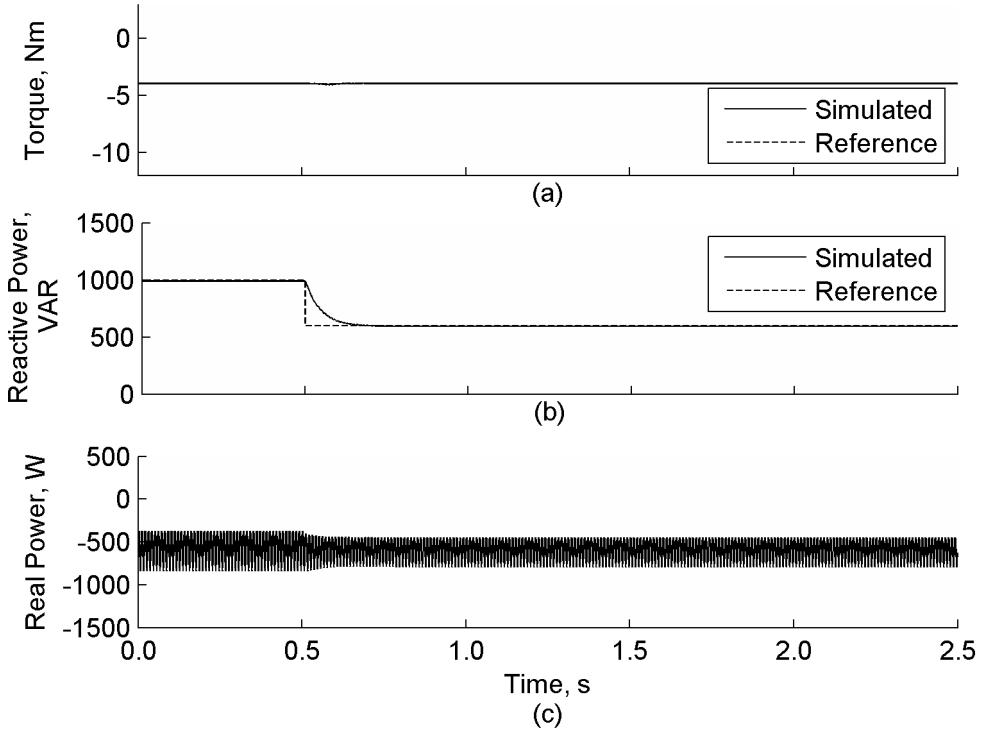

Fig. 5.5 Simulation results with torque and reactive power ripple minimization

(a) Torque, (b) Reactive power, (c) Stator real power

With similar simulation settings, the operation of the DFIG with stator real power ripple minimization is simulated, with the results as shown in Fig. 5.6. The DFIG generates a stator real power of 600 W without ripples. The average torque is at the positive sequence reference of -4 Nm, while the average reactive power follows the step change in the reference from 1000 VAR to 600 VAR. The

amplitudes of the torque and reactive power ripples are changed from 1.46 Nm to 1.08 Nm and from 222 VAR to 173 VAR, respectively, as the reactive power reference changes.

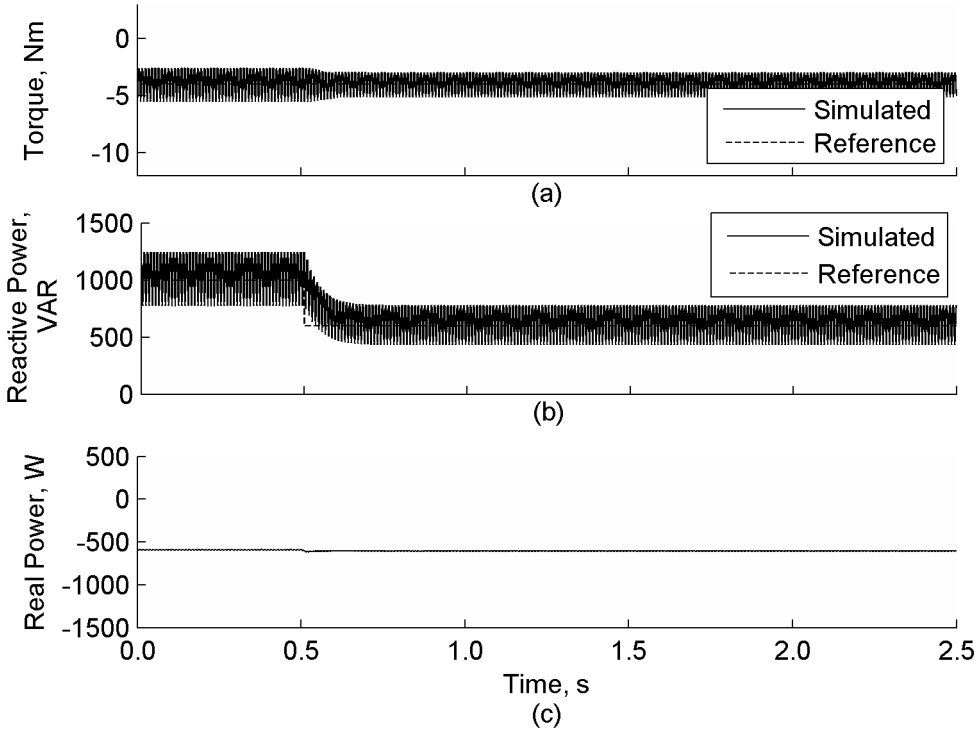

Fig. 5.6 Simulation results with stator real power ripple minimization

(a) Torque, (b) Reactive power, (c) Stator real power

5.5 Experimental Results

An experimental setup similar to Fig. 3.9, as shown in Fig. 5.7, is used to verify the proposed algorithm. A-phase and B-phase of the stator windings of the DFIG are directly connected to the three-phase mains at the rated voltage, and the Phase C winding is connected to the output of the auto-transformer, which attenuates the voltage from the mains to provide an unbalanced three-phase voltage to the DFIG, with a negative sequence ratio of 0.1.

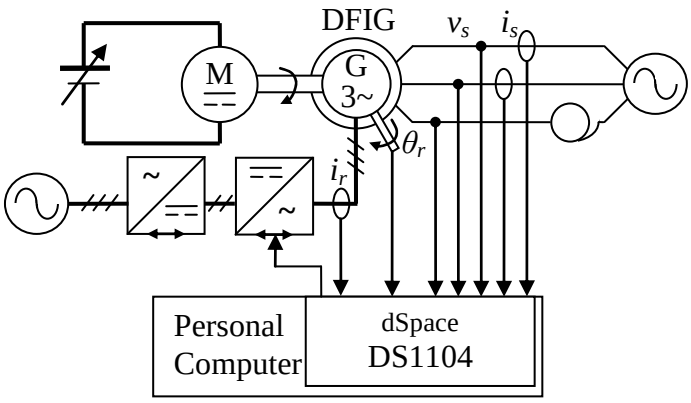

Fig. 5.7 Experimental setup

The experimental results for the DFIG operating at 1418 RPM with torque and reactive power ripple minimization, together with the simulation results are shown in Fig. 5.8 and Fig. 5.9. The average torque is regulated to the reference level of -4 Nm in the experiment. The average reactive power tracks the step change in reactive power from 1000 VAR to 600 VAR at 0.5 s. The DFIG generates an average stator power of 535 W. The amplitudes of the 100 Hz ripples in the torque and reactive power are 0.64 Nm and 28 VAR, respectively. The amplitude of the 100 Hz ripples of the stator real power is changed from 190 W to 125 W as the reactive power decreases. Fig. 5.10 and Fig. 5.11 show the experimental and simulation results of the DFIG operating with stator real power ripple minimization. The average torque, reactive power and stator real power are analogous to that of the DFIG operating with torque and reactive power ripple minimization. However, the amplitudes of the 100 Hz ripples of the torque, reactive power and the stator real power are 1.65 Nm, 135 VAR, and 12 W, respectively. The simulation results are very similar to the experimental results, which implies that the experimental results and the theoretical derivations are strongly correlated.

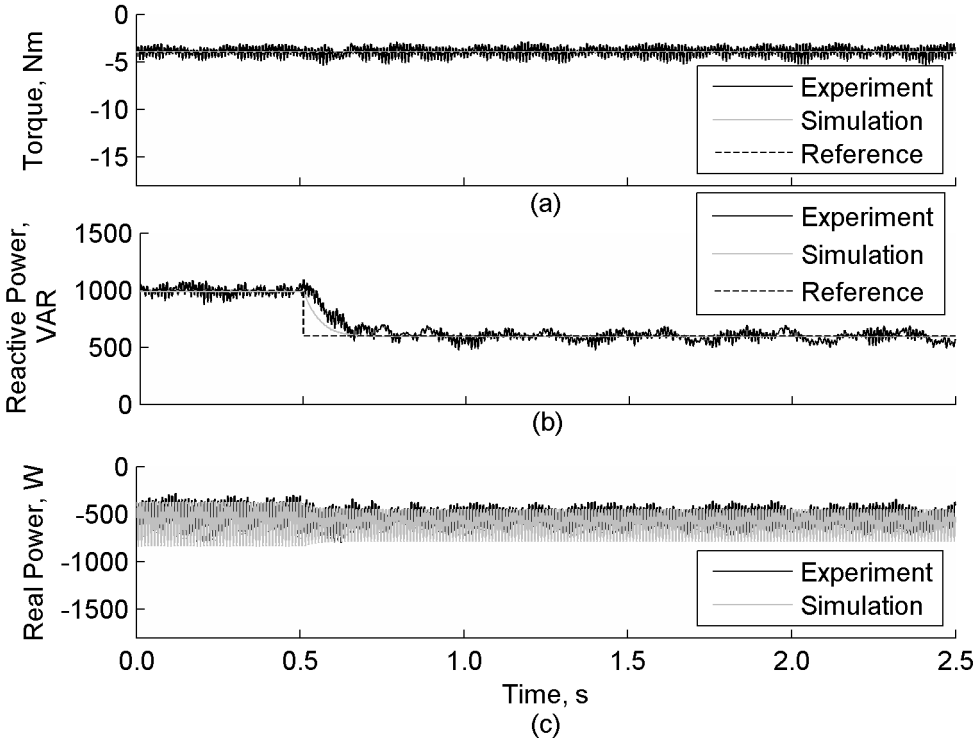

Fig. 5.8 Results with torque and reactive power ripple minimization

(a) Torque, (b) Reactive power, (c) Stator real power

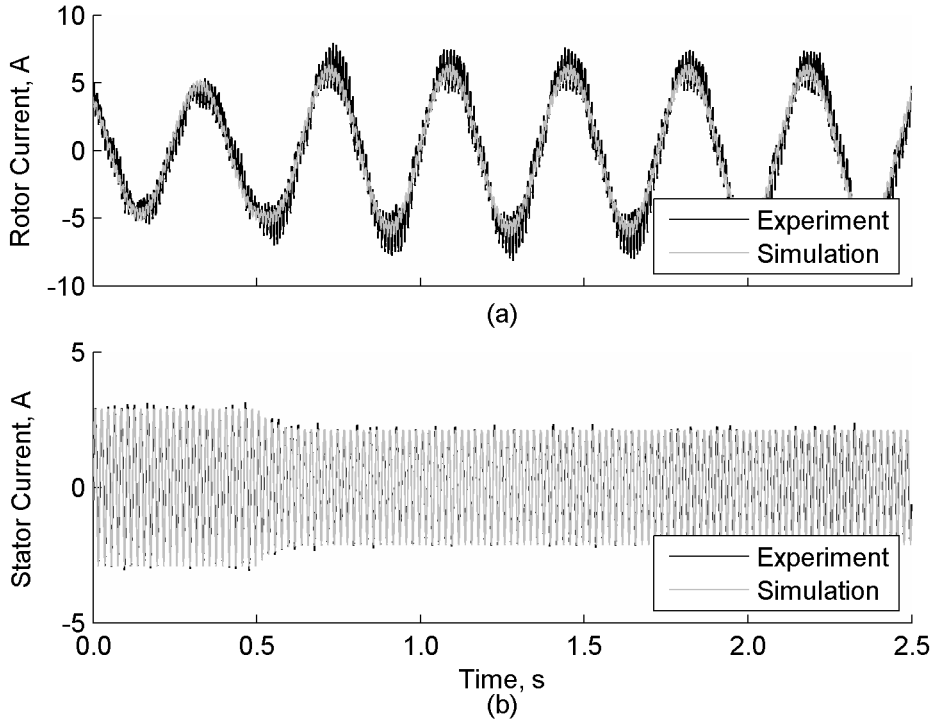

Fig. 5.9 Results with torque and reactive power ripple minimization

(a) Rotor current, (b) Stator current

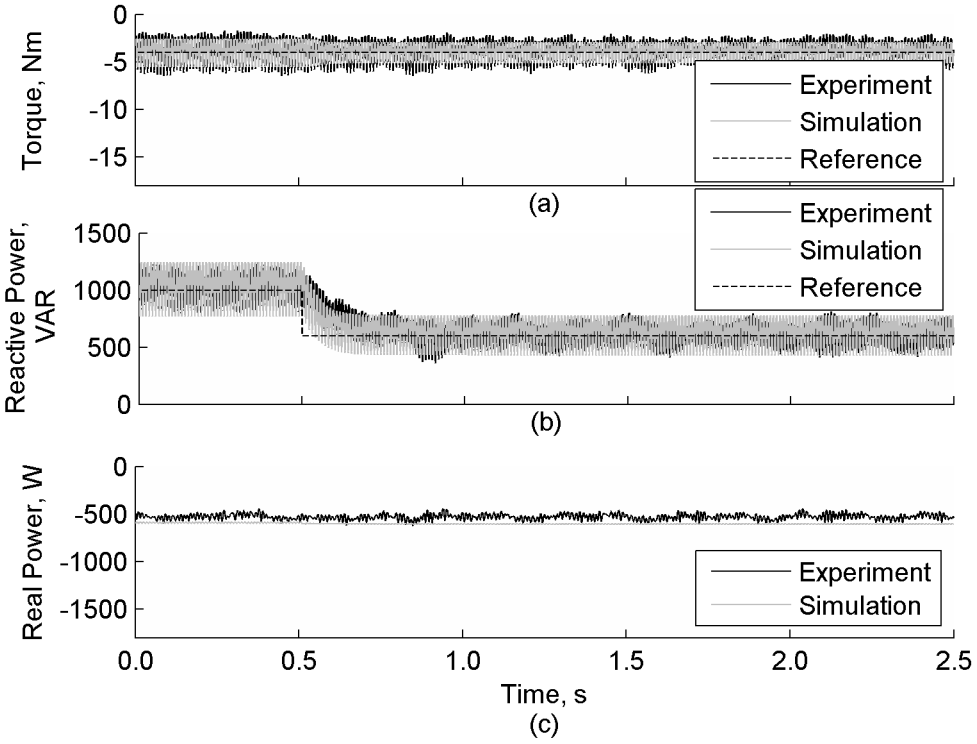

Fig. 5.10 Results with stator real power ripple minimization

(a) Torque, (b) Reactive power, (c) Stator real power

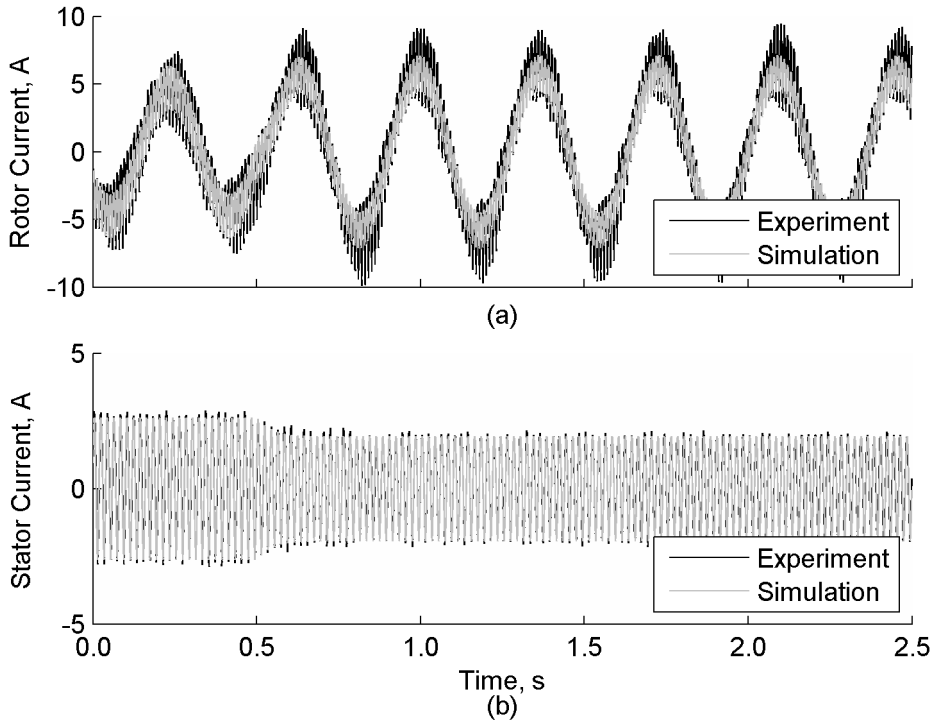

Fig. 5.11 Results with stator real power ripple minimization

(a) Rotor current, (b) Stator current

A control experiment with the algorithm, designed for balanced grid only as developed in Chapter 3, and a setup as shown in Fig. 5.7 is built to facilitate information collection on the operation of the DFIG. Since a balanced grid should have positive sequence voltage only, the direct torque control algorithm for the control experiment is implemented with neither sequence component extraction nor negative sequence component control. The torque and reactive power are calculated from the instantaneous voltage and current, and regulated by the controllers. The average and 100 Hz components of the torque, reactive and stator real power with different minimization objectives and in the control experiment are shown in

Table 5.1. The positive sequence torque and reactive power references are -8 Nm and 1000 VAR respectively, while the DFIG operates at 1400 RPM. The 100 Hz components of the torque, reactive power, and stator real power in the control experiment are 100 %, 121 %, and 105 % of their respective average components. The 100 Hz components in the control experiment are much higher than those using the proposed algorithm. It is because the 100 Hz components in the control experiment, which are comparable to the average components, are due to stator flux angle oscillations, which in turn introduce a fluctuating rotor voltage and thereby generate oscillations in torque, reactive power, and stator real power. However, with the proposed algorithm, the positive and negative sequence components of the stator flux are extracted to provide stable flux reference angles.

Table 5.1 Amplitudes of the average and 100 Hz components in the torque, reactive and stator real power

Ripples being minimized	Torque (Nm)		Reactive power (VAR)		Stator real power (W)	
	Average	100 Hz	Average	100 Hz	Average	100 Hz
Torque and reactive power	7.91	1.26	792	46	1024	203
Stator real power	8.08	2.77	808	184	1012	25
Control experiment	8.74	8.74	823	996	934	977

5.6 Summary

The direct torque control of DFIG operating with an unbalanced network has been presented. The mathematical model describing the interaction between the individual sequence components forms the basis of the control algorithm. Since the algorithm extracts the positive sequence and negative sequence torque and reactive power, and controls them independently, the DFIG can operate stably with an unbalanced network. The torque, reactive power, and stator real power ripples are introduced by the cross coupling between the sequence components of stator current, stator voltage, and stator flux. Therefore, proper coordination of the sequence components of the stator current, and hence the torque and reactive power, must be realized in order to minimize the corresponding ripples. When compared with existing algorithms for DFIGs operating in grids with unbalanced voltage, the direct feedback of the torque and reactive power used in the proposed algorithm avoids the need to align the stator current with the stator flux so as to alleviate the computational burden of the controller. The tuning of the controller using the proposed algorithm is simpler than its multi-loop counterpart. The simulation results show that either the torque and reactive power ripples, or the stator real power

ripples can be eliminated. Experimental verification provides a high degree of correlation with the simulation results. Both simulation and experimental results match the theoretical derivations well. The harmonic components of the torque, reactive power, and the stator real power confirm that the ripples, attributed to unbalance in the stator voltage, at twice mains frequency, can be substantially minimized with the proposed algorithm. Compared with algorithms designed for DFIGs operating under balanced grids only, the proposed algorithm has significantly reduced the ripples because of the extraction and the use of sequence components. The experimental results also demonstrate that the algorithm performs well in practice, and is not affected by noises from the measurement and the environment.

6 Conclusions and Further Development

In the research, direct control algorithms for i) synchronization of DFIGs to grids, ii) electric power generation of DFIGs connected to infinite bus bars, iii) power generation to grids with high source impedance, and iv) power generation to grids with unbalanced voltage are developed. All the theoretical derivations are supported by computer simulation and validated by experimental verifications.

As single-loop designs are employed in the algorithms being developed in the research, the closed-loop bandwidths of the systems are higher than those of multi-loop designs. The number of parameters and hence the effort to tune the controllers, and the computational burden of the controllers are greatly reduced in the proposed single-loop designs. Unlike other direct control schemes, the proposed algorithms employ constant switching frequencies, from which the generated harmonics and switching loss can be predicted easily. The sampling frequencies of the proposed algorithm are lower than those required by other direct control algorithms.

6.1 Synchronization to Power Grids

Direct voltage control for synchronization of DFIG is proposed in Chapter 2. The algorithm utilizes direct feedback and control of the stator voltage to track the reference voltage generated from the grid voltage. The proposed single loop design eliminates the current control loops in cascaded designs, but preserves the voltage feedback, to ensure that the magnitude, phase and frequency of the stator voltage are the same as those of the grid voltage after synchronization. Therefore, the impacts to

the power systems, at the instant at which the DFIGs are connected to the grids, are minimized.

Theoretical derivation and simulation study show that, even if a constant high switching frequency is employed in the proposed scheme, the switching operation of the rotor side converters will impress voltages composing of both high and low frequency components to the rotor windings, this in turn will induce a stator voltage comprising of high and low frequency components. To reduce the switching harmonics in the stator voltage, filtering capacitors are added to avoid possible errors due to harmonics.

Experimental results show that the algorithm is capable of rapidly synchronizing a DFIG to the grid, over a wide range of operating speed of the DFIG, and the algorithm is immune to noises in a practical environment.

6.2 Power Generation in Normal Grids

In Chapter 3, an algorithm for direct torque and reactive power control of DFIGs has been developed. Direct feedback and control of the torque and reactive power are employed in the algorithm. In addition to the elimination of current control loops, the algorithm alleviates the computation burden by reducing the number of Park transformations because the feedback variables, the torque and reactive power, can be computed in the rotor and stator reference frames readily. The transfer equations relating the reactive power, torque and the rotor voltage are derived as first order equations. Consequently, proportional-integral controllers are utilized to provide satisfactory closed-loop responses. The initial conditions of the

controllers are also derived to ensure a smooth transition from synchronization to power generation.

The simulation and experimental results demonstrate that independent control of the reactive power and torque of the DFIG can be achieved with the proposed algorithm over a wide speed range. Changes in turbine speed do not have noticeable effects on the operation of the DFIG. The disturbances on, as well as cross couplings between the torque and reactive power are compensated by the proposed algorithm and do not affect the steady state performances of the DFIG.

6.3 Power Generation in Grids with High Source Impedance

Voltage variations from power systems and their impacts to the operation of DFIGs are addressed in Chapter 4. The transfer equations between the feedback variables, the torque and reactive power, and the output variables, the direct and quadrature rotor voltages, are derived with small signal analysis. The relative gain array shows that the torque and the quadrature rotor voltage are strongly correlated, and the reactive power is related to the direct rotor voltage. For the closely related pairs of variables, they can be linked together to form independent control loops and hence two loops can be formed. In order to improve the control performance, the cross couplings between the torque and reactive power are eliminated with feed-forward compensation of them, so as to improve the system dynamics without the need to compute the direct and quadrature currents in the stator flux reference frame. With the control algorithm derived with internal model control, the closed-loop time constant can be adjusted by tuning the filter time constant of the

internal model controller. The parameters of the controller are adjusted in accordance to the stator flux so as to optimise the performance of the DFIGs even if the grid voltage fluctuates.

Robustness of the algorithm against parameter variations and disturbances is evaluated. It is confirmed that large variations in the controller parameters and the presences of disturbances do not have any detrimental effect on the control performance. Simulation and experimental results indicate that even if the stator voltage fluctuates largely as the reactive power flow changes, the DFIG still operates stably and generates reactive power and torque according to the reference values.

6.4 Power Generation in Grids with Unbalanced Voltage

Direct torque control for DFIGs in grids with unbalanced voltage is developed in Chapter 5. The mathematical model indicates that the stator real power, reactive power and the torque oscillations, at twice synchronous frequency, are originating from i) the cross product between the negative sequence voltage and the positive sequence current, and ii) the cross product between the positive sequence voltage and the negative sequence current. The conditions of minimal torque, real and reactive power ripples are derived from first principles. With the introduction of the positive and negative sequence torques and reactive powers, the conditions of minimal ripples can be interpreted in terms of the sequence torque and reactive power. With the direct and independent control of the positive and negative sequence components of the torque and reactive power, different optimization objectives, including minimization of torque and reactive power ripples, reduction of stator real power ripples and restoration of balanced stator currents, can be achieved even a

high degree of unbalance is present in the grid voltage. As the transfer equations between the torque, reactive power and rotor voltage are slightly different for the positive and negative sequence components, the structures of the controllers have a large degree of diversification for different sequence components.

Experimental verification shows that the proposed algorithm performs well in a practical environment, and whatever the optimization objective is, the proposed algorithm produces much less ripples in torque, stator real power and reactive power when compared to those of their DFIG counterparts operated with algorithms designed for balanced grid voltage only.

6.5 Further Development

Since the synchronization scheme developed in this thesis has compensated for the cross-coupling voltage with the integral action of the controllers only, there are scopes to improve the performance of the controller in terms of disturbance rejection and transients. Even if the response time is not critical during synchronization, it is likely that with the use of advanced control methods, such as internal model control with two degrees of freedom, can be exploited to improve the performance of DFIGs.

In [76], active resistance is introduced to improve disturbance rejection of DFIGs. However, the rotor current in a synchronous frame has to be evaluated in order to implement the active resistance. Active resistance could also be implemented in a direct control manner to further improve the algorithm for DFIGs in grids with voltage fluctuations. Besides, flux damping is proposed in [77] to

improve the stabilities of DFIGs by incorporating flux differential compensation in the rotor current references in FOC. It would be beneficial to employ the compensation in the torque and reactive power references of the direct torque control algorithm to increase the robustness of DFIG systems.

As the popularity of DFIG gains momentum, some features of synchronous generators, for instance the provision of fault currents, toleration of faults and voltage dip ride through [78], have to be implemented in DFIGs to improve the stability of the power systems, as it is no longer sufficient to consider power generation only. Currently, fault ride through of DFIG is implemented with current control [79]. Direct control algorithm to control DFIGs during faults can be developed to reduce the computation time, and hence the response time to faults, so as to protect the DFIGs from possible damages introduced by the faults.

In the proposed algorithm for DFIGs in grids with unbalanced voltage, the source impedance is assumed to be small. However, proper coordination of the unbalanced current can be developed to restore a balanced stator voltage, which should be useful for wind farms with weak grid connection and unbalanced grid voltage. Furthermore, as the proportion of non-linear loads increases in power systems, voltage distortions become severe, especially in networks with significant source impedance. In [80], FOC of DFIGs under distorted voltage is proposed, which requires a coordinate transformation for each of the stator harmonic current to be compensated. Direct algorithm for DFIGs in grid with distorted voltage may be developed to eliminate the possible emission of harmonic currents, without the large amount of coordinate transformation. On the other hand, harmonic current

generations for the restoration of sinusoidal grid voltage may be developed to enhance to power qualities of the wind generation systems.

7 Appendices

7.1 Parameters of the DFIG Being Simulated and Tested

Stator rated voltage: 380 V

Stator rated current: 4.5 A

Rotor rated voltage: 120 V

Rotor rated current: 10 A

Operating frequency: 50 Hz

Synchronous speed: 1500 RPM

Magnetizing inductance per phase (referred to the stator): 0.3498 H

Rotor leakage inductance per phase (referred to the stator): 0.0219 H

Stator leakage inductance per phase: 0.0219 H

Rotor winding resistance per phase (referred to the stator): 5.317 Ω

Stator winding resistance per phase: 2.670 Ω

Stator to rotor turn ratio: 3.03

Thermal insulation class: B (130 °C)

7.2 Methods to determine the DFIG parameters

The resistances are measured as the ratios between the DC voltages and currents. The self-reactances are measured as the open-circuit three-phase AC voltages to currents ratios. The ratio between the inducted voltage and the AC current is the mutual reactance. The square root of the stator to rotor self-reactance ratio is the turn ratio. The product of the mutual reactance and the turn-ratio is the magnetizing reactance. The differences between the self-reactances and the

magnetizing reactance are the leakage reactances. The reactances are divided by the supply frequency in radians to calculate the inductances.

7.3 Parameters of the Transmission Line Being Simulated and Emulated in Chapter 4

Inductance per phase: 0.0497 H

Resistance per phase: 0.412 Ω

7.4 Experimental Circuits

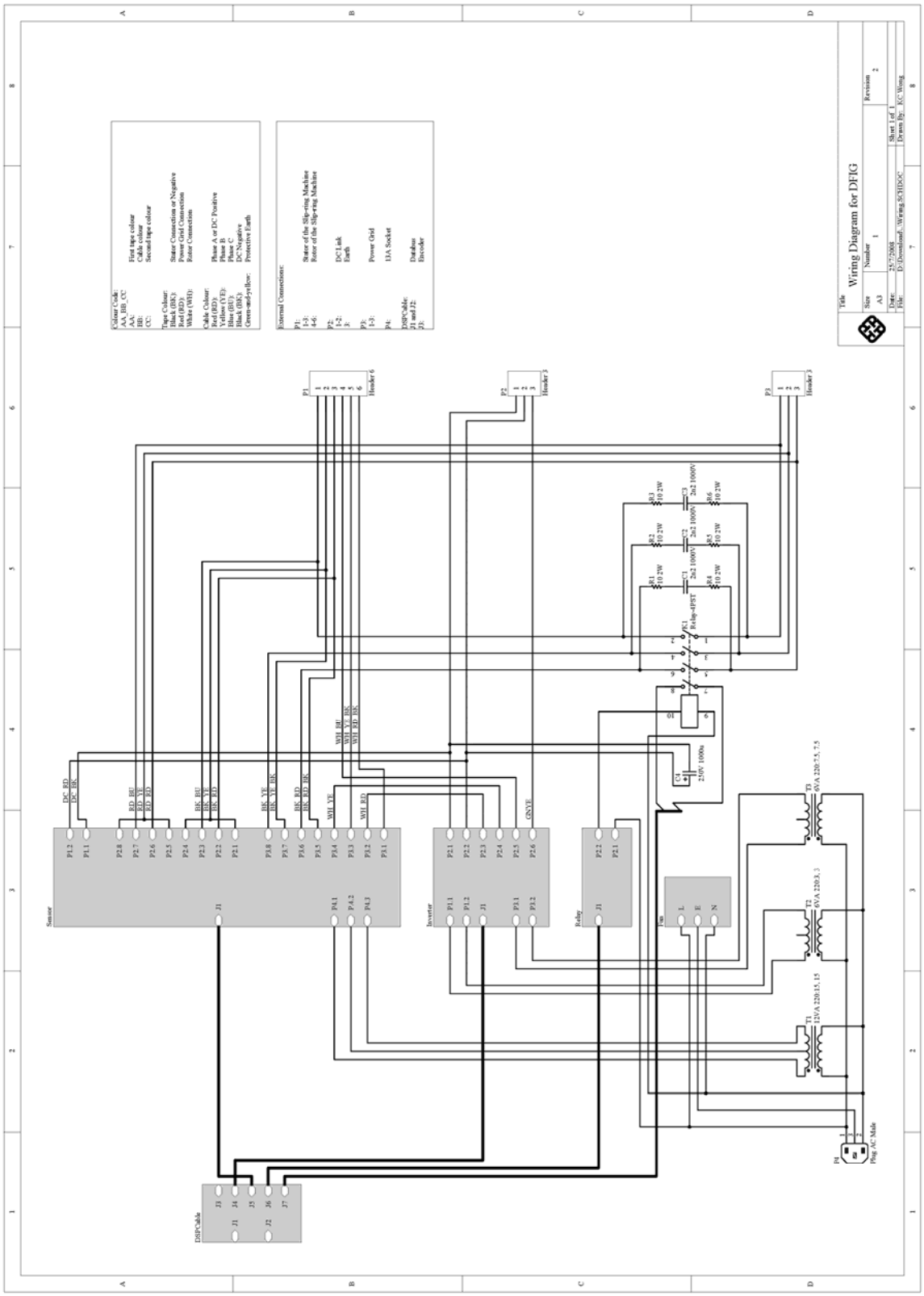

Fig. 7.1 Wiring diagram for DFIG

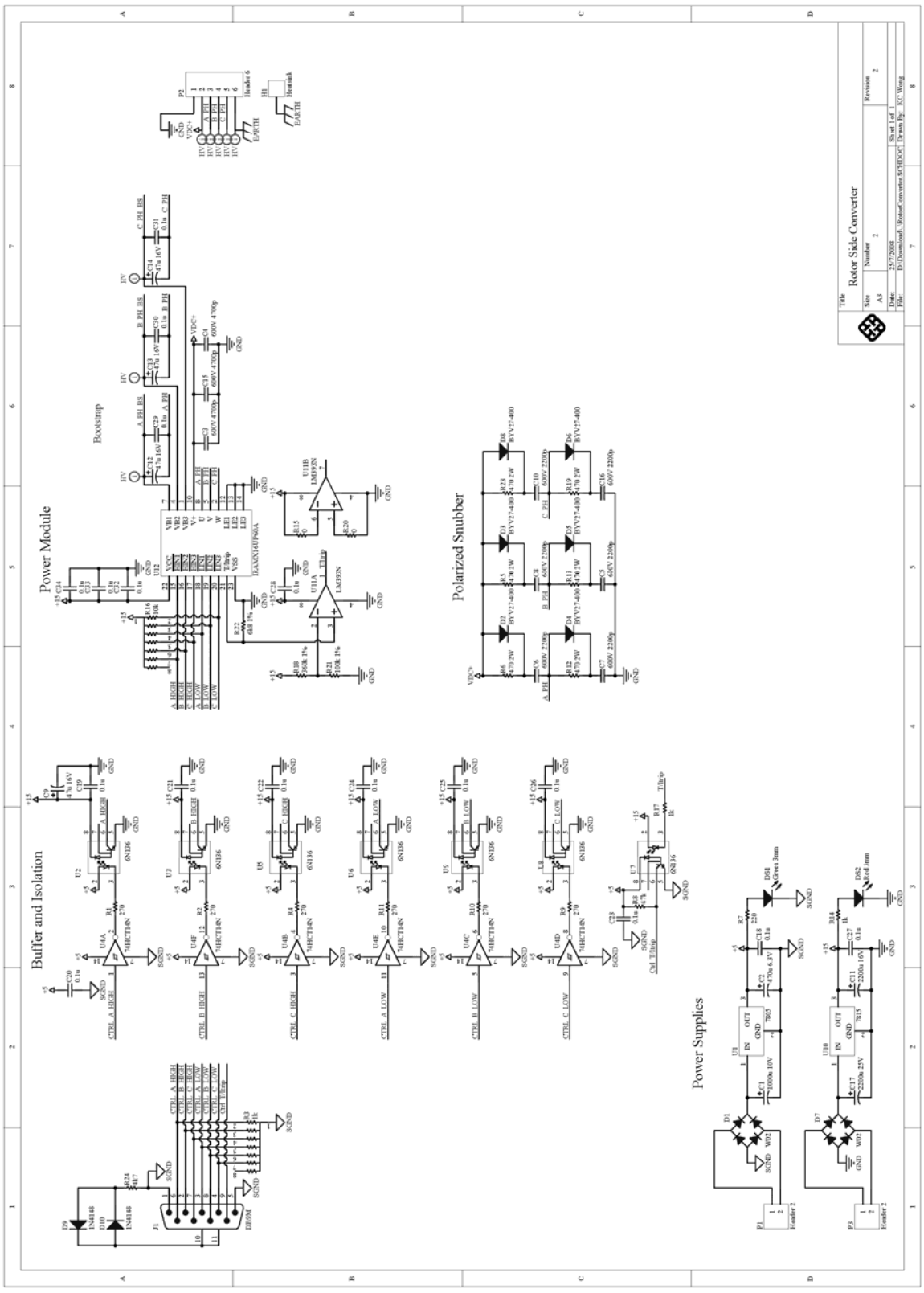

Fig. 7.2 Rotor side converter

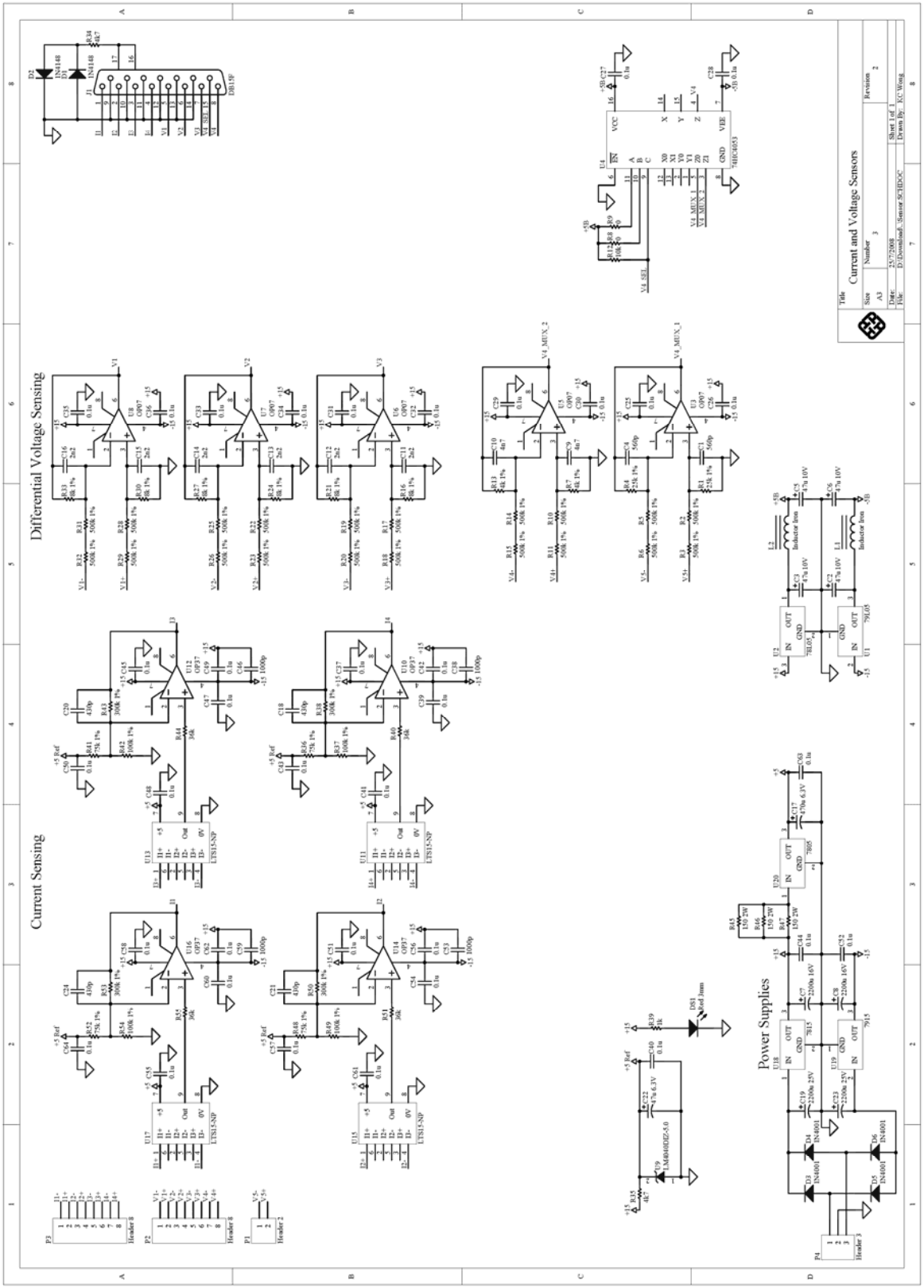

Fig. 7.3 Current and voltage sensors

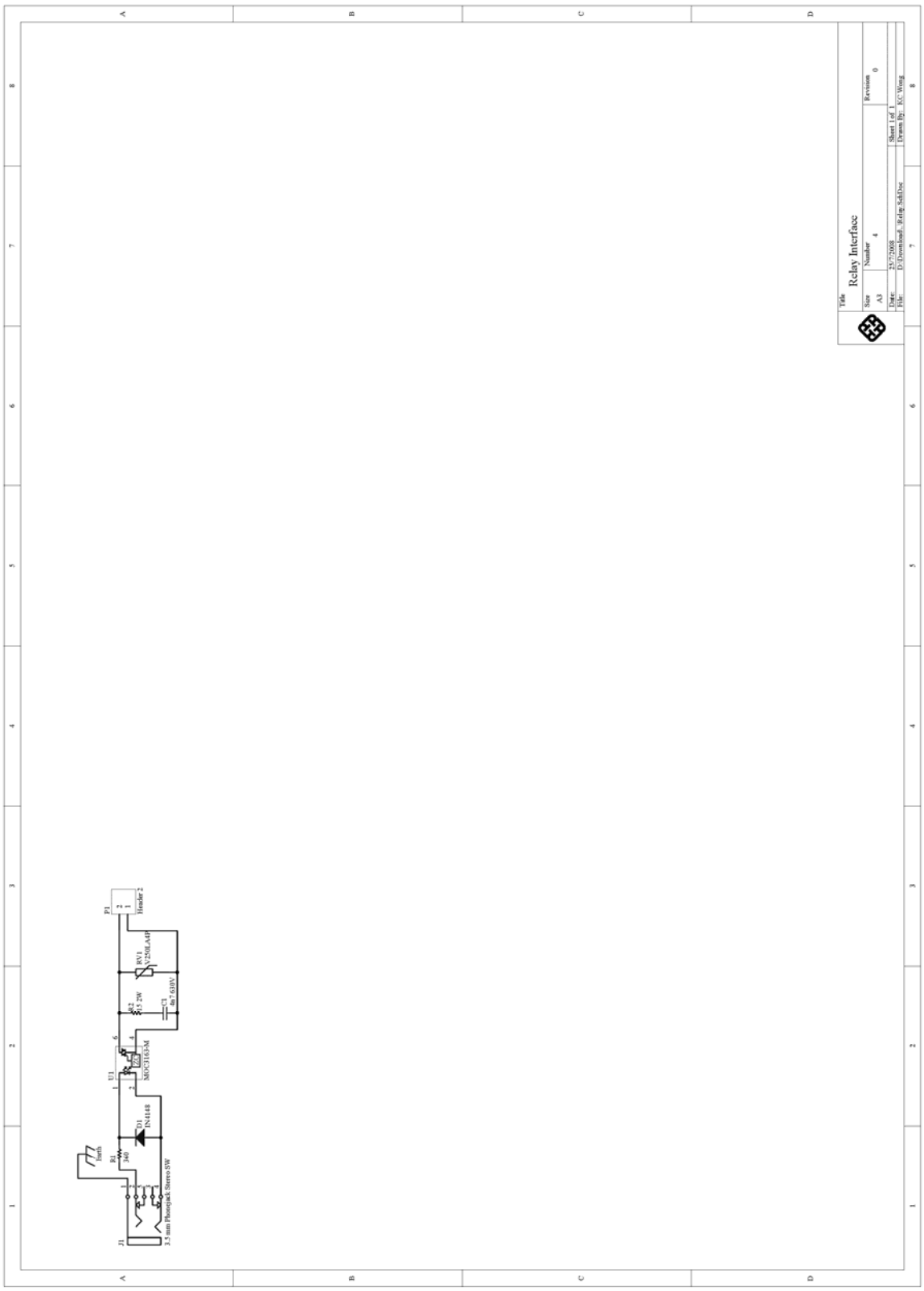

Fig. 7.4 Relay interface

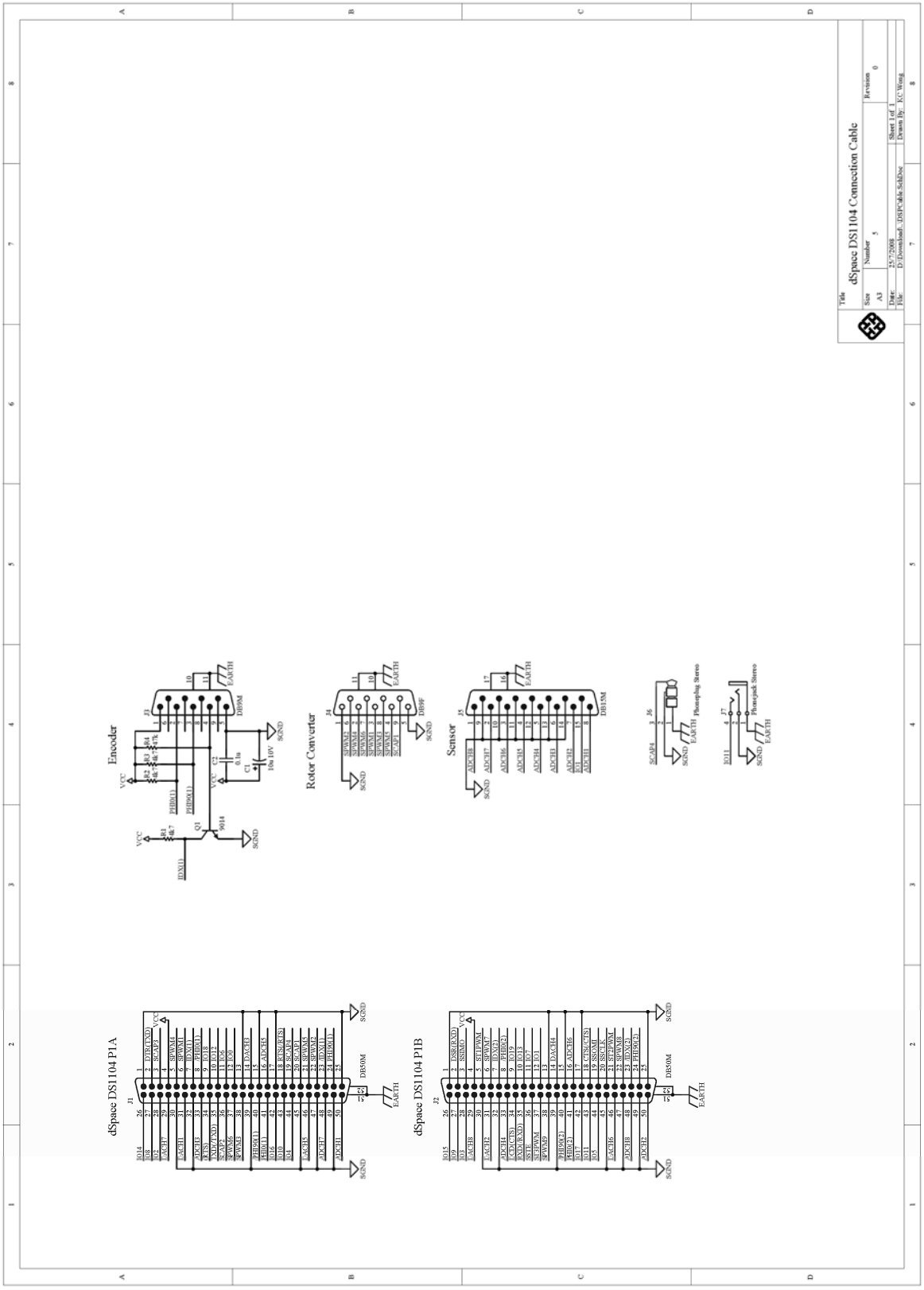

Fig. 7.5 dSpace DS1104 connection cable

8 References

[1] ‘Study on the potential applications of renewable energy in Hong Kong: stage 1 study report’ (Electrical & Mechanical Services Department Government of the Hong Kong Special Administrative Region, 2002)

[2] Mutschler, P., and Hoffmann, R.: ‘Comparison of wind turbines regarding their energy generation’. IEEE 33rd Annual Power Electronics Specialists Conference, Queensland, Australia, June 2002, pp. 6–11

[3] Goodfellow, D., Smith, G.A., and Gardner, G.: ’Control strategies for variable-speed wind energy recovery’. Proc. of 8th British Wind Energy Association Wind Energy Conference, Cambridge, England, 1986, pp. 219–228

[4] Heier, S.: ‘Grid integration of wind energy conversion systems’ (John Wiley and Sons, 2006)

[5] Hansen, A.D., Jauch, C., Sørensen, P., Iov F., and Blaabjerg F.: ‘Dynamic wind turbine models in power system simulation tool DIgSILENT’ (Risø National Laboratory, 2003)

[6] Nicolás, C.V., Blázquez, F., Ramírez, D., Lafoz, M., and Iglesias, J.: ‘Guidelines for the design and control of electrical generator systems for new grid connected wind turbine generators’. Proc. 28th Annual Conference of

the IEEE Industrial Electronics Society, Sevilla, Spain, November 2002, pp. 3317–3325

[7] Chen, H., Mang, C., and Zhao, X.: ‘Research on the switched reluctance wind generator system’. 2001 IEEE International Conference on Systems, Man, and Cybernetics, Arizona, USA ,October 2001, pp. 1936–1941

[8] Ackermann, T.: ‘Wind power in power systems’ (John Wiley and Sons, 2005)

[9] Williamson, S., Ferreira, A.C., and Wallace, A.K.: ’Generalised theory of the brushless doubly-fed machine. Part I. Analysis’, *IEE Proc. Electric Power Applications*, 1997, **144**, (2), pp. 111–122

[10] Hulle, F.V.: ‘Large scale integration of wind energy in the European supply: analysis, issues and recommendations’ (European Wind Energy Association, 2005)

[11] Datta, R., and Ranganathan, V.T.: ‘Variable-speed wind power generation using doubly fed wound rotor induction machine-a comparison with alternative schemes’, *IEEE Trans. Energy Conversion*, 2002, **17**, (3), pp. 414–421

[12] Jones, C.V.: ‘The unified theory of electrical machines’ (Butterworths, 1967)

[13] Tamura, J., Sasaki, T., Ishikawa, S., and Hasegawa, J.: 'Analysis of the steady state characteristics of doubly fed synchronous machines', *IEEE Trans. Energy Conversion*, 1989, **4**, (2), pp. 250–256

[14] Schreier, L., Chomát, M., and Bendl, J.: 'Working regions of adjustable-speed units with doubly fed machines'. IEEE International Electric Machines and Drives Conference, Seattle, USA, May 1999, pp. 457–459

[15] Leonhard, W.: 'Control of electric drives' (Springer-Verlag, 3rd edn. 2001)

[16] Yuan, G., Chai, J., and Li, Y.: 'Vector control and synchronization of doubly fed induction wind generator system'. 4th International Power Electronics and Motion Control Conference, Xi'an, China, August 2004, pp. 886–890

[17] Morel, L., Godfroid, H., Mirzaian, A., and Kauffmann, J.M.: 'Double-fed induction machine: converter optimisation and field oriented control without position sensor', *IEE Proc. Electric Power Applications*, 1998, **145**, (4), pp. 360–368

[18] Park, J., Lee, K., and Kim, D.: 'Control method of a doubly-fed induction generator with automatic grid synchronization'. 32nd Annual Conference on IEEE Industrial Electronics, Paris, France, November 2006, pp. 4254–4259

[19] Xie, Z., Zhang, C.W., Zhang, X., Yang, S.Y., and Cao, R.X.: 'Study on the rotor convertor of doubly fed induction generator used in wind turbine

system'. 2nd IEEE Conference on Industrial Electronics and Applications, Harbin, China, May 2007, pp. 2594–2598

[20] Abo-Khalil, A.G., Lee, D.C., and Ryu, S.P.: 'Synchronization of DFIG output voltage to utility grid in wind power system'. Proc. of the Sixth IASTED International Conference on European Power and Energy Systems, Rhodes, Greece, June 2006, pp. 372–377

[21] Yang, S.Y., Zhang, X., Zhang, C.W., and Chang, L.: 'Development of a variable-speed wind energy conversion system based on doubly-fed induction generator'. Twenty Second Annual IEEE Applied Power Electronics Conference, California, USA, February 2007, pp. 1334–1338

[22] Gómez, S.A, and Amenedo, J.L.R.: 'Grid synchronisation of doubly fed induction generators using direct torque control'. IEEE 28th Annual Conference of the Industrial Electronics Society, Sevilla, Spain, November 2002, pp. 3338–3343

[23] Holtz, J.: 'Pulsewidth modulation for electronic power conversion', *Proc. IEEE*, 1994, **82**, (8), pp. 1194–1214

[24] Ghandakly, A.A., and Sbeiti, Z. H.: 'A digital optimal controller for VSCF wind generators'. Conference Record of the 1991 IEEE Industry Applications Society Annual Meeting, September 1991, pp. 1618–1623

[25] Çadirci, I., and Ermis, M.: ‘Double-output induction generator operating at subsynchronous and supersynchronous speeds: steady-state performance optimisation and wind-energy recovery’, *IEE Proc.-B*, 1992, **139**, (5), pp. 429–442

[26] Xu, L., and Cheng, W.: ‘Torque and reactive power control of a doubly fed induction machine by position sensorless scheme’, *IEEE Trans. Industry Applications*, 1995, **31**, (3), pp. 636–642

[27] Pena, R., Clare, J.C., and Asher, G.M.: ‘Double fed induction generator using back-to-back PWM converters and its application to variable-speed wind-energy generation’, *IEE Proc. Electric Power Applications*, 1996, **143**, (3), pp. 231–241

[28] Hopfensperger, B., Atkinson, D.J., and Lakin, R.A.: ‘Stator-flux-oriented control of a doubly-fed induction machine with and without position encoder’, *IEE Proc. Electric Power Applications*, 2000, **147**, (4), pp. 241–250

[29] Ekanayake, J., Holdsworth, L., and Jenkins, N.: ‘Control of DFIG wind turbines’, *IEEE Power Engineer*, 2003, **17**, (1), pp. 28–32

[30] Tang, Y., and Xu, L.: ‘A flexible active and reactive power control strategy for a variable speed constant frequency generating system’, *IEEE Trans. Power Electronics*, 1995, **10**, (4), pp. 472–478

[31] Rongve, K.S., Naess, B.I., Undeland, T.M., and Gjengedal, T.: 'Overview of torque control of a doubly fed induction generator'. IEEE Bologna Power Tech Conference Proc., Bologna, Italy, June 2003, (3)

[32] Hansen, A.D., Sørensen, P., Iov, F., and Blaabjerg, F.: 'Control of variable speed wind turbines with doubly-fed induction generators', *Wind Engineering*, 2004, **28**, (4), pp. 411–432

[33] Tapia, A., Tapia, G., Ostolaza, J.X., and Sáenz, J.R.: 'Modeling and control of a wind turbine driven doubly fed induction generator', *IEEE Trans. Energy Conversion*, 2003, **18**, (2), pp. 194–204

[34] Müller, S., Deicke, M., and De Doncker, R.W: 'Doubly fed induction generator systems for wind turbines', *IEEE Industry Applications Magazine*, 2002, **8**, (3), pp. 26–33

[35] Yamamoto, M., and Motoyoshi, O.: 'Active and reactive power control for doubly-fed wound rotor induction generator', *IEEE Trans. Power Electronics*, 1991, **6**, (4), pp. 624–629

[36] Datta, R., and Ranganathan, V.T.: 'Decoupled control of active and reactive power for a grid-connected doubly-fed wound rotor induction machine without position sensors'. Conference Record of the 1999 IEEE Industry Applications Conference, Phoenix, USA, October 1999, pp. 2623–2630

[37] Park, J.W., Lee, K.W., and Lee, H.J.: 'Control of active power in a doubly-fed induction generator taking into account the rotor side apparent power'. IEEE 35th Annual Power Electronics Specialists Conference, Aachen, Germany, June 2004, pp. 2060–2064

[38] Azaza, H., and Masmoudi, A.: 'Implementation of a dual vector control strategy in a doubly-fed machine drive', *European Transactions on Electrical Power*, 2005, **15**, (6), pp. 541–555

[39] Arnalte, S., Burgos, J.C., and Rodríguez-Amenedo, J.L: 'Direct torque control of a doubly-fed induction generator for variable speed wind turbines', *Electric Power Components and Systems*, 2002, **30**, (2), pp. 199–216

[40] Wang, Z., Wang, F., Zong, M., and Zhang, F.: 'A new control strategy by combining direct torque control with vector control for doubly fed machine'. 2004 International Conference on Power System Technology, Singapore, November 2004, pp. 792–795

[41] Liu, Z., Mohammed, O.A., and Liu, S.: 'A novel direct torque control of doubly-fed induction generator used for variable speed wind power generation'. IEEE Power Engineering Society General Meeting, Tampa, USA, June 2007, pp. 1–6

[42] Buja, G.S., and Kazmierkowski, M.P.: 'Direct torque control of PWM inverter-fed AC motors – a survey', *IEEE Trans. Industrial Electronics*, 2004, **51**, (4), pp. 744–757

[43] Datta, R., and Ranganathan, V.T.: 'Direct power control of grid-connected wound rotor induction machine without rotor position sensors', *IEEE Trans. Power Electronics*, 2001, **16**, (3), pp. 390–399

[44] Arnalte, S., and Rodríguez-Amenedo, J.L: 'Sensorless direct power control of a doubly fed induction generator for variable speed wind turbines'. European Power Electronics and Drives Association 10th International Conference on Power Electronics and Motion Control, Cavtat and Dubrovnik, Croatia, September 2002, pp. 1–12

[45] de Alegria, I.M., Andreu, J., Ibañez, P., Villate, J.L., and Gabiola, I.: 'Novel power error vector control for wind turbine with doubly fed induction generator'. 30th Annual Conference of IEEE Industrial Electronics Society, Busan, South Korea, November 2004, pp. 1218–1223

[46] Xu, L., and Cartwright, P.: 'Direct active and reactive power control of DFIG for wind energy generation', *IEEE Trans. Energy Conversion*, 2006, **21**, (3), pp. 750–758

[47] Zhi, D., and Xu, L.: 'Direct power control of DFIG with constant switching frequency and improved transient performance', *IEEE Trans. Energy Conversion*, 2007, **22**, (1), pp. 110–118

[48] Lemström, B., Räkköläinen, J., and Peltola, E.: 'A wind farm's impact on the quality of electricity in a weak network'. European Wind Energy Conference, Nice, France, March 1999, pp. 747–749

[49] Koutiva, X.I., Vrionis, T.D., Vovos, N.A., and Giannakopoulos, G.B.: 'Optimal integration of an offshore wind farm to a weak AC grid', *IEEE Trans. Power Delivery*, 2006, **21**, (2), pp. 987–994

[50] Christiansen, P.: 'A sea of turbines', *IEE Power Engineer*, 2003, **17**, (1), pp. 22–24

[51] Soerensen, H.C., Larsen, J.H., Olsen, F.A., Svenson, J., and Hansen, S.R.: 'Middelgrunden 40 MW offshore wind farm, a prestudy for the Danish offshore 750 MW wind program'. Tenth International Offshore and Polar Engineering Conference, Seattle, USA, May 2000, pp. 484–491

[52] Sørensen, P., Madsen, P.H., Vikkelsø, A., Jensen, K.K., Fathima, K.A., Unnikrishnan, A.K., and Lakaparampil, Z.V.: 'Power quality and integration of wind farms in weak grids in India' (Risø National Laboratory, 2000)

[53] Muljadi, E., Yildirim, D., Batan, T., and Butterfield, C.P.: 'Understanding the unbalanced-voltage problem in wind turbine generation'. Conference Record of the 1999 IEEE Industry Applications Conference, Phoenix, USA, October 1999, pp. 1359–1365

[54] BS EN 50160: 'Voltage characteristics of electricity supplied by public distribution networks', 2007

[55] Kearney, J., and Conlon, M.F.: 'Performance of a variable speed double-fed induction generator wind turbine during network voltage unbalance

conditions'. Proc. of the 41st International Universities Power Engineering Conference, Newcastle upon Tyne, United Kingdom, September 2006, pp. 36–40

[56] Brekken, T.K.A., and Mohan, N: 'Control of a doubly fed induction wind generator under unbalanced grid voltage conditions', *IEEE Transaction on Energy Conversion*, 2007, **22**, (1), pp. 129–135

[57] Brekken, T., and Mohan, N.: 'A novel doubly-fed induction wind generator control scheme for reactive power control and torque pulsation compensation under unbalanced grid voltage conditions'. IEEE 34th Annual Power Electronics Specialist Conference, Acapulco, Mexico, June 2003, pp. 760–764

[58] Domínguez Rubira, S., and McCulloch, M.D.: 'Control method comparison of doubly fed wind generators connected to the grid by asymmetric transmission lines', *IEEE Trans. Industry Applications*, 2000, **36**, (4), pp. 986–991

[59] Bendl, J., Chomat, M., and Schreier, L.: 'Independent control of positive- and negative-sequence current components in a doubly fed machine', *European Transactions on Electrical Power*, 2005, **15**, (3), pp. 191–202

[60] Chomát, M., Bendl, J., and Schreier, L.: 'Extended vector control of doubly fed machine under unbalanced power network conditions'. International

Conference on Power Electronics, Machines and Drives, University of Bath, UK, April 2002, pp. 329–334

[61] Jang, J.I., Kim, Y.S., and Lee, D.C.: 'Active and reactive power control of DFIG for wind energy conversion under unbalanced grid voltage'. CES/IEEE 5th International Power Electronics and Motion Control Conference, Shanghai, China, August 2006, pp. 11–16

[62] Ehlert, D., and Wrede, H.: 'Wind turbines with doubly-fed induction generator systems with improved performance due to grid requirements'. IEEE Power Engineering Society General Meeting, Tampa, USA, June 2007, pp. 3841–3847

[63] Wang, Y., and Xu, L.: 'Control of DFIG-based wind generation systems under unbalanced network supply'. IEEE International Electric Machines and Drives Conference, Antalya, Turkey, May 2007, pp. 430–435

[64] Xu, L., and Wang, Y.: 'Dynamic modelling and control of DFIG-based wind turbines under unbalanced network conditions', *IEEE Trans. Power Systems*, 2007, **22**, (1), pp. 314–323

[65] Swisher, R., De Azua, C.R., and Clendenin, J.: 'Strong winds on the horizon: wind power comes of age', *Proc. of the IEEE* , 2001, **89**, (12), pp. 1757–1764

[66] Albertos, P. and Sala A.: 'Multivariable Control Systems' (Springer-Verlag, 2004)

[67] Camblong, H., Tapia, G., and Rodríguez, M.: 'Robust digital control of a wind turbine for rated-speed and variable-power operation regime', *IEE Proc. Control Theory and Applications*, 2006, **153**, (1), pp. 81–91

[68] BS EN 62114: 'Electrical insulation systems (EIS) – Thermal classification', 2001

[69] Scott, N.C., Atkinson, D.J., and Morrell, J.E.: 'Use of load control to regulate voltage on distribution networks with embedded generation', *IEEE Trans. Power Systems*, 2002, **17**, (2), pp. 510-515

[70] Brosilow, C., and Joseph, B.: 'Techniques of model-based control' (Prentice Hall, 2002)

[71] Huang, H., Fan, Y., Qiu, R.C., and Jiang, X.D.: 'Quasi-steady-state rotor EMF-oriented vector control of doubly fed winding induction generators for wind-energy generation', *Electric Power Components and Systems*, 2006, **34**, (11), pp. 1201-1211

[72] Blevins, T.L., McMillan, G.K., Wojsznis, W.K., and Brown, M.W.: 'Advanced Control Unleashed - Plant Performance Management for Optimum Benefit' (The Instrumentation, Systems, and Automation Society, 2003)

[73] Lindholm, M., and Rasmussen T.W.: 'Harmonic analysis of doubly fed induction generators'. Proc. 5th International Conference on Power Electronics and Drive Systems, Singapore, November 2003, pp. 837-841

[74] Liao, Y., Ran, L., Putrus, G.A., and Smith, K.S.: 'Evaluation of the effects of rotor harmonics in a doubly-fed induction generator with harmonic induced speed ripple', *IEEE Trans. Energy Conversion*, 2003, **18**, (4), pp. 508-515

[75] Zhang, G., and Xu, Z.: 'A new real-time negative and positive sequence components detecting method based on space vector'. Proc. IEEE Power Engineering Society Winter Meeting, 28 January 2001 – 1 February 2001, (1), pp. 275-280

[76] Petersson, A., Harnefors, L., and Thiringer, T.: 'Evaluation of Current Control Methods for Wind Turbines Using Doubly-Fed Induction Machines', *IEEE Trans. Power Electronics*, 2005, **20**, (1), pp. 227–235

[77] Petersson, A: 'Analysis, modeling and control of doubly-fed induction generators for wind turbines'. PhD thesis, Chalmers University of Technology, 2005

[78] Iov, F., Hansen, A.D., Sørensen, P., and Cutululis, N.A.: 'Mapping of grid faults and grid codes' (Risø National Laboratory, 2007)

[79] Xiang, D., Ran, L., Tavner, P.J., and Yang, S.: ‘Control of a doubly fed induction generator in a wind turbine during grid fault ride-through’, *IEEE Trans. Energy Conversion*, 2006, **21**, (3), pp. 652–662

[80] Ramos, C.J., Martins, A.P., and Carvalho, A.S.: ‘Rotor current controller with voltage harmonics compensation for a DFIG operating under unbalanced and distorted stator voltage’. Proc. 33rd Annual Conference of the IEEE Industrial Electronics Society, Taipei, Taiwan, November 2007, pp. 1287–1292